

DISSERTATION

DEVELOPMENT OF TETHERED MICELLE HYDROGEL NETWORKS THROUGH  
SPHERE-FORMING AB/ABA BLOCK COPOLYMER MELTS

Submitted by

Chen Guo

Department of Chemical and Biological Engineering

In partial fulfillment of the requirements

For the Degree of Doctor of Philosophy

Colorado State University

Fort Collins, Colorado

Fall 2013

Doctoral Committee:

Advisor: Travis S. Bailey

Matt J. Kipper

Eugene Chen

S. Ranil Wickramasinghe

Copyright by Chen Guo 2013

All Rights Reserved

## ABSTRACT

### DEVELOPMENT OF TETHERED MICELLE HYDROGEL NETWORKS THROUGH SPHERE-FORMING AB/ABA BLOCK COPOLYMER MELTS

The overriding theme of the work contained in this thesis is concerned with the preparation of tethered micelle hydrogel networks through the melt-state self-assembly of sphere-forming AB diblock and ABA triblock copolymer blends. The first chapter of this dissertation introduces the various projects pursued and provides background information for the reader.

The second chapter of this thesis contains the initial demonstration of this novel strategy using polystyrene-poly(ethylene oxide) (PS-PEO, SO) diblock and PS-PEO-PS (SOS) triblock copolymers. Included in this chapter is a discussion of the synthetic polymerization techniques used to produce the SO and SOS block copolymers, the basic melt-state fabrication and characterization strategies used to pre-structure the tethered micelle networks, and the impact of changing both the SOS concentration and temperature on the resultant properties of the hydrogels produced. In these initial studies, the SOS triblock copolymer was constructed to be exactly double the SO diblock copolymer molecular weight, such that the preferred lattice dimensions during self-assembly were "matched". These "matched" hydrogels produced equilibrium swelling ratios (3.8-36.9 g water/g polymer) and dynamic elastic moduli ( $G' = 1.7-160$  kPa) tunable across an impressive range of values using only temperature (10-50 °C) and SOS concentration (3.3-72.0 mol%).

The third chapter of this thesis describes our efforts to influence the swelling and mechanical properties exhibited by simply modifying the PEO midblock molecular weight in the

SOS tethering molecules. In doing so, we were able to show that the degree of coronal layer overlap between adjacent micelles was the primary contributing factor determining the dynamic mechanical response of the hydrogel. That is, the changes in mechanical properties produced due to altering tether concentration, tether length, or temperature, could all be understood in terms of their impact on the degree of coronal layer overlap in the system. In addition to these findings, we also discovered an interesting relationship between swelling and tether length. Increases in tether length by a factor of 1.6 compared to that of the matched system, resulted in higher swelling ratios and smaller elastic moduli (due to reduced coronal layer overlap). However, increases in tether length by a factor of 2.3 produced swelling behavior and mechanical properties nearly identical to that of the matched system. We concluded that the increase in tether length by a factor of 2.3 was sufficient to allow bridging into the second shell of the nearest neighbor micelles, negating the swelling advantage anticipated for the system.

The fourth chapter of this thesis concerns our efforts to demonstrate the modification potential of the swollen hydrogel systems of Chapters 2 and 3. In this study, the terminal hydroxyl functionality present in the aforementioned SO diblock copolymers was substituted with either an azide or alkyne functionality. Cu(I) catalyzed coupling of the azide/alkyne functional diblock copolymer was then performed in the swollen state, producing a secondary network of tethers in the system. Installation of the secondary network produced dramatic improvements in the hydrogel tensile modulus, strain at break, stress at break, and toughness, while permitting swelling ratios, small strain rheological properties, and response in unconfined compression to remain largely unchanged.

The fifth and final chapter of this thesis concerns a discussion of preliminary data supporting several promising directions for future work involving the further development of these tethered micelle networks.

## ACKNOWLEDGEMENTS

I would like to express my gratitude to my advisor Dr. Travis Bailey for his guidance and help. After seven years in his group, I'm very thankful for the scientist I have become. It has always been a great pleasure to work in the Bailey Research Group (the BRG) because of the people around, especially Vincent Scalfani (Vinny) and Mike Wells who have become my friends for life. Besides Vinny, I would also like to recognize Jackson Lewis and Miriah Schwartz for their inputs in the extension of my work.

It has been by far the best seven years in my life. I want to thank my parents Jianxue Guo and Qiuwen Wei, who wanted me to stay home the most but made the hard decision to let me follow my heart. All friends in the LifePointe Church and Fort Collins Chinese Christian Fellowship deserve infinite thanks for their friendship in GOD. Xuejia Yan and Lijun Deng are my friends in Tsinghua University who encouraged me to apply for the graduate program in Colorado State University and helped me with my application. Without their help, I could never have the chance to enjoy my life like this.

Finally, I want to give my acknowledgements to my family. My husband Lei Chen is the love of my life and my forever best friend. Getting married to him is the most amazing thing that ever happened to me. I can never make through these seven years through without his love and support. And to Kaydence, my beautiful daughter, I love you!

## TABLE OF CONTENTS

<b>ABSTRACT.....</b>	<b>II</b>
<b>ACKNOWLEDGEMENTS .....</b>	<b>V</b>
<b>CHAPTER 1</b>	
<b>INTRODUCTION TO THE DISSERTATION .....</b>	<b>1</b>
<b>1.1 Overview of Dissertation .....</b>	<b>1</b>
<b>1.2 Block Copolymer Thermodynamics .....</b>	<b>1</b>
<b>1.3 Development of a Model Block Copolymer-based Tethered Micelle Hydrogel Network         (Chapter 2) .....</b>	<b>5</b>
<b>1.4 Tether Length Adjustment in Tethered Micelle Networks (Chapter 3) .....</b>	<b>7</b>
<b>1.5 Post Swelling Modification of Hydrogel System (Chapter 4).....</b>	<b>9</b>
<b>1.6 Notes on Dissertation Main Text.....</b>	<b>10</b>
<b>1.7 References .....</b>	<b>11</b>
<b>CHAPTER 2</b>	
<b>HIGHLY DISTENSIBLE NANOSTRUCTURED ELASTIC HYDROGELS FROM AB         DIBLOCK AND ABA TRIBLOCK COPOLYMER MELT BLENDS.....</b>	<b>13</b>
<b>2.1. Summary .....</b>	<b>13</b>
<b>2.2. Introduction .....</b>	<b>14</b>
<b>2.3. Experimental.....</b>	<b>16</b>
2.3.1 Materials.....	16
2.3.2 Synthesis .....	17
2.3.3 Hydrogel Fabrication .....	19

2.3.4	Characterization .....	20
<b>2.4.</b>	<b>Results and discussion.....</b>	<b>23</b>
2.4.1	Material Synthesis.....	23
2.4.2	SO and SOS-72.0 Melt-State Morphological Characterization .....	25
2.4.3	SOS- $X_i$ Blend Characterization .....	34
2.4.4	Equilibrium Swelling Behavior .....	35
2.4.5	Mechanical Performance.....	39
2.4.6	Elastic Recovery and Aging.....	47
<b>2.5.</b>	<b>Conclusions .....</b>	<b>49</b>
<b>2.6.</b>	<b>Recognitions.....</b>	<b>50</b>
<b>2.7.</b>	<b>Supporting information available.....</b>	<b>50</b>
<b>2.8.</b>	<b>References .....</b>	<b>51</b>

## CHAPTER 3

### EFFECTS OF TAILORED CORONAL LAYER OVERLAP IN TETHERED MICELLE

	<b>HYDROGEL NETWORKS.....</b>	<b>55</b>
<b>3.1</b>	<b>Summary .....</b>	<b>55</b>
<b>3.2</b>	<b>Introduction .....</b>	<b>56</b>
<b>3.3.</b>	<b>Experimental.....</b>	<b>63</b>
3.3.1.	Materials.....	63
3.3.2.	$\omega$ -Hydroxyl-polystyrene (S-OH).....	63
3.3.3.	$\omega$ -Hydroxyl-polystyrene-b-poly(ethylene oxide) (SO-1, SO-1.6, SO-2.3).....	64
3.3.4.	Polystyrene-b-poly(ethylene oxide)-b-polystyrene (SOS-1, SOS-1.6, SOS-2.3) .....	64
3.3.5.	Fractionation.....	65
3.3.6.	SO/SOS blend formation.....	65
3.3.7.	Polymer disk formation .....	65

3.3.8. Swelling to equilibrium .....	66
3.3.9. Molecular characterization .....	66
3.3.10. Small angle X-ray scattering (SAXS) .....	66
3.3.11. Determination of swelling ratio (Q) .....	67
3.3.12. Hydrogel rheology .....	67
<b>3.4. Results and discussion .....</b>	<b>67</b>
3.4.1. Block copolymer synthesis .....	67
3.4.2. Characterization of SO/SOS blends .....	70
3.4.3. Equilibrium swelling behavior .....	76
3.4.4. Impact on mechanical properties .....	80
<b>3.5. Conclusions .....</b>	<b>83</b>
<b>3.6. Recognitions .....</b>	<b>84</b>
<b>3.7. References .....</b>	<b>85</b>

## CHAPTER 4

<b>IMPROVING TOUGHNESS IN HIGHLY SWOLLEN BLOCK COPOLYMER BASED HYDROGEL NETWORKS .....</b>	<b>87</b>
<b>4.1 Summary .....</b>	<b>87</b>
<b>4.2. Introduction .....</b>	<b>88</b>
<b>4.3. Experimental .....</b>	<b>93</b>
4.3.1 Materials .....	93
4.3.2 Synthesis of PS-PEO diblock copolymer (SO-H) and PS-PEO-PS (SOS) triblock copolymer .....	94
4.3.3 Synthesis of SO-azide <sup>21, 22</sup> .....	94
4.3.4 Synthesis of SO-alkyne <sup>23</sup> .....	95
4.3.5 SO/SO-alkyne/SO-azide/SOS blends .....	96

4.3.6	Dry polymer disk formation.....	96
4.3.7	Hydrogel swelling and general protocol of click chemistry .....	96
<b>4.4</b>	<b>Characterization.....</b>	<b>97</b>
4.4.1	Molecular characterization.....	97
4.4.2	Dynamic Shear and Unconfined Compression Testing .....	97
4.4.3	Tensile Testing.....	98
<b>4.5</b>	<b>Results and discussion.....</b>	<b>99</b>
4.5.1	Block Copolymer Synthesis, Physical Characterization and Blend Formation.....	99
4.5.2	Baseline Performance of SO/SOS Hydrogels.....	103
4.5.3	Chemical Characterization and Swelling in “Click” Enhanced Hydrogels .....	108
4.5.4	Mechanical Performance of “Click” Enhanced Hydrogels.....	113
<b>4.6</b>	<b>Conclusions .....</b>	<b>121</b>
<b>4.7</b>	<b>Recognitions.....</b>	<b>122</b>
<b>4.8</b>	<b>Supporting information found in the appendix.....</b>	<b>122</b>
<b>4.9</b>	<b>References .....</b>	<b>124</b>
 <b>CHAPTER 5</b>		
 <b>CONCLUSIONS AND FUTURE WORK.....</b>		
<b>5.1</b>	<b>Conclusion.....</b>	<b>126</b>
<b>5.2</b>	<b>Future work .....</b>	<b>127</b>
5.2.1	Sample preparation for tensile tests .....	127
5.2.2	Mass transfer properties and pore structures in the hydrogels.....	127
5.2.3	Alternate Methods Towards Porosity Control .....	128
5.2.4	Ionic liquid gels and gels swollen in biological buffer solutions.....	132
5.2.5	Small molecule immobilization .....	132
<b>5.3</b>	<b>References .....</b>	<b>134</b>

## APPENDIX

<b>SUPPLEMENTARY INFORMATION.....</b>	<b>135</b>
<b>Supplementary Information for Chapter 2: .....</b>	<b>135</b>
S 2.1 Determination of SOS triblock copolymer concentration in SOS-72.0 by regression analysis .....	135
S 2.2 Differential scanning calorimetry (DSC) data for the S-OH and SO samples .....	136
S 2.3 Melt-state rheological analysis of the SO and SOS-72.0 samples.....	138
S 2.4 Additional notes on the analysis of morphology from SAXS .....	139
<b>Supplementary Information for Chapter 3: .....</b>	<b>141</b>
S 3.1 DSC of S-OH.....	141
<b>Supplementary Information for Chapter 4: .....</b>	<b>142</b>
S4.1 <sup>1</sup> H-NMR spectrum of PS-PEO-H .....	142
S4.2 <sup>1</sup> H-NMR spectrum of PS-PEO-Ms .....	143
S4.3 <sup>1</sup> H-NMR spectrum of PS-PEO-azide.....	144
S4.4 <sup>1</sup> H-NMR spectrum of PS-PEO-alkyne.....	145
S4.5 FTIR spectrum of PS-PEO-azide.....	146
S4.6 Dynamic frequency sweep results (elastic shear moduli) for samples A1 - D1, baseline SO/SOS hydrogels of 4.1 and 20.3 mol% SOS, and a catalyst control sample .....	147
S4.7 Unconfined compression for samples A1 - D1, and a catalyst control sample .....	148
<b>Example PY fitting using MATLAB.....</b>	<b>149</b>

## CHAPTER 1

### INTRODUCTION TO THE DISSERTATION<sup>1</sup>

#### 1.1 Overview of Dissertation

The purpose of this chapter is to briefly introduce block copolymer (BCP) thermodynamics and outline the contents within this dissertation. There are three major studies in this dissertation, all of which are based on a novel BCP hydrogel platform: 1) development of a model BCP-based tethered micelle hydrogel network, 2) study of tether length adjustment in tethered micelle networks and the influence on hydrogel swelling and mechanical properties, and 3) development of post-swelling modification strategies using click chemistry to enhance hydrogel toughness. The following sections present a brief introduction to BCP phase behavior and an overview of the aforementioned studies contained within this dissertation. Detailed introductions and comprehensive literature reviews are introduced separately within each chapter, tailored to the goals of each particular major study.

#### 1.2 Block Copolymer Thermodynamics

Block copolymers (BCPs) are hybrid molecules consisting of two or more homopolymers that are covalently connected. The most attractive feature of BCPs for researchers is their ability to spontaneously self-assemble into periodic structures on the nanometer scale, which has been investigated both theoretically<sup>1-4</sup> and experimentally<sup>1, 5-7</sup> for the last several decades. Nanostructured materials based on self-assembled BCPs have been widely exploited in numerous applications such as: catalysis<sup>8</sup>, templation<sup>9</sup>, molecular separations<sup>10</sup>, polymer light-

---

<sup>1</sup> The contents of this dissertation chapter were written by Chen Guo.

emitting diodes (LEDs)<sup>11</sup>, and photovoltaic cells.<sup>12</sup> The driving force for the spontaneous self-assembly of BCPs is twofold: 1) the covalent bond between the homopolymer blocks prevents macrophase separation and thus forces the incompatible system to separate in a microscopic length scale (microphase separation), and 2) the final adopted morphology is a result of a delicate balance between interfacial surface contact and chain stretching penalties that result in the lowest overall free energy.

Detailed phase diagrams of linear AB diblock copolymers have been extensively studied both theoretically<sup>13</sup> (Figure 1.1) and experimentally<sup>6</sup> (Figure 1.2). As shown in the theoretical phase diagram (Figure 1.1), BCP phase separation is governed by the product  $\chi N$ , where  $\chi$  is the Flory-Huggins segment-segment interaction parameter and  $N$  is the number of segmental volumes. When the product  $\chi N$  exceeds a critical point, it becomes energetically more favorable to phase separate, than to form a disordered mixture. The adopted equilibrium morphology with the lowest free energy is then chosen by balancing the entropic chain stretching and enthalpic interfacial surface contact energy. Importantly, the desired morphology can be targeted through adjustment of the overall volume fraction ( $f$ ). For linear AB diblocks the following structures are confirmed to be stable both in theory and in experiment: lamellae, hexagonal-packed cylinders, body-centered cubic spheres, and bicontinuous gyroid structures. Notably, more complex self-assembled morphologies can be obtained through BCP architectures such as rod-coil diblock copolymers<sup>14</sup>, ABC triblock copolymers<sup>15-18</sup> and even multiblock copolymers<sup>19</sup>, however such complex systems were not studied in this dissertation and therefore not discussed herein.

Numerous AB diblock copolymers systems have been studied in order to map out their experimental phase diagrams including, for example, poly(ethylene oxide)- polyisoprene (PEO-

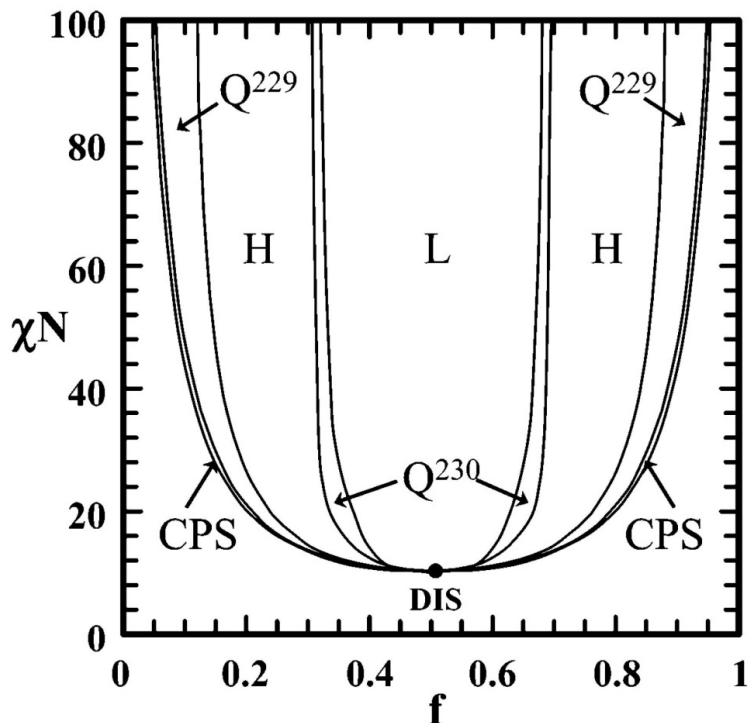
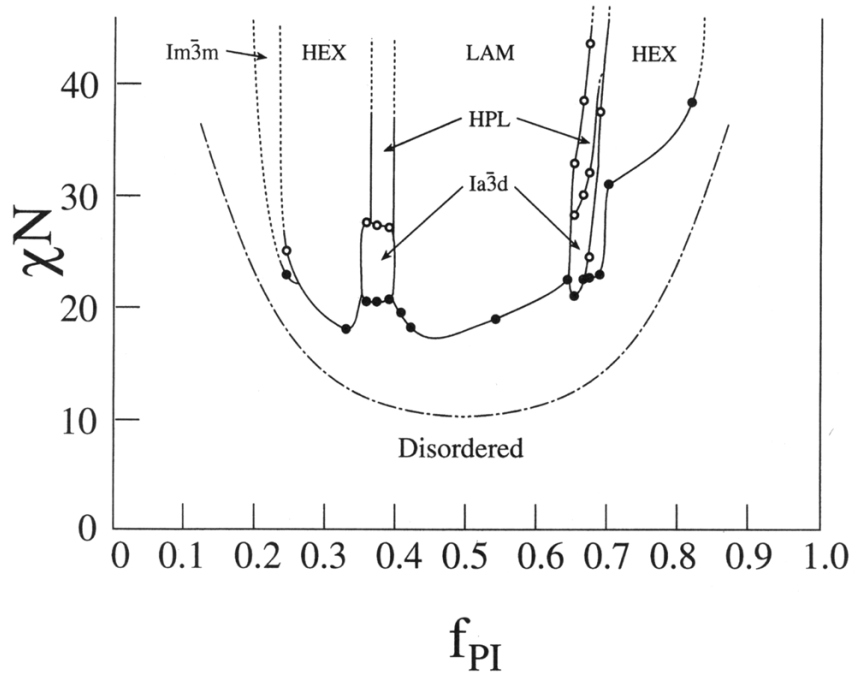


Figure 1.1. Theoretically calculated diblock copolymer phase diagram developed by Cochran et al. adapted from ref [4] with permission, (copyright (2006) American Chemical Society), using self-consistent mean-field (SCMF) theory.<sup>13</sup> CPS, Q<sup>229</sup>, H, Q<sup>230</sup> and L stand for close packed spheres, body-centered cubic spheres, hexagonally packed cylinders, bicontinuous gyroid and lamellae, respectively.

PI)<sup>7</sup>, polystyrene-polyisoprene (PS-PI)<sup>6</sup> and polystyrene-polybutyl methacrylate (PS-PBMA)<sup>5</sup>. Khandpur et al. studied the phase behavior of PS-PI diblock copolymer.<sup>6</sup> (Figure 1.2) The experimental phase diagram is very similar to the theoretical phase diagram, containing spherical, hexagonally packed cylindrical, bicontinuous gyroid, and lamellar structures. The main difference in the two phase diagrams is the slightly asymmetric shape in the experimental diagram. Nonetheless, the theoretical and experimental phase diagrams agree well and have a remarkable degree of similarity. Numerous researchers, including those involved with this dissertation, have exploited targeted areas of the phase diagram to produce nanostructured materials.<sup>20-22</sup> In this dissertation, the spherical morphology was exclusively targeted in the



**Figure 1.2.** Experimental phase diagram of polystyrene-polyisoprene diblock copolymer system by Khandpur et al., adapted with permission from ref [6]. Copyright (1995) American Chemical Society. Similarly to the theoretical phase diagram, spherical, hexagonally packed cylindrical, bicontinuous gyroid, and lamellar structures are adopted when certain values of  $\chi N$  and  $f$  are met.

phase diagram to prepare nanostructured elastic hydrogels. Instead of preparing hydrogels in the conventional way where amphiphilic block copolymers are dissolved in water to form connected micelles (sol-gel)<sup>23-28</sup>, we utilized the spherical morphology in the melt state to pre-structure the network. This, as discussed in great length in Chapters 2 and 3, produces hydrogels with greater control over nanostructure and mechanical properties when compared to the conventional hydrogel preparation methods.

### 1.3 Development of a Model Block Copolymer-based Tethered Micelle Hydrogel Network (Chapter 2)

In chapter 2, a model hydrogel system was developed utilizing sphere-forming AB diblock and ABA triblock copolymer melt blends. The pre-structured hydrogel system is comprised of an infinite network of spherical hydrophobic junctions (A block aggregates) tethered together through hydrophilic midblocks (B blocks) of the ABA triblock copolymer. The equilibrium swelling dimensions of the tethered hydrogel system are governed by the balance between the osmotic swelling forces of solvation, the entropic restoring forces of the tethering midblocks, and the density of topological entanglements among the tethers. Notably, the spherical morphologies provide three-dimensionally isolated domains with precisely controlled distances such that these model hydrogels can potentially serve as porous membrane materials with controlled and narrowly-distributed mesh sizes. In-depth analysis of the model system revealed the hydrogels swell isotropically and are highly tunable. The mechanical properties and swelling ratios could be altered by simply adjusting the relative composition of the AB diblock / ABA triblock copolymer blend. After swelling, the initial pre-swollen shape is completely preserved. Lastly, the glassy nature of the A domains eliminates the necessity to chemically crosslink the micelle cores, making the hydrogel system completely reprocessable.

Specifically, the model system was comprised of polystyrene (PS) as the A block and poly(ethylene oxide) (PEO) as the B block. PS is a strongly hydrophobic polymer with a glass transition temperature ( $T_g$ ) around 100 °C, while PEO is a semi-crystalline polymer with a melt temperature ( $T_m$ ) around 65 °C and water solubility that is temperature dependent. Importantly, PEO serves not only as a hydrophilic block but also as a widely utilized biocompatible polymer.<sup>28</sup> The  $T_g$  of PS is a strong function of molecular weight below 10,000 g/mol.<sup>29,30</sup> Well

below 10,000 g/mol chain entanglements are minimal resulting in poor mechanical properties. Therefore, we selected a PS molecular weight of about 8 kDa which has a bulk  $T_g$  of approximately 80 °C. In our studies, we found that hydrogels prepared using PS with a MW of 8000 g/mol produce nontrivial mechanical properties up to operating temperatures of about 60 °C. In order to obtain the desired spherical polystyrene domains, the volume fraction of PS in the PS-PEO diblock copolymer has to be in the range of 0.09-0.13.<sup>2,3</sup> This particular volume fraction range produces an extremely asymmetric block copolymer with a very large PEO majority block. For example, with the 8 kDa PS (minimum to obtain good mechanical properties up to 60 °C), the PEO block must be 60,000 g/mol to reach a volume fraction of 0.13. Higher molecular weight (>100,000 g/mol) PEO can also be difficult to synthesize in a controlled fashion, and therefore the use of larger PS blocks was avoided. For the fabrication of hydrogel networks, PS-PEO-PS triblock copolymer was required to physically tether adjacent spherical domains. The triblock copolymer was synthesized by coupling the PS-PEO diblock copolymer, producing triblock copolymer with MWs of exactly double (~140,000 g/mol) that of the PS-PEO diblock copolymers.

After material synthesis, hydrogels were prepared by blending a desired amount of the triblock into the diblock copolymer. Disks of the composite blends were then melt-processed, vitrified through cooling to room temperature, and swollen in water. In Chapter 2, a fundamental study of the hydrogel system was conducted by investigating the impact of varying PS-PEO-PS concentrations in the blends. The equilibrium swelling behavior, thermal response, rheological properties and unconfined compressive behavior were evaluated on these hydrogels.

In the original proposal we sought to prepare hydrogels with highly ordered body-centered cubic spherical morphologies. However, due to the large molecular weight block

copolymers used within this work, the nanostructures produced during self-assembly were not spherical domains arranged on a bcc lattice, but instead a liquid-like packing of spheres, absent of long-range order. Despite the absence of a well-ordered periodic lattice, the hydrogels swelled isotropically in three dimensions, and proved to be extremely robust and highly tunable. A more rigorous analysis of the exact structure was performed using model fits of the small-angle X-ray Scattering (SAXS) data, helping to characterize the nature of the liquid-like packing and confirm the uniformity of the average sphere-to-sphere distance in these samples. The detailed characterization information is discussed in Chapter 2.

#### **1.4 Tether Length Adjustment in Tethered Micelle Networks (Chapter 3)**

Following the studies of the lattice matched ( $M_{n,ABA} = 2M_{n,AB}$ ) systems of Chapter 2, we altered the molecular weight of the PEO midblock within the PS-PEO-PS triblock copolymer tethers in order to tailor the swelling behavior and mechanical properties of the hydrogels. Blends of PS-PEO diblock and PS-PEO-PS triblock copolymer comparable to those in the model system of Chapter 2 were prepared this time as the a control group, in order to distinguish the effects of introducing SOS molecules with longer tethers. PS-PEO-PS triblock copolymers end capped with the same PS block as the control blends but containing PEO with higher molecular weights were synthesized, fractionated and then blended with PS-PEO diblock copolymer. The blends were then used to create polymer disks, which were later swollen to produce tethered micelle hydrogel networks. Similar to the model system study, the hydrogel properties examined included equilibrium swelling ratios and rheological mechanical testing.

More specifically, a series of PS-PEO-PS triblock copolymers with different length PEO midblocks were synthesized, consisting of 152 kDa (1X control  $M_{n,ABA} = 2M_{n,AB}$ ), 243 kDa (1.6 X) and 350 kDa (2.3 X) PEO. The longer tether triblocks were blended with PS-PEO diblock

copolymer to produce PS-PEO-PS concentrations of 3, 5, 10 and 15 mol%, respectively. Similar to the matched system, the 1.6 X and 2.3 X systems were able to produce robust and elastic hydrogels whose behavior followed similar trends to the model system. That is, swelling ratios increased with decreased PS-PEO-PS concentration, and mechanical properties improved with increased PS-PEO-PS concentration. The SAXS data of all melt blends were used to verify the liquid-like packing of spherical morphology was preserved, despite of the increased tether length in the system.

As expected, increasing the tether length by 1.6X produced hydrogels with larger swelling ratios as compared to the 1X control. Based on these results, we were expecting even larger hydrogels for the 2.3X system, but found contrary results. The 2.3X system behaved similarly to the matched system in both swelling and mechanical properties. We believe that this result is caused by tether insertion into the second shell of nearest-neighbor micelles, instead of being constrained only to the first shell. We hypothesized that there is a limit between a 1.6 and 2.3 X that can produce the most absorbent hydrogels for a given system.

Importantly, the increased ability to swell in the 1.6X system was also accompanied by a severe decrease in elastic modulus. The severe decrease was a direct result of vanishing coronal layer overlap as the distance between micelles increased. It became apparent that coronal layer overlap was the major contributing factor in determination of dynamic mechanical response. From these studies, we were able to discern the roles of water content, tether concentration and tether length in controlling coronal layer overlap, and thus the mechanical performance, of the hydrogel system.

Meanwhile, it is interesting to consider the case of a tether length long enough to reach the second shell of nearest neighbor micelles, but too short to reach the third shell of nearest

neighbor micelles. In this scenario, it is plausible that an increased amount of swelling would again be achieved, however the distinction in discrete distances available to the tethering molecules would likely become less and less pronounced. It would be a fantastic future study to generate a map of hydrogel behavior regarding the longer tether lengths (e.g. 3x, 4x, 5x etc) and predict the hydrogel mechanical properties based on this map. However, the synthesis of monodispers high molecular weight PS-PEO-PS triblock copolymer would be a significant challenge.

### **1.5 Post Swelling Modification of Hydrogel System (Chapter 4)**

One of the most exciting features about our designed tethered micelle hydrogel networks compared to other conventional hydrogels is that there are hundreds of free hydroxyl terminated diblock copolymer chains ends per micelle which can be readily functionalized. In Chapter 4, click chemistry catalyzed by Cu(I) salts in aqueous solution was selected to demonstrate the modification potential of the swollen hydrogel systems of Chapters 2 and 3. In this study, the aforementioned PS-PEO diblock and PS-PEO-PS triblock copolymers were prepared and the hydroxyl groups on the PS-PEO diblock copolymers substituted with either azide or alkyne functionality. A fixed amount of PS-PEO-PS triblock copolymer was blended with the azide/alkyne functional PS-PEO diblock copolymer and used to control the swelling ratio of the produced tethered micelle network. Cu(I) catalyzed coupling of the azide/alkyne functional diblock was then performed in the swollen state, producing a secondary network of tethers in the system. To control the quantity of the additional tethers formed in the swollen state, the azide/alkyne functional group concentration was diluted through the addition of inert PS-PEO diblock copolymers (-OH end-capped) at various ratios. The tensile properties, swelling behavior, and compression test results are discussed in Chapter 4.

The targeted amount of pre-blended PS-PEO-PS tether was 9 - 10 mol% to produce hydrogel equilibrium swelling ratios in the vicinity of 20 g H<sub>2</sub>O/g polymer. The balance of the blend consisted of 1:1 ratios of PS-PEO-azide and PS-PEO-alkyne in combination with inert PS-PEO-H. Introducing the secondary network of tethers produced significant improvements to the hydrogel tensile modulus, strain at break, stress at break, and toughness, while permitting the swelling ratios, the rheological properties under dynamic shear and modulus in unconfined compression to remain largely unchanged. As anticipated, the preblended PS-PEO-PS triblock copolymer concentration was solely responsible for determining the swelling ratio of the hydrogels while the installation of the secondary tether network improved the tensile properties of the hydrogels. With this study, we successfully demonstrated the potential of post-swelling modification in these systems, in this case used as a means to enhance the tensile properties of the hydrogel. Details are included in Chapter 4.

## **1.6 Notes on Dissertation Main Text**

This dissertation concludes with Chapter 5, containing an overview of the major results in this dissertation and preliminary data supporting future work involving possible applications of these nanostructured hydrogels. Included is preliminary work aimed at 1) preparing new gels using swelling media other than water, and 2) developing alternate methods of controlling hydrogel porosity.

## 1.7 References

- [1] F. S. Bates and G. H. Fredrickson, "Block Copolymer Thermodynamics: Theory and Experiment," *Annual Review of Physical Chemistry*, vol. 41, pp. 525-557, 1990/10/01 1990.
- [2] F. S. Bates, "Polymer-Polymer Phase Behavior," *Science*, vol. 251, pp. 898-905, 1991.
- [3] F. S. Bates, M. F. Schulz, A. K. Khandpur, S. Forster, J. H. Rosedale, K. Almdal, and K. Mortensen, "Fluctuations, conformational asymmetry and block copolymer phase behaviour," *Faraday Discussions*, vol. 98, pp. 7-18, 1994.
- [4] E. W. Cochran, C. J. Garcia-Cervera, and G. H. Fredrickson, "Stability of the Gyroid Phase in Diblock Copolymers at Strong Segregation," *Macromolecules*, vol. 39, pp. 2449-2451, 2006/04/01 2006.
- [5] R. Weidisch, M. Stamm, G. H. Michler, H. Fischer, and R. J. V. Me, "Mechanical Properties of Weakly Segregated Block Copolymers. 3. Influence of Strain Rate and Temperature on Tensile Properties of Poly(styrene-b-butyl methacrylate) Diblock Copolymers with Different Morphologies," *Macromolecules*, vol. 32, pp. 742-750, 1999/02/01 1999.
- [6] S. F. Ashish K. Khandpur, Frank S. Bates, Ian W. Hamley, Anthony J. Ryan, Wim Bras, Kristoffer Almdal, Kell Mortensen, "Polyisoprene-Polystyrene Diblock Copolymer Phase Diagram near the Order-Disorder Transition," *Macromolecules*, vol. 28, pp. 8796-8806, 1995.
- [7] G. Floudas, B. Vazaiou, F. Schipper, R. Ulrich, U. Wiesner, H. Iatrou, and N. Hadjichristidis, "Poly(ethylene oxide-b-isoprene) Diblock Copolymer Phase Diagram," *Macromolecules*, vol. 34, pp. 2947-2957, 2001/04/01 2001.
- [8] Y. Z. Carlos B. W. Garcia, Surbhi Mahajan, Francis Disalvo, Ulrich Wiesner, "Self-Assembly Approach toward Magnetic Silica-Type Nanoparticles of Different Shapes from Reverse Block Copolymer Mesophases," *Journal of the American Chemical Society*, vol. 125, pp. 13310-13311, 2003.
- [9] M. Park, "Block Copolymer Lithography: Periodic Arrays of 1011 Holes in 1 Square Centimeter," *Science*, vol. 276, pp. 1401-1404, 1997.
- [10] L. Chen, W. A. Phillip, E. L. Cussler, and M. A. Hillmyer, "Robust Nanoporous Membranes Templated by a Doubly Reactive Block Copolymer," *Journal of the American Chemical Society*, vol. 129, pp. 13786-13787, 2007/11/01 2007.
- [11] Y. Heischkel and H.-W. Schmidt, "Synthesis of ABC-triblock copolymers for light emitting diodes," *Macromolecular Chemistry and Physics*, vol. 199, pp. 869-880, 1998.
- [12] A. Corma, P. Atienzar, H. Garcia, and J. Y. Chane-Ching, "Hierarchically mesostructured doped CeO<sub>2</sub> with potential for solar-cell use," *Nat Mater*, vol. 3, pp. 394-7, Jun 2004.
- [13] C. J. G.-C. Eric W. Cochran, Glenn H. Fredrickson, "Stability of the Gyroid Phase in Diblock Copolymers at Strong Segregation," *Macromolecules*, vol. 39, pp. 2449-2451, 2006.
- [14] D. G. Wentao Li, "Self-assembly of Rod-Coil Diblock Copolymers," *Macromolecules*, vol. 34, 2001.
- [15] N. Hadjichristidis, H. Iatrou, M. Pitsikalis, S. Pispas, and A. Avgeropoulos, "Linear and non-linear triblock terpolymers. Synthesis, self-assembly in selective solvents and in bulk," *Progress in Polymer Science*, vol. 30, pp. 725-782, 2005.

- [16] U. K. Ulrike Breiner, Thomas Jakob, Volker Abetz, Reimund Stadler, "Spheres on spheres - a novel spherical multiphase morphology in polystyrene-block-polybutadiene-block-poly(methyl methacrylate) triblock copolymers," *Polymer Bulletin*, vol. 40, pp. 219-226, 1998.
- [17] H. K. Yasuhiro Mogi, Yuji Kaneko, Katsuaki Mori, Yushu Matsushita, Ichiro Noda, "Preparation and morphology of triblock copolymers of the ABC type," *Macromolecules*, vol. 25, pp. 5408-5411, 1992.
- [18] C. M. H. Travis S. Bailey, Thomas H. Epps, III, Frank S. Bates, "A Noncubic Triply Periodic Network Morphology in Poly(isoprene-b-styrene-b-ethylene oxide) Triblock Copolymers," *Macromolecules*, vol. 35, pp. 7007-7017, 2002.
- [19] G. H. F. François Drolet, "Combinatorial Screening of Complex Block Copolymer Assembly with Self-Consistent Field Theory," *Physics Review Letter*, vol. 83, pp. 4317-4320, 1999.
- [20] M. A. H. Huiming Mao, "Nanoporous polystyrene by chemical etching of poly (ethylene oxide) from ordered block copolymers," *Macromolecules*, vol. 38, pp. 4038-4039, 2005.
- [21] R. O.-V. Andrew S. Zalusky, Johanna H. Wolf, Marc A. Hillmyer, "Ordered nanoporous polymers from polystyrene-poly lactide block copolymers," *Journal of American Chemical Society*, vol. 124, pp. 12761-12773, 2002.
- [22] R. O.-V. Andrew S. Zalusky, Charles J. Taylor, Marc A. Hillmyer, "Mesoporous polystyrene monoliths," *Journal of American Chemical Society*, vol. 123, pp. 1519-1520, 2001.
- [23] A. M. Bivigou-Koumba, E. Görnitz, A. Laschewsky, P. Müller-Buschbaum, and C. M. Papadakis, "Thermoresponsive amphiphilic symmetrical triblock copolymers with a hydrophilic middle block made of poly(N-isopropylacrylamide): synthesis, self-organization, and hydrogel formation," *Colloid and Polymer Science*, vol. 288, pp. 499-517, 2010.
- [24] A. P. Vogt and B. S. Sumerlin, "Temperature and redox responsive hydrogels from ABA triblock copolymers prepared by RAFT polymerization," *Soft Matter*, vol. 5, pp. 2347-2351, 2009.
- [25] L. Yu and J. Ding, "Injectable hydrogels as unique biomedical materials," *Chem Soc Rev*, vol. 37, pp. 1473-81, Aug 2008.
- [26] A. Khademhosseini and R. Langer, "Microengineered hydrogels for tissue engineering," *Biomaterials*, vol. 28, pp. 5087-92, Dec 2007.
- [27] S. W. K. Byeongmoon Jeong, You Han Bae, "Thermosensitive sol-gel reversible hydrogels," *Advanced Drug Delivery Reviews*, vol. 54, pp. 37-51, 2002.
- [28] K. B. K. Nikolaos A Peppas, Madeline Torres-Lugo, Anthony M Lowman, "Poly(ethylene glycol)-containing hydrogels in drug delivery," *Journal of Controlled Release*, vol. 62, pp. 81-87, 1999.
- [29] P. J. F. T. G. Fox, "The Glass Temperature and Related Properties of Polystyrene. Influence of Molecular Weight," *Journal of Polymer Science*, vol. 14, pp. 315-319, 1954.
- [30] C. M. R. P. G. Santangelo, "Molecular Weight Dependence of Fragility in Polystyrene," *Macromolecules*, vol. 31, pp. 4581-4585, 1998.

## CHAPTER 2

### HIGHLY DISTENSIBLE NANOSTRUCTURED ELASTIC HYDROGELS FROM AB DIBLOCK AND ABA TRIBLOCK COPOLYMER MELT BLENDS<sup>2</sup>

#### 2.1. Summary

A new structural motif for the generation of highly distensible, highly elastic, nanostructured hydrogels is presented. Based on the swelling of vitrified melt-phase blends of sphere-forming polystyrene-poly(ethylene oxide) diblock and polystyrene-poly(ethylene oxide)-polystyrene triblock copolymers, the equilibrium swelling ratio (3.8 – 36.9 g H<sub>2</sub>O/g polymer) and dynamic elastic modulus ( $G' = 1700 - 160000$  Pa) of these novel hydrogel systems were found to be remarkably tunable through simple manipulation of temperature (10 – 50 °C) and triblock copolymer content (3.3 – 72.0 mol%). Mechanical properties were found to be almost exclusively a function of triblock copolymer content, independent of temperature induced changes in swelling ratio. The resulting hydrogels were highly elastic at all swelling ratios with  $G'/G'' \sim 10^2$  for the range of triblock copolymer concentrations examined. Hydrogel samples exhibited excellent preservation of dry polymer shape upon swelling, with complete recovery of both shape and mechanical performance following repeated compression-decompression cycles.

---

<sup>2</sup> The contents of this dissertation chapter have been adapted by permission of The Royal Society of Chemistry from a manuscript published in *Soft Matter*: Chen Guo and Travis S. Bailey. *Soft Matter*, 2010, **6**, 4807-4818. Chen Guo and Travis S. Bailey developed and designed the experiments. Chen Guo performed the experiments. The manuscript and dissertation chapter were written by Chen Guo with editing by Travis S. Bailey.

## 2.2. Introduction

The development of highly absorbant polymeric hydrogels continues to have significant implications in a range of biomedical, personal hygiene, therapeutic delivery, optical, and dynamic mechanical applications.<sup>1-13</sup> Effective design requires explicit control, not only over mass transfer characteristics, chemical or biocompatibility, and mechanical performance, but equilibrium water content and long term shape behavior, as well. Classical strategies for hydrogel synthesis are largely based on the formation of lightly crosslinked single or double networks of water soluble polymers. For these systems, mass transfer, equilibrium water content, and mechanical properties are a strong function of the crosslink density and largely interdependent. High modulus gels are attainable, but equilibrium water content suffers accordingly. Shape is fixed during the crosslinking event, and is largely permanent over the hydrogel's lifetime. Chemical or biological compatibility is principally related to the polymer selected, and the nature of the crosslinking agent.

A considerable fraction of hydrogel research in the last decade has focused on the development of reversible solution based hydrogels systems, where gelation is triggered by the removal of shear flow fields, or more commonly, by thermal or pH induced hydrophobicity of certain segments of the polymer chain. ABA triblock copolymers of various forms have been employed in many of these systems, with the induced phase separation of the A blocks, coupled by the tethering B mid-blocks, responsible for the percolating networks formed.<sup>14-27</sup> Most of these systems are being studied for their potential as chemical or drug release vehicles, which can be injected in sol form, followed by in situ gelation upon application of the appropriate trigger. Such hydrogel systems are often multicomponent mixtures, in which mass transfer characteristics and mechanical properties can be tuned somewhat independently, through

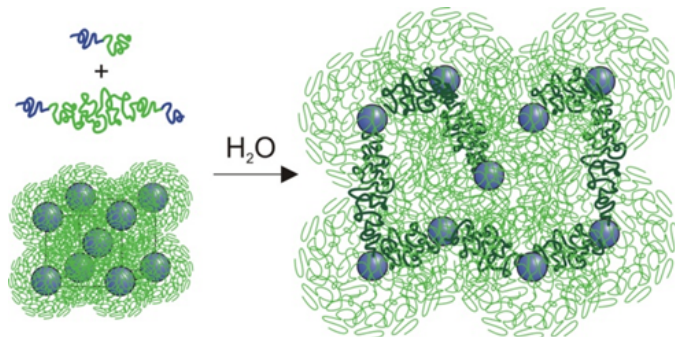


**Figure 2.1. Nanostructured hydrogel formation based on sphere forming AB diblock and ABA triblock copolymer blends. Hydrophilic B blocks (matrix) are selectively solvated, while hydrophobic A blocks (spherical domains) remain vitreous. The ABA triblock copolymer in the blend can span adjacent spherical domains, creating an elastic network at high enough concentrations. Equilibrium swelling dimensions are the product of a balance between osmotic swelling forces produced by the solvent and entropic restoring forces in the tethering mid-block of the ABA triblock copolymer chains (highlighted in bold).**

composition changes in the original sol. Water content is predetermined in the sol and usually far lower than that possible through equilibrium swelling, while shape is predicated on the local environment into which the sol is placed. Shape is therefore reversible, but also susceptible to changes in local conditions over time. Moduli of these injectible hydrogels are typically of the order of 10 – 1000 Pa, limited by the nature of the solution-based reversible gelation mechanism.

Recently, we have been exploring new approaches to hydrogel formation, based on the swelling of vitrified melt-phase blends of sphere-forming AB diblock and ABA triblock copolymers. The original dry polymers are based on selecting AB/ABA blends which adopt the sphere morphology<sup>28, 29</sup> in the melt, and retain that morphology upon cooling to room temperature. The generalized strategy, portrayed pictorially in Figure 2.1, is based on the selection of AB block combinations for which aqueous media selectively solvates the majority component or matrix (B block), while the minority component spherical domains (A block) remain vitrified (not plasticized) in that same media. The added ABA triblock copolymer then acts to tether the spherical domains and physically crosslink the material without disrupting the inherent structural lattice. Typical aggregation numbers for spherical domains are of the order

100 – 300, suggesting that as little as 1 – 3 mol% ABA triblock copolymer should be sufficient to form infinite network gels.<sup>30</sup> The equilibrium dimensions of the swollen hydrogel are expected to be a strong function of the mid-block molecular weight, the bridging to looping ratio of ABA triblock, the temperature dependent solvent-polymer interaction, and the entanglement density created through topological pinning of the tethers at fixed points along the AB domain interfaces. In contrast to the solution-based gels described previously, hydrogel shape under this approach is established during melt processing of the dry polymer, and remains fixed during swelling. However, as the network is the product of physically tethered spherical domains, the materials remain reprocessable, similar to traditional thermoplastic elastomers.

Here, we report the results of our initial investigations of hydrogels formed via this strategy, using a model system based on polystyrene-poly(ethylene oxide) (PS-PEO) diblock and PS-PEO-PS triblock copolymer blends. Within, we examine the unique ability of this simple structural motif to produce highly elastic hydrogels of widely varying equilibrium swelling dimensions and mechanical properties, accessible using only moderate changes in temperature and PS-PEO-PS triblock copolymer concentrations. The high fidelity with which both shape and mechanical performance are preserved is also evaluated.

## **2.3. Experimental**

### **2.3.1 Materials**

Styrene (99%, 4-tert-butylcatechol inhibitor, Aldrich) and ethylene oxide (99.5+%, compressed gas, Aldrich) monomer were each purified by successive distillations (10-20 mTorr) from dried dibutylmagnesium (0.1mmol/g monomer, 1.0 M solution in heptane, Aldrich) before use. Both purified styrene and ethylene oxide monomer were stored in glass burets in the dark, at room temperature (styrene) and 0°C (ethylene oxide), respectively, until use (typically less

than 24 hrs). Argon degassed cyclohexane (CHX) was purified by passing the solvent over activated alumina followed by Q-5-like supported copper catalyst (Glass Contour, proprietary). Argon degassed tetrahydrofuran (THF) was purified by passing the solvent over activated alumina. High-purity argon (99.998%, General Air) was passed through additional oxygen and moisture traps prior to use. All other materials were used as received.

## 2.3.2 Synthesis

### 2.3.2.1 $\omega$ -hydroxy-polystyrene (S-OH).<sup>31</sup>

Purified styrene monomer (99.72 g, 0.957 mol, 20 °C) was added under argon (~3 psig) to a vigorously stirring solution of sec-butyl lithium (10.23 mL, 1.3 M in cyclohexane, Aldrich) and dry, air-free cyclohexane (~ 1 L, 20 °C) in a 2 L reaction vessel. The temperature of the reaction mixture was raised to 40 °C and stirring continued for approximately 8 hours. At this point the reactor pressure was reduced to approximately 1 psig and purified ethylene oxide (5.85 g, 0.133 mol, 0 °C, liquid) was added to the reaction vessel. The reaction was maintained at 40 °C for an additional 24 hours, after which all excess ethylene oxide (toxic!) was purged from the reactor under a constant argon flow. The reaction was terminated by direct addition of methanol (50 ml, degassing unnecessary). The polymer was precipitated in a 1:3 mixture of isopropanol:methanol (5 L total) to give a fluffy white solid. The polymer was dried under vacuum at room temperature over a 48 hr period. Yield 98.1 g, 98+%. SEC (THF, PS stds):  $M_n = 8390 \text{ g mol}^{-1}$ ,  $M_w = 8660 \text{ g mol}^{-1}$ ,  $M_w/M_n = 1.03$ .  $^1\text{H}$  (300 MHz;  $\text{CDCl}_3$ ): 6.20-7.26 (b, - $(\text{C}_6\text{H}_5)$ ), 3.2-3.5 (m,  $-\text{CH}_2\text{OH}$ ), 0.84-2.60 (b,  $-\text{CH}(\text{C}_6\text{H}_5)\text{CH}_2-$ ,  $\text{CH}_3\text{CH}(\text{CH}_2\text{CH}_3)-$ ,  $-\text{CH}_2\text{CH}_2\text{OH}$ ), 0.5-0.78 (m,  $\text{CH}_3\text{CH}(\text{CH}_2\text{CH}_3)-$ ).

### 2.3.2.2 $\omega$ -Hydroxy-polystyrene-*b*-poly(ethylene oxide) (SO).

**S-OH** (2.91 g, 0.347 mmol) was placed into a 2 L reaction vessel (glass coated magnetic stir bar). The reactor was evacuated and backfilled with purified argon (5x) before the addition of approximately 1 L of dry, air-free THF. Concentrated potassium naphthalenide in THF was added to the polymer solution via cannula until a light green color persisted for at least 20 minutes. The temperature of the reaction mixture was raised to 40 °C and purified ethylene oxide monomer (26.9 g, 0.611 mol, 0 °C) was added under argon (~1 psi) with vigorous stirring. Stirring was continued for approximately 48 hours. The reaction was terminated by direct addition of methanol (50 ml, degassing unnecessary). The polymer was precipitated in pentane (~4 L) to give a fluffy white solid. The polymer was dried under vacuum at room temperature over a 48 hr period. Yield 29.+ g, 98+%. SEC (DMF, PEO stds):  $M_w/M_n = 1.05$ .  $M_n = 91450 \text{ g mol}^{-1}$  (calculated using  $^1\text{H NMR}$  and SEC measured **S-OH**  $M_n$ ),  $M_w = 96000 \text{ g mol}^{-1}$  (calculated using SEC measured  $M_w/M_n$ );  $\delta_{\text{H}}$  (300 MHz;  $\text{CDCl}_3$ ): 6.20-7.26 (b,  $-\text{C}_6\text{H}_5$ ), 3.1-4.0 (b,  $-\text{CH}_2\text{CH}_2\text{O}-$ ,  $-\text{CH}(\text{C}_6\text{H}_5)\text{CH}_2\text{CH}_2\text{O}-$ ), 1.0-2.30 (b,  $-\text{CH}_2\text{CH}(\text{C}_6\text{H}_5)-$ ,  $\text{CH}_3\text{CH}(\text{CH}_2\text{CH}_3)-$ ,  $-\text{CH}(\text{C}_6\text{H}_5)\text{CH}_2\text{CH}_2\text{O}-$ ), 0.5-0.78 (m,  $\text{CH}_3\text{CH}(\text{CH}_2\text{CH}_3)-$ ).

### 2.3.2.3 Polystyrene-*b*-poly(ethylene oxide)-*b*-polystyrene (SOS-72.0).

Dibromoxylene (DBX) (0.283g, 1.072 mmol) was dissolved in dry, air-free THF (78.83 mL) to produce a master solution (0.0136 M). SO diblock copolymer (4.977 g, 0.0544 mmol) was added to 300 mL flask, which was then evacuated and backfilled with Ar (5x). 150 mL of dry, air-free THF was then added to dissolve the polymer. Concentrated potassium naphthalenide in THF was added to the polymer solution via cannula until a light green color persisted for at least 20 minutes. A catalytic amount of  $\text{CsI}^{31}$  was added to the reaction under Ar prior to the addition of 5 mL (0.068 mmol DBX) of the master solution via syringe pump (0.5

mL hr<sup>-1</sup>). The reaction was allowed to stir overnight and the crude product was precipitated into pentane twice to remove excess DBX. The solid was collected via vacuum filtration and dried under vacuum at room temperature overnight to give the final (very) pale yellow solid. Yield 4.9+ g, 98+%. SEC (DMF, PEO stds): 83.7 wt%, 72.0 mol% triblock copolymer.  $M_{n,SOS} = 183000 \text{ g mol}^{-1}$ , (calculated using SO  $M_n$ );  $\delta_H$  (300 MHz; CDCl<sub>3</sub>): 6.20-7.26 (b, -C<sub>6</sub>H<sub>5</sub>, -OCH<sub>2</sub>(C<sub>6</sub>H<sub>4</sub>)CH<sub>2</sub>O-), 4.55 (s, -OCH<sub>2</sub>(C<sub>6</sub>H<sub>4</sub>)CH<sub>2</sub>O-), 3.1-4.0 (b, -CH<sub>2</sub>CH<sub>2</sub>O-, -CH(C<sub>6</sub>H<sub>5</sub>)CH<sub>2</sub>CH<sub>2</sub>O-), 1.0-2.30 (b, -CH<sub>2</sub>CH(C<sub>6</sub>H<sub>5</sub>)-, CH<sub>3</sub>CH(CH<sub>2</sub>CH<sub>3</sub>)-, -CH(C<sub>6</sub>H<sub>5</sub>)CH<sub>2</sub>CH<sub>2</sub>O-), 0.5-0.78 (m, CH<sub>3</sub>CH(CH<sub>2</sub>CH<sub>3</sub>)-).

### 2.3.3 Hydrogel Fabrication

#### 2.3.3.1 SO/SOS blends.

With the exception of SOS-72.0, each SOS- $X_i$  sample was produced by solution blending (0.2 g total polymer/mL CHCl<sub>3</sub>) the appropriate amounts of SO and SOS-72.0 to reach the specified molar concentration  $X_i$  of triblock copolymer. Solutions were made in small glass vials and frozen using an ethanol/liquid N<sub>2</sub> slush bath, then placed in vacuo (10 – 20 mTorr) at room temperature for at least 24 hours. Removal of solvent was confirmed by <sup>1</sup>H NMR.

#### 2.3.3.2 Dry polymer disk formation.

8 mm diameter x 0.9 mm thick disks were melt pressed (Carver Press) directly from powders using a stainless steel cutout sandwiched between teflon covered kapton sheets. Disks were held under a constant pressure of 500 psi at 150 °C for approximately 5 minutes, before being removed from the press and cooled (unassisted) to room temperature. The formed polymer was easily removed from the stainless steel cutout to give homogeneous, slightly

opaque (due to PEO crystallinity), disks. Disk dimensions (diameter and thickness) and dry weight were recorded for subsequent swelling experiments.

### **2.3.3.3 Hydrogel swelling.**

Dry polymer disks were placed into 125 ml jars filled with DI water for at least 24 hours to ensure equilibrium swelling conditions were reached. The filled jars were then submerged in a large thermostated water bath. Previously swollen hydrogels were typically given at least 8 hours to adapt to any 10 °C step change in bath temperature. Swelling kinetics were observed to be a strong function of hydrogel dimensions, as expected with mass transfer limited diffusion. For example, 30 µm thick films (not reported here) were found to adopt their equilibrium dimensions within several minutes.

## **2.3.4 Characterization**

### **2.3.4.1 Molecular Characterization of polymers and blends.**

<sup>1</sup>H NMR spectra were collected at room temperature in CDCl<sub>3</sub> on either a Varian Inova 300 MHz or Varian Inova 400 MHz Spectrometer (n = 32, delay = 30 s). Size exclusion chromatography (SEC) was performed on a Viscotek GPC-Max chromatography system fitted with three 7.5x340 mm Polypore™ (Polymer Laboratories) columns in series, an Alltech external column oven, and a Viscotek differential refractive index (RI) detector. **S-OH** molecular weight characterization was performed using a THF (40 °C) mobile phase (1 mL min<sup>-1</sup>) with PS standards (Polymer Laboratories). Characterization of all other samples (**SO**, **SOS-X<sub>i</sub>**) was performed using a DMF (55 °C) mobile phase (1 mL min<sup>-1</sup>) with PEO standards (Polymer Laboratories). Note: The **S-OH** SEC data portrayed in Figure 2.2 was run in DMF, but

for comparison purposes only; DMF is a poor eluent for PS and unsuitable for characterization of molecular characteristics.

#### **2.3.4.2 Melt-State Rheology.**

Melt-state rheological analysis of the **SO** and **SOS-72.0** samples was performed using a TA Instruments ARES rheometer using a 8 mm parallel plate geometry. Dynamic temperature ramps (oscillatory shear) were performed for each sample using a 2% shear strain (verified in the linear viscoelastic region) at a frequency of 1 rad s<sup>-1</sup>. All heating and cooling was performed using the TA Instruments convection oven under N<sub>2</sub> gas at a ramp rate of 1 °C min<sup>-1</sup>. Data can be found in the appendix.

#### **2.3.4.3 Small angle X-ray scattering (SAXS).**

Scattering data was collected on a Rigaku S-Max 3000 High Brilliance 3 Pinhole SAXS System outfitted with a MicroMax-007HFM Rotating Anode (CuK $\alpha$ ), Confocal Max-Flux™ Optic, Gabriel Multiwire Area Detector, and a Linkham thermal stage. Dry polymer sample disks were pressed as described above. Samples were mounted without the use of kapton windows (traditionally used) to avoid the associated additional background scattering. Samples were exposed under vacuum (10 mTorr) for 120 min at 100 °C.

#### **2.3.4.4 Swelling Analysis.**

Swollen hydrogels were removed from DI water and placed on a teflon surface. Excess water was blotted from the hydrogel surface, and the weight determined. The diameter of the hydrogel was then measured with vernier calipers at six unique positions. The hydrogel was then re-weighed once again to verify no significant water loss occurred between weighings. This (roughly 3 minute) procedure was repeated for each hydrogel at 10 °C, 20 °C, 30 °C, 40 °C and

50 °C. No significant water loss was detected for any of the samples, suggesting changes in equilibrium water content due to thermal drift during measurement were negligible. For photographic purposes only, very small quantities of water soluble dyes were added to the DI water solutions (2-3 drops/125 ml DI water) to provide contrast. The color key adopted can be found in Table 2.2. The addition of the dyes did not correlate to any measurable difference in swelling properties. All hydrogels were otherwise translucent and virtually isorefractive with water.

#### **2.3.4.5 Hydrogel Rheology and Unconfined Compression.**

Both rheological and unconfined compression tests were performed using a TA Instruments ARES rheometer using a custom recirculating bath fixture in which an infinite lower plate (50 mm stainless steel) forms the bottom of an integrated glass cup. Temperature at the lower plate (or of solution in the cup) can be controlled via recirculating fluid passing through the base of the mounted fixture. Hydrogel samples were taken directly from their jars in the thermostated bath and placed onto the lower plate held at an identical temperature. The swollen hydrogels were centered between the lower infinite plate and a 25 mm parallel upper plate and excess water was blotted away. Dynamic frequency sweeps (oscillatory shear) were performed for each sample using a 0.4 - 0.5% shear strain (verified in the linear viscoelastic region) over a frequency range of 0.1 to 10 rad s<sup>-1</sup>. Slip was eliminated by placing each sample under a fixed 10% compressive strain (compression normal to the disk face) throughout the duration of the experiment. Unconfined compression experiments were performed similarly, but using an 8 mm upper plate. Compression normal to the disk face was carried out at strain rate of 5% min<sup>-1</sup>. Compression-decompression cycles were also performed at 5% min<sup>-1</sup>. In all cases, the unstrained

hydrogel diameter exceeded 8 mm, and thus stress values reported are based on the fixed upper plate dimensions.

## 2.4. Results and discussion

### 2.4.1 Material Synthesis

The anionic synthesis of both the **S-OH** precursor and the **SO** diblock copolymer were carried out using standard synthetic protocols which have been previously reported by several groups.<sup>32, 33</sup> Importantly, both the addition of the hydroxyl group at the PS terminus and its subsequent reinitiation are quantitative, leaving no residual homopolymer in the **SO** sample (Figure 2.2). The targeted composition and overall molecular weight of the **SO** diblock copolymer represent a compromise among several important design criteria. The formation of the sphere morphology requires compositionally asymmetric molecules, with the volume fractions of the minority component ( $f_{PS}$ ) in the 0.09 – 0.13 range.<sup>34, 35</sup> Highly asymmetric block copolymers require larger molecular weights to induce phase separation in the melt state, particularly for systems with only moderate Flory interaction parameters ( $\chi$ ), such as the PS/PEO system studied here. Reinforcing this need for larger molecular weights is the criteria that the PS domains must remain glassy under the expected range of hydrogel use. The PS bulk glass transition is a strong function of molecular weight below about 10 kDa.<sup>36, 37</sup> Unfortunately, larger molecular weight block copolymer systems,<sup>38-41</sup> and especially those in the spherical domain region of the phase diagram,<sup>42-44</sup> have a strong kinetic resistance to forming phase separated systems with long range periodic order. The targeted molecular weight (8390 g mol<sup>-1</sup>) of the **S-OH** precursor (which corresponds to an overall **SO** diblock molecular weight of 91450 g mol<sup>-1</sup> at  $f_{PS} = 0.10$ ) ultimately represents a compromise between achieving a PS glass transition high enough to ensure preservation of the tethered spherical network upon swelling, while

simultaneously minimizing the kinetic resistance to ordering prevalent at high molecular weights.

Differential scanning calorimetry (DSC) of the bulk **S-OH** sample shows a broad glass transition at approximately 80 °C (Appendix), consistent with the expected values reported for PS at this molecular weight.<sup>36, 37</sup> However, we were unable to discern the presence of a PS glass transition in the **SO** sample (Appendix), for which the thermal response is dominated by the melting/crystallization transition of the PEO matrix ( $65 \pm 4$  °C, heating). Since the hydrogels formed show excellent preservation of shape and high levels of elasticity (vide infra), it is probable that the limited PS content of the samples, combined with domain aggregation numbers on the order of only several hundred chains, makes observation of this transition difficult at our resolution limits (Table 2.1). The hydrogels do become irreversibly deformable around 60 – 70 °C, suggesting that the PS domains are indeed softening in this temperature range.

Exploration of various synthetic strategies for incorporating PEO as the mid-block between two PS end-blocks led us to ultimately adopt a coupling approach using dibromoxylene (DBX). The molecular weight of the PEO mid-block required to reach an overall PS volume fraction favoring the sphere morphology ( $f_{PS} < \sim 0.13$ ) made addition of a terminal PS block to a PS-PEO diblock by various controlled radical polymerization techniques difficult to control and characterize. The DBX coupling approach has been used to produce decent coupling efficiencies in other polymer systems (80 – 95 wt%),<sup>31, 46, 47</sup> which was sufficient for our investigations concentrating on the low end of the triblock copolymer concentration spectrum. Importantly, the net result of non-quantitative coupling is a blend of SO diblock and SOS triblock copolymer; i.e., the remaining uncoupled diblock copolymer in the sample is simply **SO** diblock copolymer, the same diblock copolymer subsequently used in the blends. All experiments reported here are

based on the exclusive use of a triblock copolymer sample produced from a single reaction with a coupling efficiency of 83.7%. This corresponds to a molar triblock copolymer concentration of 72.0% (**SOS-72.0**), and sets the maximum triblock copolymer concentration available in the blends. Fractionation to obtain the pure triblock copolymer was avoided due to the significant material losses associated with the equilibrium based separation technique. The determination of coupling efficiency is discussed in the sections below. A summary of the key characterization data for these samples can be found in Table 2.1.

#### **2.4.2 SO and SOS-72.0 Melt-State Morphological Characterization**

Both rheology (Appendix) and SAXS data (Figure 2.4) confirmed the presence of an ordered-state morphology in both the **SO** and **SOS-72.0** samples, with elastic moduli ( $G'$ ) in the  $10^3$ - $10^6$  Pa range, and principal scattering wave vectors ( $q^*$ ) nearly coincident at  $0.02107 \text{ \AA}^{-1}$  and  $0.02083 \text{ \AA}^{-1}$  (100 °C), respectively. The similarities in the scattering indicate the basic morphological characteristics are similar between the two samples, and that the presence of more or less triblock copolymer does not dramatically change the morphology of the system.

Based on the wealth of documented diblock copolymer phase behavior in this compositional region ( $f_{\text{PS}} < \sim 0.13$ ),<sup>34, 35, 42, 43</sup> the ordered-state morphology expected is one of spherical (micelle-like) aggregates of PS chains surrounded by PEO coronas (Figure 2.1). In low molecular weight systems, these spherical domains have been found to order into a highly periodic bcc lattice, like that portrayed in Figure 2.1. However, higher molecular weight systems or those in the vicinity of the order-disorder transition (to an isotropic phase) are commonly characterized by diminished long range order, with a more “liquid-like” packing of spherical domains. These phenomena are often associated with limited chain diffusion and mobility; a

**Table 2.1. Chemical and Melt-State Morphological Characterization Data**

Sample	$M_n$ (g mol <sup>-1</sup> )	$M_w$ (g mol <sup>-1</sup> )	$M_w/M_n$	$f_{PS}^d$	bcc Model			Percus-Yevick Hard Sphere Model						
					$a_{bcc}^f$ (nm)	$R_{PS}^f$ (nm)	$\theta_{PS}^f$	$R_c^g$ (nm)	$\sigma_c^g$ (nm)	$\xi^g$ (nm)	$R_{hs}^g$ (nm)	$\phi_{hs}^g$	$\phi_c^h$	$\theta_{PS}^i$
S-OH	8390 <sup>a</sup>	8660 <sup>a</sup>	1.03 <sup>a</sup>	0.995	-	-	-	-	-	-	-	-	-	-
SO	91450 <sup>b</sup>	96000 <sup>c</sup>	1.05 <sup>c</sup>	0.100	42.2	9.6	261	9.2	0.94	0.15	16.4	0.514	0.090	228
SOS-72.0	183000 <sup>c</sup>	-	bimodal	0.100	42.7	9.7	270	8.9	0.41	0.43	17.2	0.513	0.070	209

<sup>a</sup> determined from SEC (THF, PS stds).

<sup>b</sup> calculated from <sup>1</sup>H NMR in combination  $M_{n,S-OH}$ .

<sup>c</sup> determined from SEC (DMF, PEO stds).

<sup>d</sup> volume fraction of PS, based on <sup>1</sup>H NMR and nominal densities at 140 °C ( $\rho_{PS}=0.969$ ,  $\rho_{PEO}=1.064$  g cm<sup>-3</sup>).<sup>45</sup>

<sup>e</sup> nominal value for the coupled triblock component of the blend only.

<sup>f</sup> calculated unit cell lattice constant,  $a_{bcc}$ , mean PS sphere radius,  $R_{PS}$ , and mean aggregation number (i.e., PS chains per sphere),  $\theta_{PS}$ , based on SAXS data on dry melts, assuming a bcc arrangement of spheres with  $\mathbf{q}^* = \mathbf{q}_{110}$  (100 °C;  $\rho_{PS}=0.969$  g cm<sup>-3</sup>).

<sup>g</sup> optimized scattering fit parameters using the PY model. From left to right, micelle core radius,  $R_c$ , standard deviation of the micelle core radius,  $\sigma_c$ , diffuse sphere boundary parameter,  $\xi$ , apparent hard sphere radius,  $R_{hs}$ , and hard sphere volume fraction,  $\phi_{hs}$ .

<sup>h</sup> micelle core overall volume fraction,  $\phi_c=(R_c/R_{hs})^3\phi_{hs}$ , based on the PY model fits.

<sup>i</sup> mean aggregation number (i.e., PS chains per sphere),  $\theta_{PS}$ , based on the PY model fits.

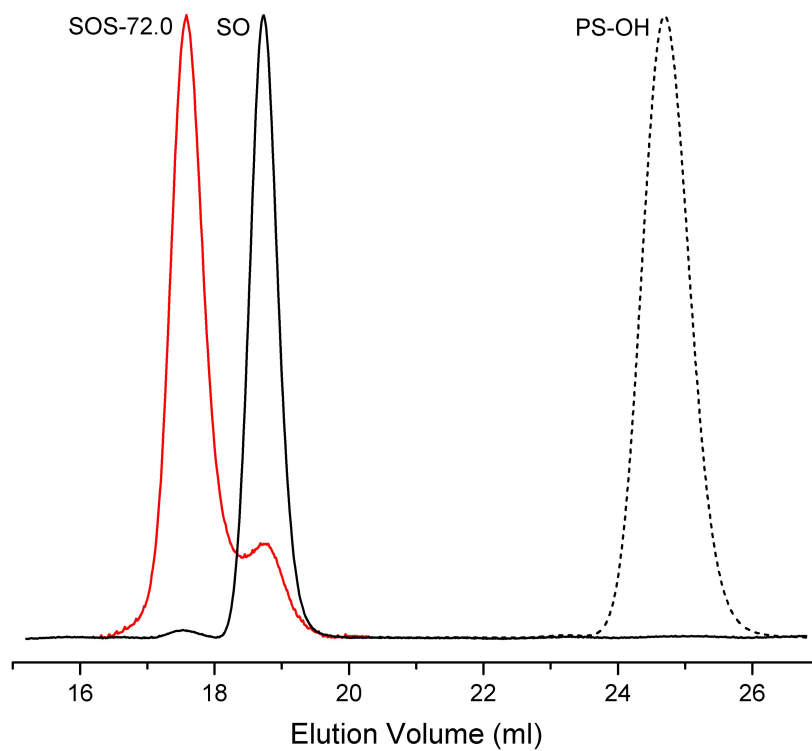
**Table 2.2. Blend Characterization Data**

Sample	$i$	$x_i^a$	$w_i^b$	color <sup>c</sup>
SOS-72.0	0	0.720	0.837	Red
SOS-16.2	1	0.162	0.279	Orange
SOS-11.7	2	0.117	0.209	Yellow
SOS-7.5	3	0.075	0.140	Green
SOS-4.9	4	0.049	0.093	Blue
SOS-3.3	5	0.033	0.064	Violet

<sup>a</sup> mol fraction of SOS triblock copolymer in each blend, determined from calculated  $w_i$  values.

<sup>b</sup> weight fraction of SOS triblock copolymer in each blend.  $w_0$  determined by linear regression (vide infra);  $w_1$ - $w_5$  calculated based on  $w_0$ .

<sup>c</sup> produced using water soluble dyes, added for photographic purposes only.

**Figure 2.2. SEC chromatograms for S-OH, SO, and SOS-72.0 (DMF, 55 °C).**

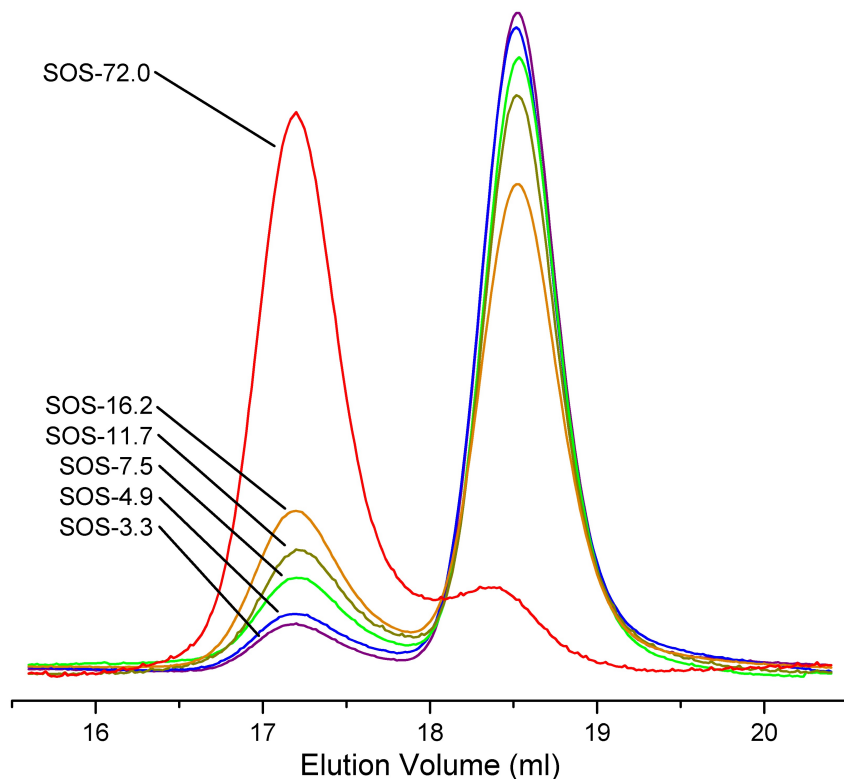


**Figure 2.3.** SEC chromatograms of dry polymer blends from which  $w_0$  was determined. Combined peak areas are normalized to the same total sample mass. Left and right peak positions correspond to the elution of SOS triblock and SO diblock copolymer in each blend, respectively.

product of the isolated nature of the spherical domains in the former,<sup>42-44</sup> and significant entanglements and long relaxation times in the latter.<sup>38</sup> In fact, the transition from a highly ordered lattice to one with liquid-like disorder has been studied in detail by several groups using SAXS as the primary characterization tool.<sup>44, 48-53</sup> Comparison of the **SO** and **SOS-72.0** data presented in Figure 2.3 with SAXS data from other confirmed sphere-forming block copolymer systems reveals that the scattering profiles in Figure 2.3 are prototypical; the emergence of the prominent (bragg) scattering peak at low  $q$  is indicative of some lattice-like (bcc-like) character on the local scale, but the prominent shoulder (and lack of higher order bragg reflections) at the

same time indicates significant disorder, or liquid-like packing, when longer range organization is considered.

Rudimentary characterization of the morphological characteristics of these systems can be achieved by simply assuming the local bcc lattice structure is representative of the sample. In this case, the principal scattering wave vector is taken to be the first allowed reflection of the  $Im\bar{3}m$  (bcc) space group, that is  $q_{110}$ . From there, geometrical arguments based on the bcc lattice, combined with the volume fraction of PS in the **SO** and **SOS-72.0** samples ( $f_{PS} = 0.10$ ), leads to calculated values for PS domain radii ( $R_{PS}$ ) of 9.6 nm and 9.7 nm, respectively, and a bcc unit cell lattice constant ( $a_{bcc}$ ) of 42.2 nm and 42.7 nm, respectively. Notably, these values correspond to PS chain aggregation numbers ( $\theta$ ) in each spherical domain of about 261 and 270 chains, respectively. The details of these calculations can be found in the appendix.

A far more rigorous analysis of the morphological characteristics of sphere forming diblock copolymers has been accomplished quite successfully using model fits to SAXS data by several groups, including Kinning and Thomas,<sup>54</sup> Schwab and Stühn,<sup>52, 53</sup> and more recently Lodge et al.<sup>44</sup> The scattering intensity for sphere forming systems can be expressed as a mathematical function which is proportional to the product of the form factor  $P(q)$ , which describes the intraparticle correlations, and the structure factor,  $S(q)$ , which describes the interparticle correlations. Adopting an approach similar to that used by these three groups, we were able to model the scattering data from these two samples using  $P(q)$  for polydisperse solid spheres, coupled with  $S(q)$  given by the Percus-Yevick (PY) model<sup>55</sup> for hard sphere liquids. Lodge et al.<sup>44</sup> give an excellent description of this approach, and the interested reader should consult this reference for the additional details. Here we present only the basic functions and the critical parameters used in the model.

The model is based on the use of the form factor for monodisperse hard spheres,

$$P(q, R) = \left( \frac{3 \cdot (\sin(qR) - qR \cos(qR))}{(qR)^3} \right)^2 \quad (1)$$

where  $R$  is taken to be the radius of the PS domain core. This expression is modified to account for (a) polydispersity in the spherical PS core by convolution with a Gaussian distribution of  $R$  characterized by a standard deviation  $\sigma_c$ , and (b) the diffuse nature of the actual interface between PS and PEO domains through the introduction of a diffuse sphere boundary parameter  $\xi$ . The result is the following modified form factor,

$$P(q, R_c, \sigma_c, \xi) = \frac{e^{-(2\pi\xi q)^2}}{\sigma_c \sqrt{2\pi}} \int_0^\infty e^{-\frac{1}{2} \left( \frac{R-R_c}{\sigma_c} \right)^2} P(q, R) dR \quad (2)$$

where  $R_c$  is mean PS core radius. The inter-micelle correlations can be represented by a hard sphere potential in the manner first described by Ornstein and Zernike,<sup>56</sup> for which Percus and Yevick<sup>55</sup> later developed an approximate analytical expression. Solution leads to the following representation of  $S(q)$ ,

$$S(q, R_{hs}, \phi_{hs}) = \frac{1}{1 + \frac{24\phi_{hs} G(q, R_{hs}, \phi_{hs})}{2qR_{hs}}} \quad (3)$$

In this expression,  $G(q, R_{hs}, \phi_{hs})$  is a nonlinear algebraic function which depends on the apparent hard sphere radius,  $R_{hs}$ , and hard sphere volume fraction,  $\phi_{hs}$ . The full expression is provided in the appendix. In this description, the hard sphere radius corresponds to the radius over which the micelle acts as a hard sphere relative to other micelles, and therefore extends beyond the PS core to include a significant fraction of the dense PEO corona. The overall volume fraction of the sample occupied by these hard sphere constructs is then given by  $\phi_{hs}$ . Finally, the model can be smeared to reflect the resolution limits of the SAXS instrumentation itself, which can be

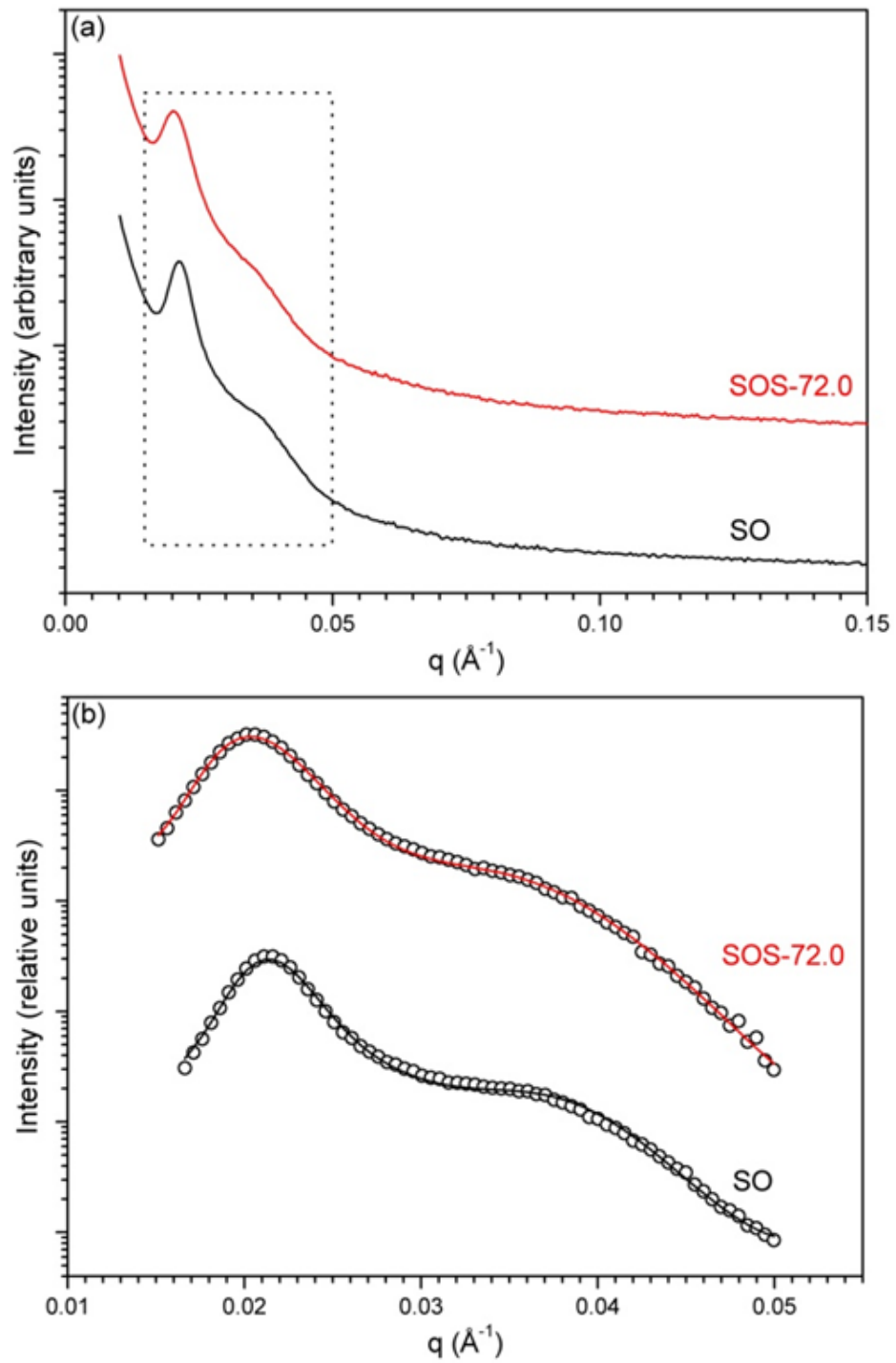


Figure 2.4. (a) SAXS data (as collected) for melts (100 °C) of SO and SOS-72.0 samples. (b) background subtracted SAXS data for SO and SOS-72.0 overlaid with nonlinear least squares fits to the Percus-Yevick hard sphere model for systems with liquid-like disorder.

approximated using a Gaussian form of the instrument resolution function with a standard deviation  $\sigma_q$ .<sup>57</sup> The final scattering intensity can then be expressed as a function of  $q$  and the described five parameters,

$$I(q_0, R_c, \sigma_c, \xi, R_{hs}, \phi_{hs}) \propto \frac{1}{\sqrt{2\pi}\sigma_q} \int P(q, R_c, \sigma_c, \xi) \cdot S(q, R_{hs}, \phi_{hs}) \cdot e^{-\frac{1}{2}\left(\frac{q-q_0}{\sigma_q}\right)^2} dq \quad (4)$$

For these analyses, the variance of the instrument resolution was estimated as  $\sigma_q^2(\text{\AA}^{-2}) = 0.0028q^2$ . The values of each of the described physical parameters which produce the optimum nonlinear least squares fit of the scattering data to the PY model are given in Table 1. The background corrected scattering data and PY model fits are given in Figure 2.3b for both the **SO** and **SOS-72.0** samples. Note that the fits were performed on the regions of the data containing significant structural information, namely,  $0.015 \text{\AA}^{-1} < q < 0.05 \text{\AA}^{-1}$ . Beyond  $q = 0.05 \text{\AA}^{-1}$ , the both samples were dominated by background scattering and accurate extraction of additional structural information was not possible.

Fits of the **SO** and **SOS-72.0** scattering data to the PY model are consistent with PS core domains  $R_c$  of 9.2 nm and 8.9 nm, respectively. This is only slightly smaller (of order 5 -10%) than the corresponding values of  $R_{PS}$  (9.6 nm and 9.7 nm, respectively) estimated using the bcc lattice as an approximate model. Our bcc approximation inherently overestimates the radius because it assumes all PS chains are contained within spherical domains. Previous investigations of other sphere-forming diblock copolymer systems have suggested that a small fraction of block copolymer chains exist as free chains within the surrounding matrix,<sup>44, 49</sup> and therefore do not contribute to the core domain size. The PY model is able to capture that characteristic as the value of  $R_c$  is influenced not only on the position of the principal peak (as is the case in the bcc approximation) but on the relative position of the higher  $q$  shoulder as well. Notably, the

difference in core domain size implies smaller chain aggregation numbers when compared with that expected from the bcc approximation; however the values remain on the order of 200+ chains (see Table 2.1). The consequence of such high aggregation numbers on the amount of SOS triblock copolymer required for gel formation is discussed in more detail below.

The existence of free chains in the matrix, reducing the expected core size by a small amount, is also suggested if one compares the volume fraction of all PS cores in the sample,  $\phi_c$ , with the actual volume fraction of PS in the sample,  $f_{PS}$ . The former can be calculated from the PY fitting parameters as  $\phi_c = (R_c / R_{hs})^3 \phi_{hs}$ , and gives  $\phi_c$  values for the **SO** and **SOS-72.0** samples of 0.09 and 0.07, respectively. In agreement with the previous observation, these values are, in fact, also slightly smaller than the value of 0.10 anticipated if all PS chains contributed to the core. Notably, these trends are very similar to those observed by Lodge et al.<sup>44</sup> in sphere-forming systems of poly(ethylenepropylene-*b*-dimethylsiloxane), for which the PY model also suggested core volume fractions several hundredths lower than expected if all the PDMS was located within the spherical cores. Comparison of these two values of  $\phi_c$  also seems to suggest that the higher concentration of SOS triblock copolymer tends to produce more free chains, or at least chain ends, isolated in the matrix. Of course, a more elaborate study would be needed to confirm this preliminary observation, but we speculate that placing both ends of the SOS triblock copolymer into nonuniformly distributed spherical domains presents a unique challenge, relative to diblock copolymer alone.

This seems to also be reflected in the PS/PEO interfacial width in the two systems, which can be estimated from the diffuse sphere boundary parameter as  $(2\pi)^{1/2} \xi$ .<sup>58</sup> Calculated values for the **SO** and **SOS-72.0** samples gives 0.4 and 1.1 nm, respectively. Although the

accuracy of these predicted values has been questioned,<sup>44</sup> the trend seems to suggest that, at higher concentrations of SOS triblock copolymer, the thermodynamic compromise for wanting to placing both ends of each triblock copolymer molecule into the core of a spherical domain is to contend with greater interfacial contact between the two dislike polymer segments.

Finally, the distribution of core domain sizes appears to be quite narrow, with  $\sigma_c$  values on the order of 10 and 5%, respectively for the **SO** and **SOS-72.0** samples. These values are also consistent with those observed in other sphere-forming polymer systems, including the poly(ethylenepropylene-*b*-dimethylsiloxane) systems mentioned previously.<sup>44</sup> Interestingly, while the values of  $\sigma_c$  suggest the variation in core size is much smaller in the **SOS-72.0** system, this is likely correlated directly to the broader interfacial width also associated with this higher SOS triblock containing sample.

### 2.4.3 SOS- $X_i$ Blend Characterization

The series of **SOS- $X_i$**  blends were generated using simple solution blending in chloroform, with  $X_i$  representing the molar concentration of triblock in sample  $i$ .  $X_i$  was determined using the relative weights of **SO** and **SOS-72.0** used to make the blend. The coupling efficiency of the **SOS-72.0** sample (referred to as SOS- $X_0$  below) was determined using linear least squares regression of the following equation:

$$w_{i,SEC} = w_0 \cdot \left( \frac{m_{SOS-X_0}}{m_{SOS-X_0} + m_{SO}} \right) \quad (5)$$

Here,  $w_{i,SEC}$  represents the weight fraction of triblock copolymer in blend sample  $i$ , determined by integrating the relative areas under the SEC chromatogram, and the term in parentheses represents the weight fraction of the SOS- $X_0$  sample added to the blend. By plotting the pairs of these values for each blend in Table 2.2, the mass fraction of triblock copolymer in

SOS- $X_0$ ,  $w_0$ , could be obtained from the slope of the regressed line. This analysis (appendix) gave  $w_0 = 0.837$ , which equates to a molar concentration of triblock copolymer,  $X_0 = 72.0$  mol%. The determination of  $w_0$  by linear regression helps to minimize error associated with integrating relative chromatogram peak intensities in cases (such as those found here) where peaks are both partially overlapping and of significantly different intensities (Figure 2.4). A summary of the key characterization data for the blend samples can be found in Table 2.2.

#### 2.4.4 Equilibrium Swelling Behavior

For each of the six hydrogel blends, the equilibrium water content (by mass) and overall mean diameter (calipers) were measured over ten degree increments from 10 to 50 °C. The swelling ratios (g H<sub>2</sub>O/g dry polymer) as a function of the molar triblock copolymer concentration are plotted in Figure 2.5. Photographic images of each of the hydrogels at 10, 30, and 50 °C, showing the swollen dimensions relative to the native dry polymer are given in Figure 2.6. Finally, A comparison of the actual mass of water absorbed and that predicted using the a single linear expansion coefficient obtained from the mean diameter (and an assumed a density of 1.0 g cm<sup>-3</sup>) are shown in Figure 2.7. This last plot gives a sense of the degree to which the swelling is isotropic, with the data following the 45 degree line quite closely with the exception of the 3.3 mol% samples. Error in these highly swollen samples is likely a product of the inherent error associated with the two measurement techniques; that is, the subjective blotting of excess water from the hydrogel prior to weighing, and the difficulty of obtaining accurate diameter measurements on soft, easily deformable solids. It appears the latter may be the more significant issue. Notably, the assumption of a nominal density of 1.0 g cm<sup>-3</sup> for the overall

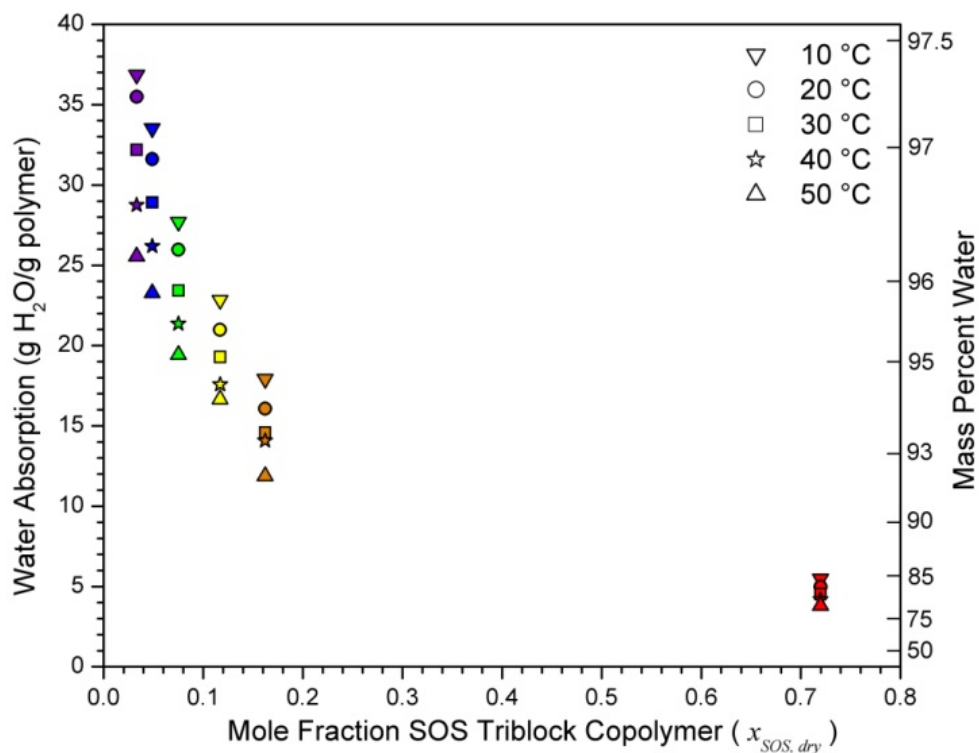


Figure 2.5. Equilibrium water absorption (left axis) and mass percent water (right axis) for each blend sample at temperatures between 10 °C and 50 °C. All values determined gravimetrically.

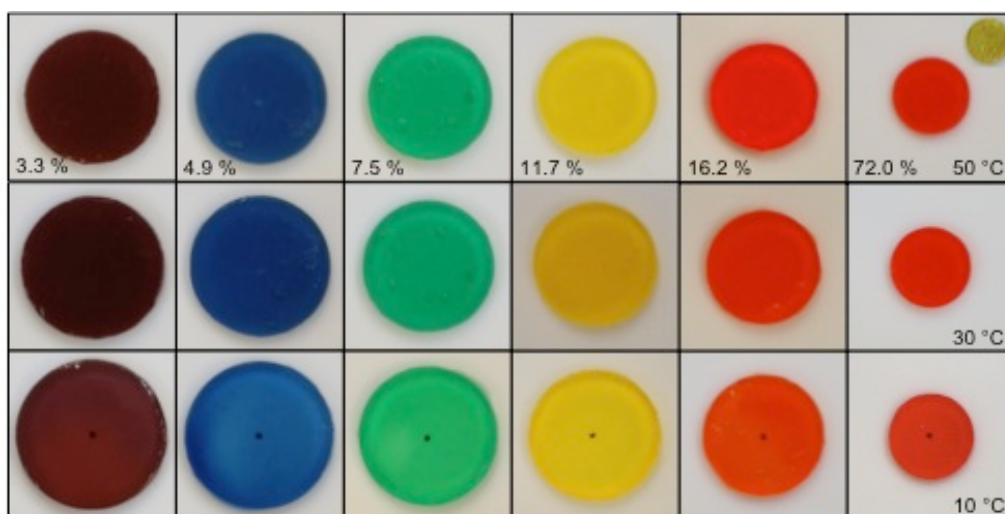


Figure 2.6. Equilibrium swollen hydrogels for each of the six SO/SOS blend concentrations, photographed at 10 °C, 30 °C, and 50 °C. Image frames measure 40 x 40 mm. The original dry polymer dry disk (8 mm diameter) is included in the upper right corner of the figure for reference.

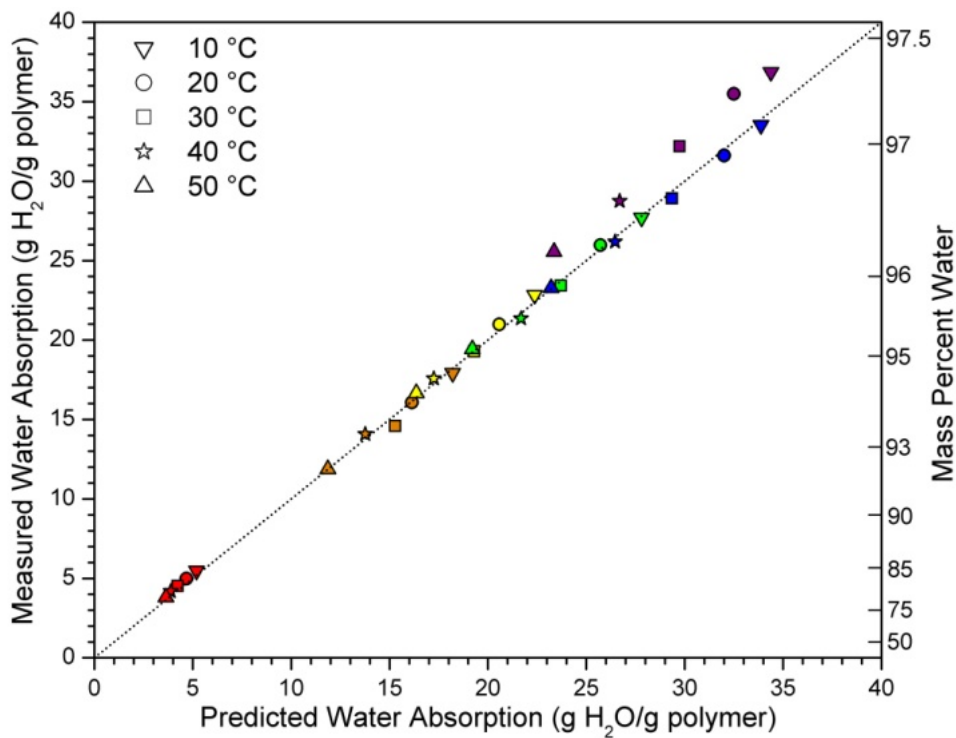


Figure 2.7. Comparison between the gravimetrically measured water uptake and the mass predicted using the linear expansion ratio obtained from the mean diameter of the hydrogel. The latter calculation assumes isotropic swelling and a nominal hydrogel density of  $1.0 \text{ g cm}^{-3}$ . The 45 degree line demarcates the expected equivalence of these values if isotropic swelling predominates.

hydrogel appears to be justified, at least for this coarse comparison made namely to verify the isotropic nature of the swelling.

The swelling results themselves are quite remarkable, and show the influence of triblock copolymer concentration and temperature to be extremely influential on the ability of the hydrogel to absorb water. The measured thermal response of the hydrogel is expected, based on the reduced solubility of the PEO matrix in water at higher temperatures. The equilibrium swelling dimensions are a simple balance between the osmotic driving force to dilute the hydrogel interior, and the entropic restoring force imparted by the tethering PEO midblocks which must stretch to accommodate more water. At higher temperatures the osmotic driving force

is diminished and a contraction in hydrogel dimensions results. On average, the hydrogels suffered about a one third reduction in volume and in equilibrium water content over the 40 °C increase in temperature from 10 to 50 °C.

The more significant impact on water uptake, by far, is associated with the triblock copolymer concentration, which is responsible for a 500+% increase in equilibrium water content when reduced from 72.0 to 3.3 mol%. It is important to consider that there is a minimum triblock copolymer concentration that will yield an infinite gel network, and that amount is in the vicinity of several tethering triblocks per sphere. This corresponds to molar ratio of triblock in the range of 1 mol% for this specific system which involves PS chain aggregation numbers in the 200+ range in each spherical domain. Thus, as we approach the gelation limit, the ability of the spherical domains to expand from one another increases dramatically. In future work we hope to be able to identify this gel point transition precisely, but note that at this stage the softness of the samples in this region has made handling materials difficult below the 2 - 3% range. We are also in the process of developing a model to help predict this transition computationally, and note that it is not just a function of the amount of triblock copolymer, but also of the inherent bridging to looping ratio adopted by the collection of triblock copolymer chains, not to mention the apparent presence of free chains and chain ends in the system suggested by the PY model fits.

It is clear the addition of triblock copolymer increases the average number of tethers between spheres, but it also increases the number of topologically trapped entanglements produced from the interdigitation of bridging tethers spanning locally adjacent sphere pairs. In the original melt, when chains are virtually unstretched, these topological constraints have little influence on the overall average distance between spheres (Table 1). However, as water is imbibed by the sample and spherical domains begin to disperse, these topologically trapped

entanglements have a striking influence on the ability of the spheres to be displaced from their original positions within the hydrogel. Interestingly, while the number of these topological entanglements present changes with the amount of tethering triblock copolymer, the number of principal junction points (spheres) per unit dry polymer volume remains constant. At high triblock copolymer content, topologically trapped loop-bridge, and loop-loop entanglements must also be playing a significant factor in the observed swelling behavior (*vide infra*). The potential variation in the number of free chains and chain ends as a function of SOS concentration as suggested by the PY model fits may also be a factor.

#### **2.4.5 Mechanical Performance**

The dynamic mechanical response of each of the hydrogel blends at 20 °C, under oscillatory shear is given in Figure 2.8a. The data portray both the elastic ( $G'$ ) and loss ( $G''$ ) moduli of each of the hydrogels as a function of angular frequency under 0.4 - 0.5% strain. Both the strain magnitude and range of frequencies examined were selected to ensure measurement in the linear viscoelastic region, and avoid slip at the hydrogel fixture interface (typical at higher frequencies). The observed plateau behavior in  $G'$  and  $G''$ , combined with consistent ratios of  $G'/G'' \sim 10^2$  for the entire frequency range, are characteristics typical of elastic materials. As with the swelling behavior, the concentration of triblock copolymer in the blend has significant influence over the behavior of the hydrogel; in this case increasing triblock copolymer concentration results in significant increases in the magnitude of the complex modulus.

In direct contrast with changes in triblock block copolymer concentration, which influence the magnitude of the elastic modulus over a two decade span, changes in hydrogel temperature have virtually no effect. Figure 2.8b shows the elastic and loss moduli for **SOS-16.2**

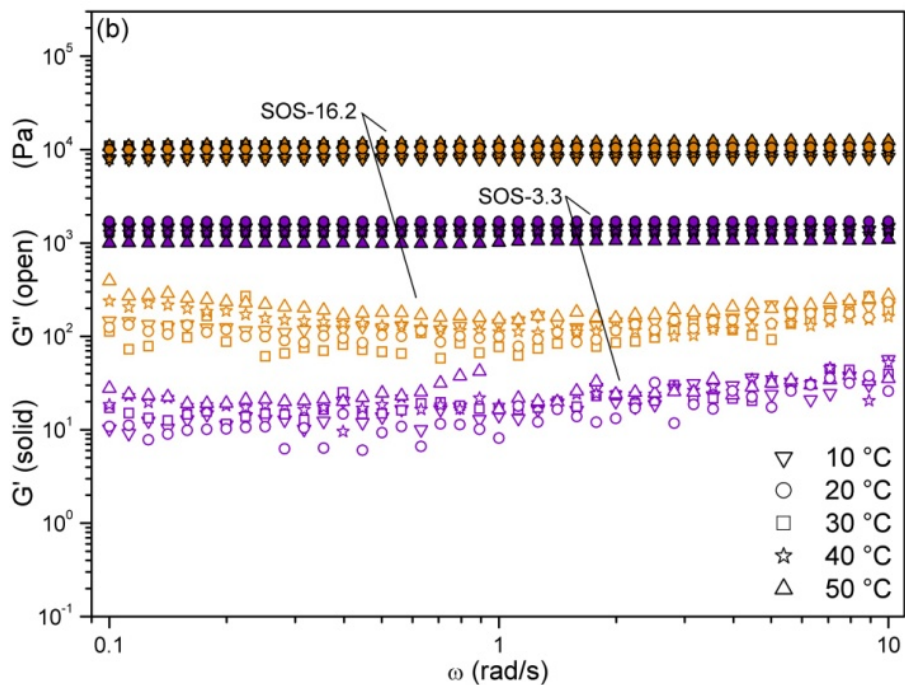
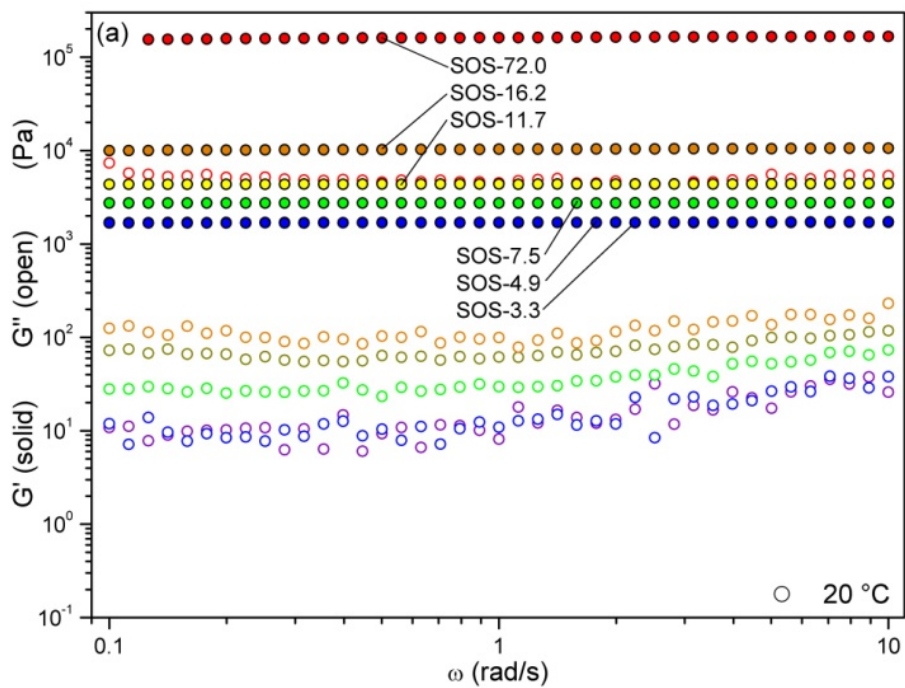


Figure 2.8. (a) Dynamic frequency sweeps for each hydrogel blend under oscillatory shear (20 °C, 0.5% strain). (b) Dynamic frequency sweeps for hydrogels SOS-16.2 and SOS-3.3 under oscillatory shear (0.5% strain) at ten degree increments between 10 and 50 °C.

and **SOS-3.3** collected at ten degree increments between 10 and 50 °C. The data presented are representative of the behavior at all triblock copolymer concentrations examined. The recorded moduli at each temperature are closely distributed over a limited range of  $G'$  and  $G''$  with no apparent experimental correlation to temperature. This suggests the sample to sample variation is at least as significant as temperature itself in the observed behavior of these systems. Thus, while changing temperature has considerable influence on the overall equilibrium water content of the system (as shown in Figure 2.5), the modulus remains essentially unaffected within the noise of sample variation. This clearly indicates that the mechanical properties exhibited are almost exclusively a function of the number of physical tethers and topological entanglements among the spherical domains. The implications of these results are significant; the equilibrium water content of the hydrogel can be tuned over a significant range without significantly influencing the mechanical properties of the hydrogel.

Unconfined compression experiments verify this effective independence of the mechanical properties on the equilibrium water content of the hydrogel. Figure 2.9 shows the stress versus compressive strain data for each of the blend compositions, and as a function of temperature for the **SOS-16.2** sample. Again, the temperature behavior documented in Figure 2.9 is representative of that found for all triblock copolymer concentrations. Compression was performed at a strain rate of  $5\% \text{ min}^{-1}$  for each hydrogel tested, up to approximately 40% strain. The data show that the modulus under compression is linear to at least 40% for all hydrogel blends, and again the sample to sample variation appears to mask any clear temperature dependence present. The addition of triblock copolymer dramatically changes the slope of the stress-strain data, which is directly related to the compressive modulus ( $K$ ) of these materials. Again, it is apparent that triblock copolymer content can be used to tailor the mechanical

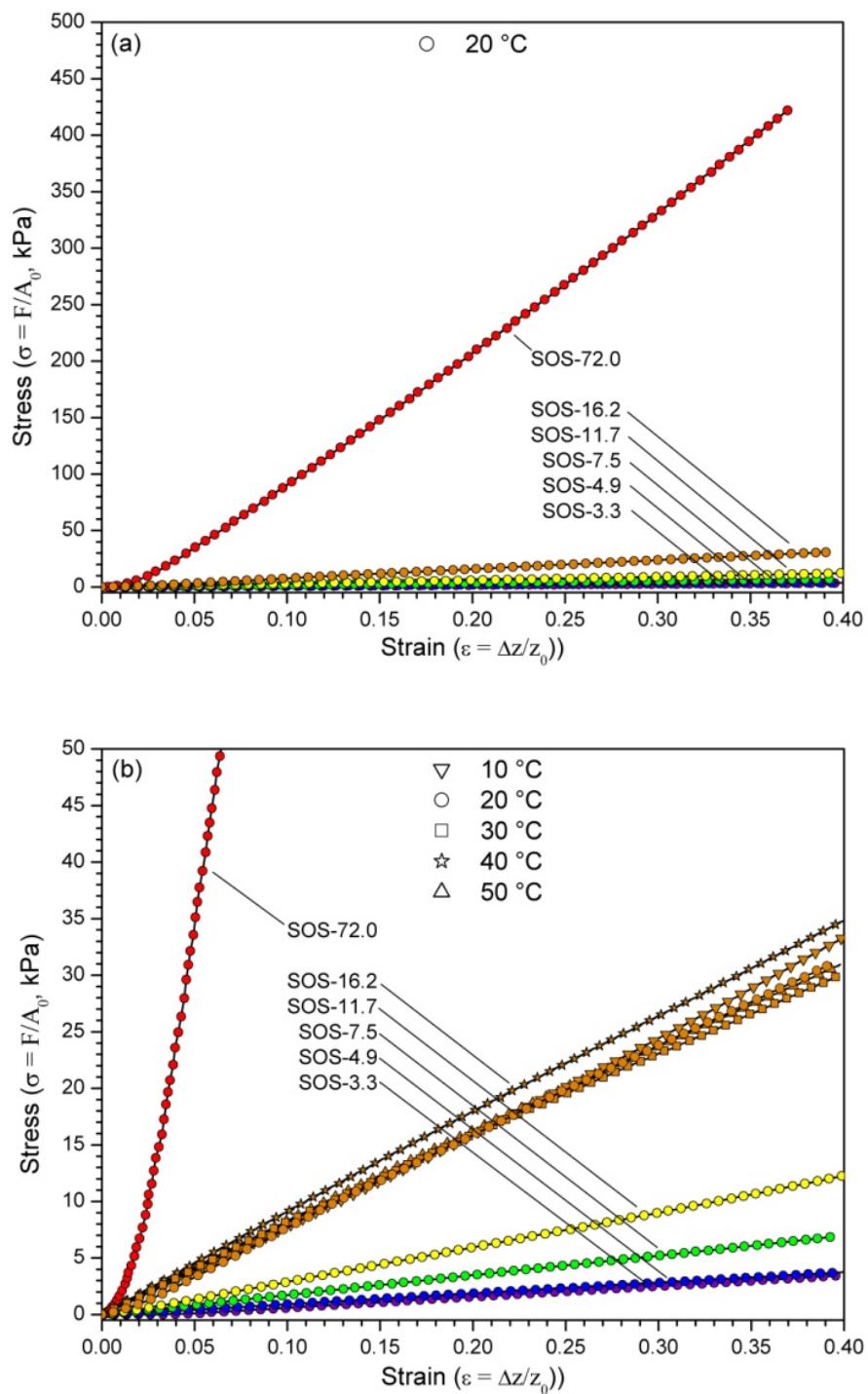


Figure 2.9. (a) Stress (in kPa) versus strain under unconfined compression (strain rate =  $5\% \text{ min}^{-1}$ ) for each hydrogel blend at 20 °C. (b) 10x magnification showing the effects of changing triblock copolymer concentration (at 20 °C) more clearly for low concentration samples. The effects of temperature in ten degree increments between 10 and 50 °C are also plotted for the SOS-16.2 sample.

response of the hydrogel, while temperature can be used as a secondary handle to independently tune the equilibrium water content over a moderate range. We also note that there appears to be a small region (0 – 2%) of nonlinearity present at the very initial stages of the compression experiment, and is likely associated with excess water trapped (but eventually displaced) between the hydrogel and parallel plate surfaces. This initial nonlinearity is most significant for the systems of higher triblock copolymer content, where water is less likely to be absorbed by the system.

It is interesting to compare the mechanical behavior of these hydrogel systems with what is expected for a swollen ideal elastomer.<sup>30, 59</sup> In general,

$$Modulus : T \cdot \phi_2^{1/3} \cdot \left( \frac{\nu_e}{V_0} \right) \quad (6)$$

where  $T$  is absolute temperature,  $\phi_2$  is the volume fraction of polymer in the swollen state, and  $(\nu_e/V_0)$  is the effective number of cross-linking strands (polymer chains spanning two junction points) per unit volume of the unswollen dry polymer. When the current hydrogels are viewed in this context, the largest difference in modulus one could expect to produce from the imposed temperature (from 283 K to 323 K), and associated equilibrium water content changes (at a fixed triblock copolymer concentration) is on the order of only 20%. This small difference is consistent with the hypothesis that sample to sample variation is a more dominant factor in determining modulus than either temperature or equilibrium water content in these systems. On the other hand, the number of tethering triblock copolymers is changing dramatically across the blend series, and the strong increase in modulus with increasing concentration is in qualitative agreement with relationship (6). If one assumes that the hydrogels in question approximate swollen ideal elastomers, it is possible to evaluate the correlation between the number of triblock copolymer chains ( $\nu_{SOS}$ ) and the number of effective strands ( $\nu_e$ ) in the system. The results are

shown in Figure 2.10. The left axis represents a type of reduced modulus based on relationship (6) above, extracted from the data plotted in Figures 2.5, 2.8, and 2.9. Note that the effects of polymer volume fraction and temperature have been, in theory, removed through normalization of the moduli by the assumed dependence on these parameters for a swollen ideal elastomer. The residual spread in the **SOS-3.3** and **SOS-16.2** data series after normalization by temperature and polymer volume fraction supports the previous arguments that sample to sample variation is more influential on modulus than changes in temperature or equilibrium water content. If the correlation between each triblock copolymer chain added and the number of effective strands produced was exactly 1:1, the data plotted in Figure 2.10 would be linear with a slope of one. The dotted line in Figure 2.10 represents this limiting behavior. Indeed, it appears that at very low concentrations of triblock copolymer the system is approaching the anticipated 1:1 correlation between triblock copolymer added and effective strands produced. In this low concentration limit, the number of junction points per unit dry volume ( $V_0$ ) is fixed by the density of spherical domains in the dry polymer. The addition of each triblock copolymer chain acts to create another effective strand between these fixed numbers of spherical domains. At higher triblock copolymer concentrations, the reduced modulus deviates from this limiting behavior. The data suggests a progressively stronger dependence of effective strands on triblock copolymer concentration. That is,

$$\left(\frac{\nu_e}{V_0}\right) \sim \left(\frac{\nu_{SOS}}{V_0}\right)^x \quad x \geq 1, \quad x = f(\nu_{SOS}) \quad (7)$$

The implication is that every triblock copolymer added acts to create, on average, more than one additional effective strand. We believe this is a product of the additional topological entanglements produced when the added triblock copolymer chain is forced to interact with other

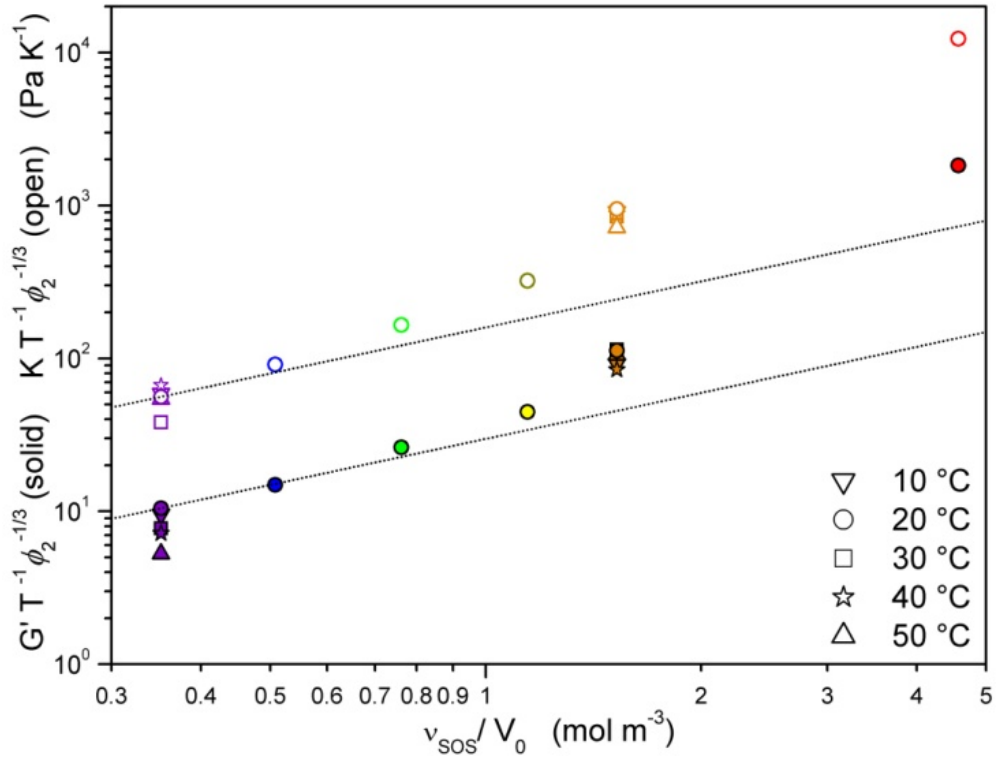


Figure 2.10. Reduced modulus plotted as a function of the SOS triblock copolymer concentration. The dotted reference lines have a slope equal to one.

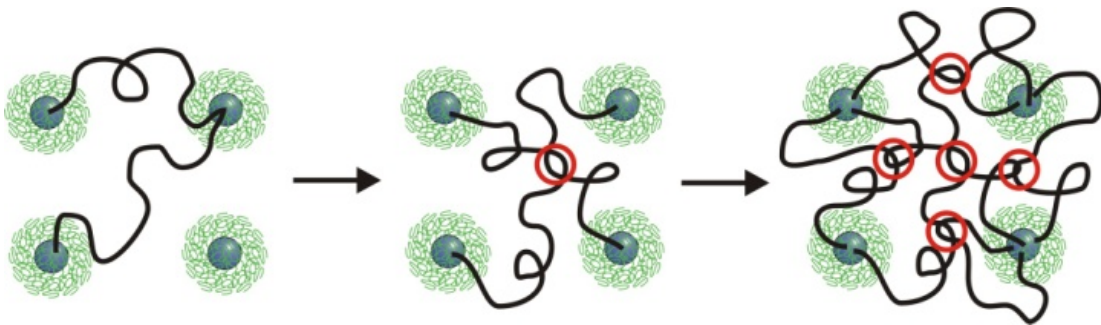
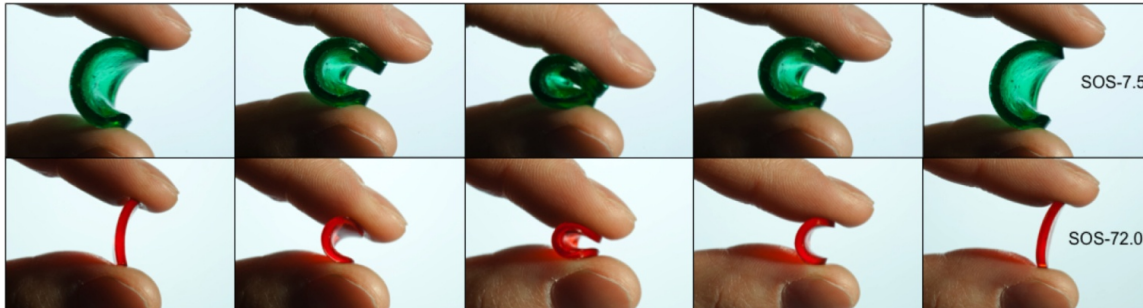


Figure 2.11. Addition of each triblock copolymer molecule creates additional topological entanglements that act to increase the effective number strands in the system beyond that expected from the triblock copolymer chain alone.

triblock copolymers in its vicinity; triblock copolymers that are in many cases spanning neighboring sets of spheres. As the concentration of triblock copolymer in the sample increases, the probability of these topological entanglements also increases, giving rise to the observed nonlinear dependence evident in Figure 2.10. The sum of all topological entanglements in the system acts to increase the number of effective junction points, and therefore the cross-link density (Figure 2.11). It follows that the average molecular weight between cross-links is thus continuously decreasing from its maximum value in the low triblock copolymer concentration regime, where it is effectively the the tethering mid-block molecular weight.

Of course, not all triblock copolymers bridge separate spherical domains, and the bridging to looping ratio and fraction of free chains and chain ends adopted by the collection of triblock copolymer chains is undoubtedly playing a major role in the behavior of these hydrogels. In the low triblock copolymer concentration regime such ratios necessarily play a significant role in determination of the gel point of the system. At high concentrations of triblock copolymer, topological entanglements would be reproduced in both bridging and looping populations, regardless. The nonlinear increase in the reduced modulus in Figure 2.10, at the very least, suggests that, even if the bridging to looping ratio and the fraction of free chains and chain ends and is a complex function of increasing triblock copolymer concentration, their net effect still produces a monotonically increasing modulus. To date, we have found no theoretical analysis of the bridging to looping ratio in sphere-forming blends of AB diblock and ABA triblock copolymer. Li et al.,<sup>60</sup> have, however, used computational models to investigate bridging to looping ratios in pure ABA systems for the sphere morphology (among others) and found the ratio to be a function of chain stiffness and Flory interaction parameter. They even investigate the influence of this ratio on the equilibrium swelling of the various mesophases. It would be of



**Figure 2.12. Manual compression and release of hydrogels formed from SOS-7.5 (96.3 wt% H<sub>2</sub>O) and SOS-72.0 (83.3 wt% H<sub>2</sub>O).**

great value, given the experimental results presented here, to extend such analyses to include blended systems of diblock and triblock copolymer chains.

#### **2.4.6 Elastic Recovery and Aging**

The elastic nature of these hydrogels and their mechanical integrity under applied stress is evident from simple qualitative bending experiments shown for SOS-7.5 and SOS-72.0 in Figure 2.12. Note that the decrease in triblock copolymer concentration by a factor of ten still produces a hydrogel with excellent recovery characteristics with no visually detectable deformation. The extent of this behavior was quantitatively examined for all blends by performing multiple unconfined compression-decompression cycles at a constant strain rate of 5% min<sup>-1</sup>. Figure 2.13 shows two cycles for each blend, compressed to approximately 40% strain. In all cases, each hydrogel was able to achieve complete recovery, after an initial period in the decompression segment in which small degrees of hysteresis were present. The magnitude of this hysteresis appears to be qualitatively proportional to the triblock copolymer concentration, which may be rooted in the degree to which entanglements slow the recovery phase. This recovery phase is a

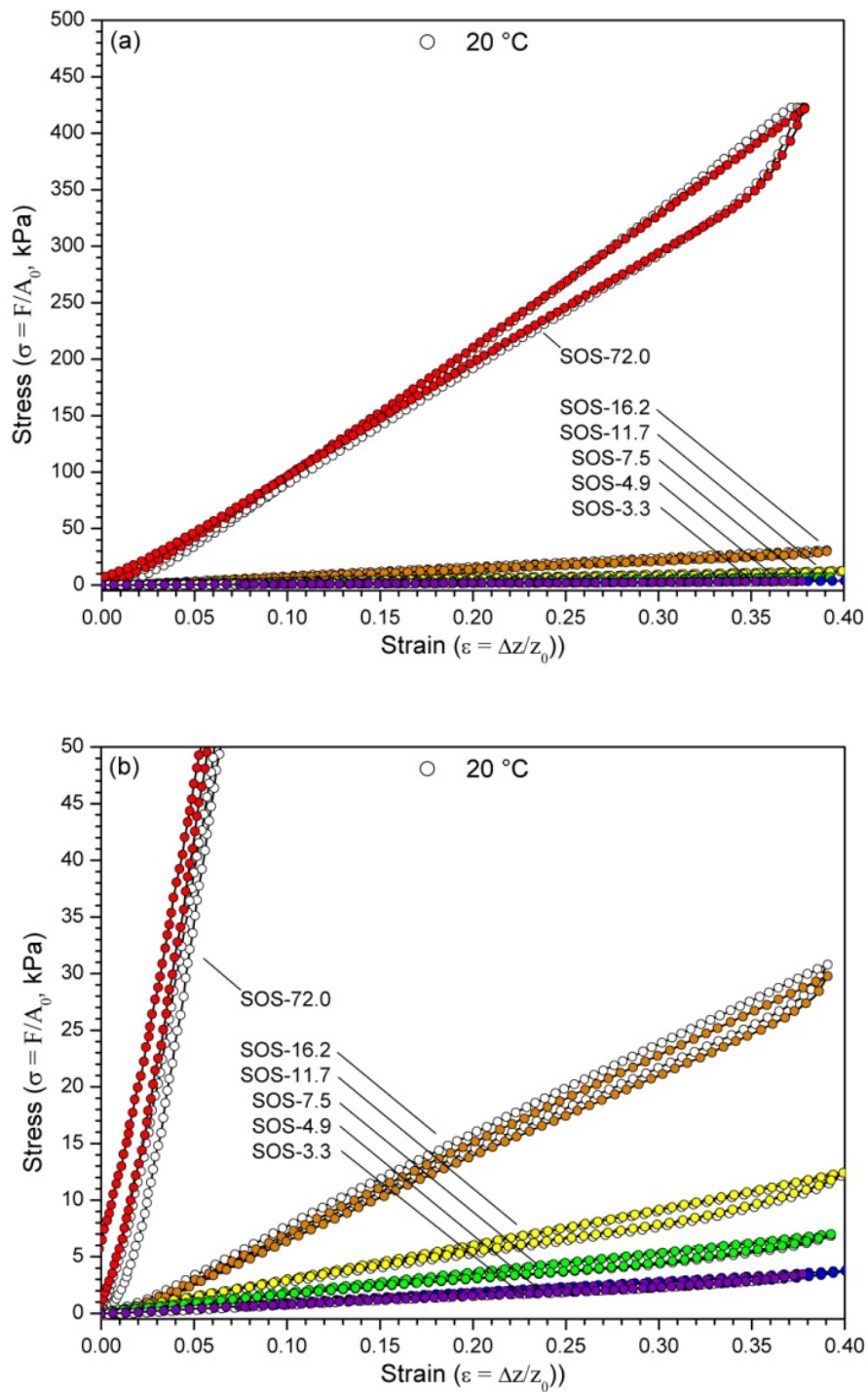


Figure 2.13. (a) Unconfined compression-decompression cycles for each of the hydrogel blends at 20 °C. (b) 10x magnification. Both compression and release were performed at a strain rate of  $5\% \text{ min}^{-1}$ . Two cycles are shown. Solid circles denote the second cycle.

direct product of the osmotic forces present which act to redistribute water molecules throughout hysteresis appears to be qualitatively proportional to the triblock copolymer concentration, which may be rooted in the degree to which entanglements slow the recovery phase. This recovery phase is a direct product of the osmotic forces present which act to redistribute water molecules throughout the sample; the hysteresis, on the other hand, is a product of the mass transfer limitations in the material. Importantly, there is excellent agreement between the first and second cycles at all concentrations of triblock copolymer. Such excellent recovery suggests that very little if any water is being exuded from the hydrogel under compressive strains to 40%. Future examination of these hydrogels at larger strains and strain rates will reveal the limitations of these materials in this regard, but the current measurements show an impressive ability to retain shape and elasticity following applied stress.

Finally, it should be noted that all hydrogel compositions examined show complete preservation of shape over a three month period when stored in DI water solutions. Clearly, the vitreous PS domains are sufficiently glassy at room temperature to inhibit long term rearrangement of the PS domain structure. As such, the applicability of such hydrogels in more enduring applications is quite promising.

## **2.5. Conclusions**

Simple blends of sphere-forming amphiphilic PS-PEO diblock and PS-PEO-PS triblock copolymers can be used to produce highly elastic, nanostructured hydrogels with excellent mechanical properties and long-term preservation of shape. Mechanical performance can be tuned using the relative concentration of triblock copolymer in the blend, and the equilibrium swelling ratio tuned using a combination of triblock copolymer concentration and temperature. Ultimately, the breadth over which one can control the moduli and equilibrium water content in

these hydrogels has significant implications for the widespread utility of these materials throughout the biomedical and membrane communities. This potential is further solidified with the anticipated facility with which the hydrogel interior may be chemically modified at the dangling hydroxylated PEO chain ends. As such, this generalized hydrogel fabrication strategy stands as an incredibly versatile platform from which a wealth of new hydrogel materials can be synthesized.

## **2.6. Recognitions**

The authors would like to thank both M. Kipper and Q. Wang for their many discussions and critical input. This work was supported by the National Science Foundation (DMR-0645781) and Colorado State University. The photographs shown in Figure 2.12 were taken by Joe Mendoza of CSU Photography.

## **2.7. Supporting information available**

Determination of SOS triblock copolymer concentration in SOS-72.0 by regression analysis; Differential scanning calorimetry (DSC) data for the S-OH and SO samples; Melt-state rheological analysis of the SO and SOS-72.0 samples; Additional notes on the analysis of morphology from SAXS in Appendix.

## 2.8. References

- [1] P. Calvert, "Hydrogels for Soft Machines," *Advanced Materials*, vol. 21, pp. 743-756, Feb 16 2009.
- [2] Y. Tanaka, J. P. Gong, and Y. Osada, "Novel hydrogels with excellent mechanical performance," *Progress in Polymer Science*, vol. 30, pp. 1-9, Jan 2005.
- [3] C. C. Lin and K. S. Anseth, "PEG Hydrogels for the Controlled Release of Biomolecules in Regenerative Medicine," *Pharmaceutical Research*, vol. 26, pp. 631-643, Mar 2009.
- [4] J. M. G. Swann and A. J. Ryan, "Chemical actuation in responsive hydrogels," *Polymer International*, vol. 58, pp. 285-289, Mar 2009.
- [5] J. Jagur-Grodzinski, "Polymers for tissue engineering, medical devices, and regenerative medicine. Concise general review of recent studies," *Polymers for Advanced Technologies*, vol. 17, pp. 395-418, Jun 2006.
- [6] J. Jagur-Grodzinski, "Polymeric gels and hydrogels for biomedical and pharmaceutical applications," *Polymers for Advanced Technologies*, vol. 21, pp. 27-47, Jan 2010.
- [7] N. A. Peppas, J. Z. Hilt, A. Khademhosseini, and R. Langer, "Hydrogels in biology and medicine: From molecular principles to bionanotechnology," *Advanced Materials*, vol. 18, pp. 1345-1360, Jun 6 2006.
- [8] J. S. Mohammed and W. L. Murphy, "Bioinspired Design of Dynamic Materials," *Advanced Materials*, vol. 21, pp. 2361-2374, Jun 19 2009.
- [9] M. C. Branco and J. P. Schneider, "Self-assembling materials for therapeutic delivery," *Acta Biomaterialia*, vol. 5, pp. 817-831, Mar 2009.
- [10] L. Yu and J. D. Ding, "Injectable hydrogels as unique biomedical materials," *Chemical Society Reviews*, vol. 37, pp. 1473-1481, 2008.
- [11] J. Kopecek, "Hydrogels: From Soft Contact Lenses and Implants to Self-Assembled Nanomaterials," *Journal of Polymer Science Part a-Polymer Chemistry*, vol. 47, pp. 5929-5946, Nov 15 2009.
- [12] B. V. Slaughter, S. S. Khurshid, O. Z. Fisher, A. Khademhosseini, and N. A. Peppas, "Hydrogels in Regenerative Medicine," *Advanced Materials*, vol. 21, pp. 3307-3329, Sep 4 2009.
- [13] P. Gupta, K. Vermani, and S. Garg, "Hydrogels: from controlled release to pH-responsive drug delivery," *Drug discovery today*, vol. 7, pp. 569-79, 2002.
- [14] W. A. Petka, J. L. Harden, K. P. McGrath, D. Wirtz, and D. A. Tirrell, "Reversible hydrogels from self-assembling artificial proteins," *Science*, vol. 281, pp. 389-392, Jul 17 1998.
- [15] V. Castelletto and I. W. Hamley, "Microstructure and Physical Properties of a pH-Responsive Gel Based on a Novel Biocompatible ABA-Type Triblock Copolymer," *Langmuir*, vol. 20, 2004.
- [16] V. Castelletto, I. W. Hamley, M. Crothers, D. Attwood, Z. Yang, and C. Booth, "Structure of Aqueous Gels Formed by Triblock and Diblock Copolymers with Oxyethylene and Oxyphenylethylene Blocks," *J. Macromol. Sci. Phys.*, vol. B43, pp. 13-27, 2004.
- [17] M. Branco, N. Wagner, D. Pochan, and J. Schneider, "Release of Model Macromolecules from Self-Assembling Peptide Hydrogels for Injectable Delivery," *Biopolymers*, vol. 92, pp. 318-318, 2009.

- [18] T. Vermonden, S. S. Jena, D. Barriet, R. Censi, J. van der Gucht, W. E. Hennink, and R. A. Siegel, "Macromolecular Diffusion in Self-Assembling Biodegradable Thermosensitive Hydrogels," *Macromolecules*, vol. 43, pp. 782-789, Jan 26 2010.
- [19] L. Yu, G. T. Chang, H. Zhang, and J. D. Ding, "Injectable block copolymer hydrogels for sustained release of a PEGylated drug," *International Journal of Pharmaceutics*, vol. 348, pp. 95-106, Feb 4 2008.
- [20] N. Stavrouli, T. Aubry, and C. Tsitsilianis, "Rheological properties of ABA telechelic polyelectrolyte and ABA polyampholyte reversible hydrogels: A comparative study," *Polymer*, vol. 49, pp. 1249-1256, Mar 3 2008.
- [21] A. P. Vogt and B. S. Sumerlin, "Temperature and redox responsive hydrogels from ABA triblock copolymers prepared by RAFT polymerization," *Soft Matter*, vol. 5, pp. 2347-2351, 2009.
- [22] S. A. Angelopoulos and C. Tsitsilianis, "Thermo-reversible hydrogels based on poly(N,N-diethylacrylamide)-block-poly(acrylic acid)-block-poly(N,N-diethylacrylamide) double hydrophilic triblock copolymer," *Macromolecular Chemistry and Physics*, vol. 207, pp. 2188-2194, Dec 1 2006.
- [23] D. W. Grijpma and J. Feijen, "Hydrogels by stereo-complexation of water-soluble PLLA-PEO-PLLA and PDLA-PEO-PDLA triblock-copolymers," *Journal of Controlled Release*, vol. 72, pp. 247-249, May 14 2001.
- [24] Z. Q. Jiang, Y. J. You, X. M. Deng, and J. Y. Hao, "Injectable hydrogels of poly(epsilon-caprolactone-co-glycolide)-poly(ethylene glycol)-poly(epsilon-caprolactone-co-glycolide) triblock copolymer aqueous solutions," *Polymer*, vol. 48, pp. 4786-4792, Jul 27 2007.
- [25] S. E. Kirkland, R. M. Hensarling, S. D. McConaughy, Y. Guo, W. L. Jarrett, and C. L. McCormick, "Thermoreversible hydrogels from RAFT-synthesized BAB triblock copolymers: Steps toward biomimetic matrices for tissue regeneration," *Biomacromolecules*, vol. 9, pp. 481-486, Feb 2008.
- [26] X. P. Ni, A. Cheng, and J. Li, "Supramolecular hydrogels based on self-assembly between PEO-PPO-PEO triblock copolymers and alpha-cyclodextrin," *Journal of Biomedical Materials Research Part A*, vol. 88A, pp. 1031-1036, Mar 15 2009.
- [27] M. X. Qao, D. W. Chen, T. N. Hao, X. L. Zhao, H. Hu, and X. C. Ma, "Injectable thermosensitive PLGA-PEG-PLGA triblock copolymers-based hydrogels as carriers for interleukin-2," *Pharmazie*, vol. 63, pp. 27-30, Jan 2008.
- [28] F. S. Bates and G. H. Fredrickson, "Block copolymers-designer soft materials," *Physics Today*, vol. 52, pp. 32-38, 1999.
- [29] E. W. Cochran, C. J. Garcia-Cervera, and G. H. Fredrickson, "Stability of the gyroid phase in diblock copolymers at strong segregation," *Macromolecules*, vol. 39, pp. 2449-2451, Apr 4 2006.
- [30] P. J. Flory, *Principles of polymer chemistry*. Ithaca,: Cornell University Press, 1953.
- [31] R. P. Quirk and J. J. Ma, "Characterization of the functionalization reaction product of poly(styryl)lithium with ethylene oxide," *J. Polym. Sci., Part A: Polym. Chem.*, vol. 26, pp. 2031-7, 1988.
- [32] P. G. Fragouli, H. Iatrou, and N. Hadjichristidis, "Synthesis and characterization of linear diblock and triblock copolymers of 2-vinyl pyridine and ethylene oxide," *Polymer*, vol. 43, pp. 7141-7144, Dec 2002.

- [33] L. J. Fetters, D. J. Lohse, D. Richter, T. A. Witten, and A. Zirkel, "Connection between Polymer Molecular Weight, Density, Chain Dimensions, and Melt Viscoelastic Properties," *Macromolecules*, vol. 27, pp. 4639-47, 1994.
- [34] M. A. Hillmyer and F. S. Bates, "Synthesis and Characterization of Model Polyalkane-Poly(ethylene oxide) Block Copolymers," *Macromolecules*, vol. 29, pp. 6994-7002, 1996.
- [35] F. S. Bates, "Polymer-Polymer Phase-Behavior," *Science*, vol. 251, pp. 898-905, Feb 22 1991.
- [36] F. S. Bates, M. F. Schulz, A. K. Khandpur, S. Foerster, and J. H. Rosedale, "Fluctuations, conformational asymmetry and block copolymer phase behavior," *Faraday Discuss.*, vol. 98, pp. 7-18, 1995.
- [37] T. G. Fox and P. J. Flory, "The Glass Temperature and Related Properties of Polystyrene - Influence of Molecular Weight," *Journal of Polymer Science*, vol. 14, pp. 315-319, 1954.
- [38] P. G. Santangelo and C. M. Roland, "Molecular weight dependence of fragility in polystyrene," *Macromolecules*, vol. 31, pp. 4581-4585, Jul 14 1998.
- [39] N. P. Balsara, B. A. Garetz, M. Y. Chang, H. J. Dal, and M. C. Newstein, "Identification of the molecular parameters that govern ordering kinetics in a block copolymer melt," *Macromolecules*, vol. 31, pp. 5309-5315, Aug 11 1998.
- [40] C. R. Harkless, M. A. Singh, S. E. Nagler, G. B. Stephenson, and J. L. Jordansweet, "Small-Angle X-Ray-Scattering Study of Ordering Kinetics in a Block Copolymer," *Physical Review Letters*, vol. 64, pp. 2285-2288, May 7 1990.
- [41] J. K. Kim, H. H. Lee, M. Ree, K. B. Lee, and Y. Park, "Ordering kinetics of cylindrical and spherical microdomains in an SIS block copolymer by synchrotron SAXS and rheology," *Macromolecular Chemistry and Physics*, vol. 199, pp. 641-653, Apr 1998.
- [42] T. H. Epps, III and F. S. Bates, "Effect of Molecular Weight on Network Formation in Linear ABC Triblock Copolymers," *Macromolecules*, vol. 39, pp. 2676-2682, 2006.
- [43] K. A. Cavicchi and T. P. Lodge, "Self-diffusion and tracer diffusion in sphere-forming block copolymers," *Macromolecules*, vol. 36, pp. 7158-7164, Sep 23 2003.
- [44] K. A. Cavicchi and T. P. Lodge, "Domain size equilibration in sphere-forming block copolymers," *Journal of Polymer Science Part B-Polymer Physics*, vol. 41, pp. 715-724, Apr 1 2003.
- [45] X. H. Wang, E. E. Dormidontova, and T. P. Lodge, "The order-disorder transition and the disordered micelle regime for poly(ethylenepropylene-b-dimethylsiloxane) spheres," *Macromolecules*, vol. 35, pp. 9687-9697, Dec 17 2002.
- [46] H. L. Hsieh, *Rubber Chem. Technol.*, vol. 49, p. 1305, 1976.
- [47] H. L. Hsieh and R. P. Quirk, *Anionic polymerization : principles and practical applications*. New York: Marcel Dekker, 1996.
- [48] J. L. Adams, D. J. Quiram, W. W. Graessley, R. A. Register, and G. R. Marchand, "Ordering dynamics of compositionally asymmetric styrene isoprene block copolymers," *Macromolecules*, vol. 29, pp. 2929-2938, Apr 8 1996.
- [49] E. E. Dormidontova and T. P. Lodge, "The order-disorder transition and the disordered micelle regime in sphere-forming block copolymer melts," *Macromolecules*, vol. 34, pp. 9143-9155, Dec 18 2001.
- [50] C. D. Han, N. Y. Vaidya, D. Kim, G. Shin, D. Yamaguchi, and T. Hashimoto, "Lattice disordering/ordering and demicellization/micellization transitions in highly asymmetric

- polystyrene-block-polyisoprene copolymers," *Macromolecules*, vol. 33, pp. 3767-3780, May 16 2000.
- [51] N. Sakamoto, T. Hashimoto, C. D. Han, D. Kim, and N. Y. Vaidya, "Order-order and order-disorder transitions in a polystyrene-block-polyisoprene-block-polystyrene copolymer," *Macromolecules*, vol. 30, pp. 1621-1632, Mar 24 1997.
- [52] M. Schwab and B. Stuhn, "Thermotropic transition from a state of liquid order to a macrolattice in asymmetric diblock copolymers," *Physical Review Letters*, vol. 76, pp. 924-927, Feb 5 1996.
- [53] M. Schwab and B. Stuhn, "Asymmetric diblock copolymers - Phase behaviour and kinetics of structure formation," *Colloid and Polymer Science*, vol. 275, pp. 341-351, Apr 1997.
- [54] D. J. Kinning and E. L. Thomas, "Hard-Sphere Interactions between Spherical Domains in Diblock Copolymers," *Macromolecules*, vol. 17, pp. 1712-1718, 1984.
- [55] J. K. Percus and G. J. Yevick, "Analysis of Classical Statistical Mechanics by Means of Collective Coordinates," *Physical Review*, vol. 110, pp. 1-13, 1958.
- [56] L. S. Ornstein and F. Zernike, "Accidental deviations of density and opalescence at the critical point of a simple substance," *Proceedings of the Koninklijke Akademie Van Wetenschappen Te Amsterdam*, vol. 17, pp. 793-806, 1914.
- [57] J. S. Pedersen, D. Posselt, and K. Mortensen, "Analytical Treatment of the Resolution Function for Small-Angle Scattering," *Journal of Applied Crystallography*, vol. 23, pp. 321-333, Aug 1 1990.
- [58] T. Hashimoto, M. Fujimura, and H. Kawai, "Domain-Boundary Structure of Styrene-Isoprene Block Co-Polymer Films Cast from Solutions .5. Molecular-Weight Dependence of Spherical Microdomains," *Macromolecules*, vol. 13, pp. 1660-1669, 1980.
- [59] P. C. Hiemenz and T. Lodge, *Polymer chemistry*, 2nd ed. Boca Raton: CRC Press, 2007.
- [60] B. Q. Li and E. Ruckenstein, "The equilibrium fraction of bridging chains and the swelling behavior of ABA triblock copolymer mesophases," *Macromolecular Theory and Simulations*, vol. 7, pp. 333-348, May 1998.

## CHAPTER 3

### EFFECTS OF TAILORED CORONAL LAYER OVERLAP IN TETHERED MICELLE HYDROGEL NETWORKS<sup>3</sup>

#### 3.1 Summary

Solvent-free fabrication of tethered micelle networks via melt-state self-assembly of sphere-forming polystyrene-*b*-poly(ethylene oxide) (SO) diblock and SOS triblock copolymers blends is capable of producing highly elastic and mechanically robust hydrogel systems not typically achievable using solution assembly techniques. Here, we explore the impact of using PEO midblocks of different lengths within the SOS tethers, in an effort to elucidate the role played by water content, tether concentration, and tether length in mechanical property determination. In doing so, we were able to establish coronal layer overlap as the primary contributing factor in regulating the dynamic elastic moduli exhibited by tethered micelle systems. Variation of either tether concentration or tether length could be used to tune the degree of coronal layer overlap, enabling direct and accurate control over hydrogel mechanical properties. We contend such control is a unique feature of the melt-state fabrication approach to tethered micelle networks.

---

<sup>3</sup> The contents of this dissertation chapter have been adapted from a manuscript submitted to *Soft Matter*. Chen Guo and Travis S. Bailey developed and designed the experiments. Chen Guo performed the experiments. The manuscript and dissertation chapter were written by Chen Guo with editing by Travis S. Bailey.

### 3.2 Introduction

Polymer-based hydrogel networks have become increasingly important targets for a range of applications beyond simple commodity based absorbents, such as wound dressings, chemical and drug delivery agents,<sup>1-5</sup> tissue growth scaffolds,<sup>6-9</sup> ocular lenses, and biomedical-related implant technologies. However, extension to these types of applications requires hydrogel designs through which functionality, biocompatibility, mass transport and mechanical response can be carefully tailored to meet highly specific performance criteria.<sup>10</sup> At the center of this development challenge lays the need for synthetic protocols capable of producing basic hydrophilic polymer networks with spatial homogeneity at length scales in the nanoscale range, where precision, accuracy, and reproducibility of performance are ultimately determined.

Producing networks with submicron homogeneity in mesh size can be challenging using traditional crosslinking of multifunctional monomer, oligomer, or polymer chains. The use of tethered micelle networks formed from solution-based self-assembly of amphiphilic ABA triblock copolymers has been one of the most prevalent alternate strategies explored over the last decade, particularly as injectable media for local delivery of therapeutics. Using the micelle morphology as a fundamental structural unit provides a number of unique opportunities not available in traditional systems fabricated from simple crosslinking of hydrophilic polymers. Notably, each micelle becomes a multifunctional junction point within the network, which lends itself towards a number of useful design advantages. For example, the core domains can be used as hydrophobic reservoirs for small molecule encapsulation. Release can, in theory, be controlled through the size, or degradation rate of these cores, depending on the polymer systems employed. Tethering of these micelle structural units, due to highly uniform size distributions, can be used to generate fairly homogenous mesh sizes and distances between junction points.

And finally, because each micelle contains tens to hundreds of chains, the number of effective network strands between junction points can be quite large, providing a *potential* for forming very mechanically robust materials. Unfortunately, the mechanical properties of tethered micelle networks formed are often limited in practice, a consequence of the solution-based fabrication methods used to produce them. For applications such as controlled or targeted delivery through an injectable medium, the mechanical properties are often quite sufficient and of minimal concern. However, our group has been focused on ways to tap the intrinsic potential of the tethered micelle framework to produce more mechanically robust hydrogel constructs, ones capable of reproducing, for example, the impressive mechanical function exhibited by biologically derived hydrated soft tissues.

Tethered micelle network formation is typically accomplished through the use of solvated ABA systems in which the A blocks can be thermodynamically triggered to phase separate (precipitate) out of solution, producing spherical micelle aggregates containing (hydrophobic) collapsed cores of polymer A and (hydrophilic) coronal layers of solvated polymer B. If the concentration of the polymer in solution is low, precipitating block copolymers form flower-like micelles characterized by looping chains, in which opposite ends of a chain predominantly occupy the same micelle core. When the concentration of ABA triblock exceeds a critical value, a sufficient fraction of opposing chains ends form bridges between adjacent micelle cores, and an infinite network of tethered micelles is formed. Not surprisingly, bridging fractions, micelle size distribution, aggregation number, and network uniformity can all be quite sensitive to changes in concentration, precipitation kinetics, differences in solvent selectivity between blocks, and the rate at which the conditions for precipitation are invoked. An inability to control such factors is one facet of tethered micelle network synthesis that makes optimizing mechanical properties in

these systems difficult. However, in most cases, the mechanical deficiency of these network materials can almost always be traced to the limited mechanical integrity of the micelle cores formed during the precipitation step.<sup>5, 11, 12, 13</sup> As the formal junction points through which stress is distributed across the hydrogel, the physical state of the micelle core is central to the mechanical potential of the network. In some cases, small aggregation numbers in the tens of chains are not of sufficient size to produce bulk-like mechanical properties. In other cases, residual solvent trapped during chain aggregation effectively plasticizes the micelle core, a kinetic problem faced even in systems for which very sharp thermodynamic transitions in chain end solubility have been achieved. Successful attempts to improve the mechanical stability have involved integration of chain end blocks for which post-precipitation crystallization or cross-linking is possible. For example, dramatic improvements in mechanical response have been achieved through in situ cross-linking of micelle cores composed of functionalized polylactides.<sup>14</sup> However, these examples are few, and the promise of solution assembly as a generalized means to tethered micelle networks of extensive mechanical elasticity, strength, and toughness appears limited.

Our group has been exploring the use of solvent free assembly of tethered micelle networks as a route to hydrogel materials of improved mechanical (and chemical) function. Recently,<sup>15</sup> we introduced a novel approach exploiting the self-assembly of sphere-forming block copolymers, allowing us to establish the tethered micelle network in the melt-state, sans solvent. Self-assembly in the melt state permits pre-structuring of the network prior to swelling, in direct contrast with the majority of hydrogel preparations.<sup>1-7, 9, 11, 14, 16</sup> Either vitrification<sup>15</sup> or chemical crosslinking<sup>17</sup> of the spherical domains following self-assembly was used to fix the network structure, prior to the introduction of a matrix selective solvent. Because of the very high

bridging fractions found in sphere-based ABA block copolymer morphologies (approaching 80%)<sup>18</sup>, we found we could introduce considerable amounts of non-tethering AB diblock copolymer (up to 96.7 mol%) to the standard ABA triblock copolymer systems and still achieve infinitely tethered networks. This is a direct consequence of the very high aggregation numbers found in sphere based block copolymer morphologies. For example, in polystyrene-poly(ethylene oxide) (PS-PEO, SO) diblock and PS-PEO-PS (SOS) triblock copolymer blends used as a model system in our previous work, each spherical domain was found to have a mean aggregation number of over 200 PS chains. With high bridging fractions, and only several bridging chains per sphere necessary to reach the infinite network gel point<sup>19</sup>, very little SOS triblock copolymer was actually required to form infinitely connected systems.

In the SO/SOS systems previously studied,<sup>15</sup> we discovered that melt-state self-assembly of the tethered micelle structure was incredibly effective at producing highly elastic, mechanically robust hydrogel systems. Hydrogels fabricated using this strategy preserved their original shape with high fidelity and had properties that could be easily tuned over a large range using a combination of either SOS concentration or hydrogel temperature. For example, by adjusting the amount of SOS content from 3.3 mol% to 72 mol% in the SO/SOS blend, the dynamic elastic moduli of the hydrogel could be tuned from values as low as  $10^3$  Pa on the low end, to values exceeding  $10^5$  Pa on the high end. Mechanical performance in unconfined compression was also highly tunable through adjustment of SOS triblock copolymer content. Samples with only 3.3 mol% SOS produced compressive moduli of 7.5 kPa, while samples with 72 mol% SOS produced compressive moduli of over 1000 kPa. In all cases, regardless of SOS triblock copolymer concentration, the compression was linear to 40% strain, with complete elastic recovery over multiple cycles.

Coincident with the large increases in dynamic elastic and compressive moduli with increased SOS triblock copolymer concentration, was an equally dramatic decrease in the equilibrium water content absorbable by the system. Swelling ratios ( $Q$ ), could be tuned all the way from 35.5 g water/g polymer (at 20 °C) down to 5.0 g water/g polymer simply by increasing the SOS triblock copolymer concentration of the system. At a fixed temperature, there appeared to be a clear (and not particularly interesting) relationship: more tethers, less solvent, higher modulus. This seemed to be in general agreement with what would be expected for an ideal swollen elastomer, in which

$$Modulus \propto T \cdot \phi_2^{1/3} \cdot \left( \frac{\nu_e}{V_0} \right) \quad (6)$$

where  $T$  is absolute temperature,  $\phi_2$  is the volume fraction of polymer in the swollen state, and  $(\nu_e/V_0)$  is the effective number of cross-linking strands (polymer chains spanning two junction points) per unit volume of the unswollen dry polymer. However, in taking advantage of the decreasing solubility of PEO in water with increasing temperature, we found we could decrease the swelling ratio by as much as 33% simply by heating the hydrogels from 10°C to 50°C. In doing so, however, we found that the mechanical properties of the system remained essentially unchanged, despite the increases in both  $T$  and  $\phi_2$ . Furthermore, we found that the addition of SOS triblock copolymer tethers appeared to increase modulus at a much faster rate than expected, such that each additional SOS triblock copolymer molecule added was acting to create more than one additional effective strand. So although we could see there were evident correlations between SOS triblock copolymer concentration, equilibrium swelling ratio, and mechanical performance, our understanding of the origin of the mechanical properties in these tethered micelle networks appeared quite limited.

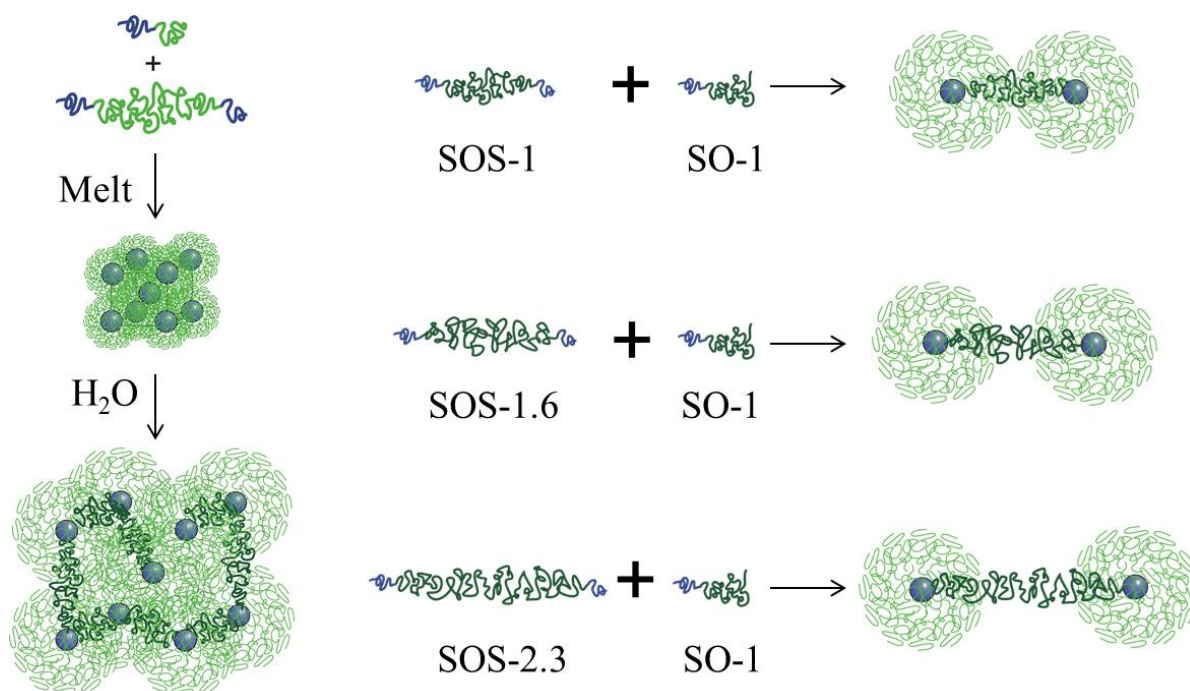


**Figure 3.1. Illustration showing the use of sphere-forming AB diblock and ABA triblock copolymer blends to prestructure tethered micelle networks in the absence of solvent (left). In this study, the molecular weight of the bridging tethers is varied help expose the contribution of various structural elements towards the resultant hydrogel mechanics.**

In this report, we expand our investigation of the model SO/SOS systems in an attempt to resolve the degree to which the various structural elements are contributing to the mechanics of these melt-prestructured tethered micelle networks. In the previously described model SO/SOS system, the SOS triblock copolymer used was always twice the molecular weight of the SO diblock copolymer, such that their preferred lattice dimensions during self-assembly were roughly "matched". Here, we introduce SOS triblock copolymer for which the PEO midblock has been extended in molecular weight relative to the length generated by simply coupling SO diblock copolymer. As shown in Figure 3.1, the study revolves around hydrogels produced from three blends involving distinct pairings of a single SO diblock copolymer and three different SOS triblock copolymer molecules. Importantly, the SO diblock copolymer was kept identical

throughout the series, and the PS chain ends for all molecules originate from the same PS-OH parent block. Thus, the PEO midblock molecular weight is designed as the only variable among blends of similar SO:SOS molar ratios. Each SOS triblock copolymer is designated as SOS-Y, where Y is the ratio of the PEO midblock molecular weight present in the SOS-Y triblock copolymer relative to midblock molecular weight if the SOS triblock copolymer were "matched".

The premise behind studying these three sets of blends is tied to the tether's critical role in determining the equilibrium swelling dimensions of the hydrogel. At low SOS concentrations, the equilibrium swelling dimensions are determined by the balance of solvent-induced osmotic swelling force trying to disperse the micelles, and the entropic restoring force of the tethering midblocks which resist chain stretching associated with the swelling process. As concentrations of tethering midblocks increase, topologically constrained entanglements among the tethers restrict swelling even further. The increasing number of entanglements is responsible for the decreased swelling ratios produced at higher SOS concentrations. By increasing the tether lengths exclusively, we hypothesized we could increase the swelling ratio independently from SOS triblock copolymer concentration, providing a means of decoupling the mechanical contributions of those two quantities. As we show within, it is actually the degree of coronal overlap dictated by the length and quantity of tethers that is the major contributor to the mechanics of the hydrogel network. Notably, the use of melt-state pre-structuring (in contrast to solution assembly) provides the means to accurately control both.

### 3.3. Experimental

#### 3.3.1. Materials

Styrene (99%, 4-tert-butylcatechol inhibitor, Aldrich) and ethylene oxide (99.5+%, compressed gas, Aldrich) monomer were each purified by successive vacuum distillations (10–20 mTorr) from dried dibutylmagnesium ( $0.1 \text{ mmol g}^{-1}$  monomer, 1.0M solution in heptane, Aldrich) before use. Both purified styrene and ethylene oxide monomer were stored in glass burettes in the dark, at room temperature (styrene) and  $0 \text{ }^{\circ}\text{C}$  (ethylene oxide), respectively, until use (typically less than 24 h). Argon degassed cyclohexane (CHX) was purified by passing the solvent over activated alumina followed by Q-5-like supported copper catalyst (Glass Contour, proprietary). Argon degassed tetrahydrofuran (THF) was purified by passing the solvent over activated alumina. High-purity argon (99.998%, Airgas) was passed through additional oxygen and moisture traps prior to use. Glassware and polymerization reactors were flamed under vacuum and backfilled with argon (3x). Materials added to the reactors were added while Ar was blowing for all air-free chemical reactions. All other materials were used as received.

#### 3.3.2. $\omega$ -Hydroxyl-polystyrene (S-OH)

S-OH was prepared as described previously<sup>15, 20</sup> using anionic polymerization of polystyrene followed by quantitative hydroxyl functionalization using ethylene oxide. SEC (THF, PS std):  $M_n=8390 \text{ g mol}^{-1}$ ,  $M_w=8660 \text{ g mol}^{-1}$ ,  $M_w/M_n=1.03$ .  $\delta\text{H}$  (300MHz,  $\text{CDCl}_3$ ): 6.20–7.26 (br,  $-(\text{C}_6\text{H}_5)$ ), 3.2–3.5 (m,  $-\text{CH}_2\text{OH}$ ), 0.84–2.60 (br,  $-\text{CH}(\text{C}_6\text{H}_5)\text{CH}_2-$ ,  $\text{CH}_3\text{CH}(\text{CH}_2\text{CH}_3)-$ ,  $-\text{CH}_2\text{CH}_2\text{OH}$ ), 0.5–0.78 (m,  $\text{CH}_3\text{CH}(\text{CH}_2\text{CH}_3)-$ ).

### 3.3.3. $\omega$ -Hydroxyl-polystyrene-b-poly(ethylene oxide) (SO-1, SO-1.6, SO-2.3)

SO-1, SO-1.6 and SO-2.3 were prepared as described previously<sup>15</sup> by treating different amounts of S-OH (SO-1: 3.71g, 0.442 mmol; SO-1.6: 0.6g, 0.072mmol; SO-2.3: 1.128g, 0.134mmol) with potassium naphthalenide to generate the alkoxide macroinitiator and adding ethylene oxide (SO-1: 29.9 grams, 0.679 mol; SO-1.6: 11.1g, 0.252 mol; SO-2.3: 21.6g, 0.488mol, 0°C) accordingly. For SO-1, Yield 32.4 g, 96.4%. SEC (THF, PS std.):  $M_w/M_n=1.026$ ,  $M_n=84380 \text{ g mol}^{-1}$  (calculated using <sup>1</sup>H-NMR and SEC measured S-OH  $M_n$ ). For SO-1.6, Yield 7.27g, 63.0%. SEC (THF, PS std.):  $M_w/M_n=1.040$ ,  $M_n=129658 \text{ g mol}^{-1}$  (calculated using <sup>1</sup>H-NMR and SEC measured S-OH  $M_n$ ). For SO-2.3, Yield 20.16g, 89.1%. SEC (THF, PS std.):  $M_w/M_n=1.148$ ,  $M_n=183201 \text{ g mol}^{-1}$  (calculated using <sup>1</sup>H-NMR and SEC measured S-OH  $M_n$ ).  $\delta$ H (400MHz, CDCl<sub>3</sub>): 6.20-7.26 (br, -C<sub>6</sub>H<sub>5</sub>), 3.1-4.0 (br, -CH<sub>2</sub>CH<sub>2</sub>O-, -CH(C<sub>6</sub>H<sub>5</sub>)CH<sub>2</sub>CH<sub>2</sub>O), 1.0-2.30 (br, -CH<sub>2</sub>CH(C<sub>6</sub>H<sub>5</sub>)-, CH<sub>3</sub>CH(CH<sub>2</sub>CH<sub>3</sub>)-, -CH(C<sub>6</sub>H<sub>5</sub>)CH<sub>2</sub>CH<sub>2</sub>O-), 0.5-0.78 (m, CH<sub>3</sub>CH(CH<sub>2</sub>CH<sub>3</sub>)-).

### 3.3.4. Polystyrene-b-poly(ethylene oxide)-b-polystyrene (SOS-1, SOS-1.6, SOS-2.3)

SOS-1, SOS-1.6 and SOS-2.3 were prepared as described previously<sup>15</sup> in which the alkoxide forms of SO-X diblock copolymers were coupled using dibromoxylene as a coupling agent. Crude reaction products included both SOS-Y triblock and residual SO-X diblock copolymer. Yields: 98+ % (containing SOS-Y and undesired SO-X).  $\delta$ H (400MHz, CDCl<sub>3</sub>): 6.20-7.26 (br, -C<sub>6</sub>H<sub>5</sub>), 3.1-4.0 (br, -CH<sub>2</sub>CH<sub>2</sub>O-, -CH(C<sub>6</sub>H<sub>5</sub>)CH<sub>2</sub>CH<sub>2</sub>O), 1.0-2.30 (br, -CH<sub>2</sub>CH(C<sub>6</sub>H<sub>5</sub>)-, CH<sub>3</sub>CH(CH<sub>2</sub>CH<sub>3</sub>)-, -CH(C<sub>6</sub>H<sub>5</sub>)CH<sub>2</sub>CH<sub>2</sub>O-), 0.5-0.78 (m, CH<sub>3</sub>CH(CH<sub>2</sub>CH<sub>3</sub>)-).

### 3.3.5. Fractionation

SOS-Y was isolated through fractionation of the crude product using chloroform/*n*-hexane as a solvent/non-solvent pair. The crude product was dissolved in chloroform in a beaker (1 wt% solution) and heated to 40 °C. *n*-hexane was added slowly to the slowly stirring polymer solution held at 40 °C until first detection of cloudiness. At that point stirring was stopped and the beaker was covered to prevent loss of solvent. After several hours, the solution formed two separate layers. The upper layer was slowly decanted into another container leaving the sticky bottom layer behind. Both layers were redissolved, concentrated, and recovered through precipitation in pentane. Samples from both layers were characterized using SEC. Fractionation solutions were maintained above 40 °C to avoid solvent induced crystallization of PEO.<sup>11</sup> Several fractionations were typically repeated until the bottom layer contained 98% SOS-Y.

### 3.3.6. SO/SOS blend formation

Each sample was prepared by solution blending (0.2 g polymer per mL CHCl<sub>3</sub>). The polymer mixtures were then freeze-dried using an ethanol/liquid nitrogen slush bath, and dried under vacuum at room temperature for at least 24 hours.

### 3.3.7. Polymer disk formation

Polymer disks of 8mm in diameter and about 0.9 mm thick were melt pressed (Carver Press) using a stainless steel mold sandwiched between two pieces of Teflon<sup>®</sup> coated Kapton<sup>®</sup> sheets. The disks were held under a constant pressure of 500 psi at 150 °C for approximately 5 minutes before being removed. After cooling slowly to room temperature, the vitrified polymer

disks were removed from the mold. The diameters and thicknesses of the disks were recorded for subsequent swelling experiments.

### **3.3.8. Swelling to equilibrium**

Polymer disks were immersed in 125mL of DI water (sealed jars) for at least 24 hours to ensure swelling equilibrium was reached. The jars were then placed in a large thermostated water bath held at the appropriate temperature (10 °C, 20 °C, 30 °C, 40 °C and 50 °C) for at least eight hours before any measurements were conducted on the hydrogels.

### **3.3.9. Molecular characterization**

Size exclusion chromatography (SEC) was performed on a Viscotek GPC-Max chromatography system fitted with three 7.5 ×340 mm Polypore<sup>TM</sup> (Polymer Laboratories) columns in series, an Alltech external column oven, and a Viscotek differential refractive index (RI) detector. S-OH molecular weight and polydispersity, and the polydispersity of the SO and SOS samples were determined using a THF (40 °C) mobile phase (1mL min<sup>-1</sup>) with PS standards (Polymer Laboratories). <sup>1</sup>H-NMR spectra were collected at room temperature in CDCl<sub>3</sub> on a Varian Inova 400 MHz spectrometer (n=32, delay=30s).

### **3.3.10. Small angle X-ray scattering (SAXS)**

SAXS data were collected on a Rigaku S-Max 3000 High Brilliance 3 Pinhole SAXS system outfitted with a MicroMax-007HFM Rotating Anode (CuK $\alpha$ ), Confocal Max-Flux<sup>TM</sup> Optic, Gabriel Multiwire Area Detector and a Linkham thermal stage. Polymer disks described above were mounted on the thermal stage and heated to 120 °C, then cooled down to 100 °C and kept in vacuum for 120 minutes before exposure.

### **3.3.11. Determination of swelling ratio (Q)**

Hydrogels were removed from solution and quickly placed on a Teflon<sup>®</sup> surface. Excess water was gently blotted from the surface prior to massing. This process was repeated four times. Hydrogels were returned to their thermostated DI solutions for at least one hour between each weighing.

### **3.3.12. Hydrogel rheology**

Rheological tests were performed on a TA Instruments ARES rheometer with a customized recirculating bath fixture. In this test setup, an infinite lower plate (63 mm stainless steel) served as the bottom of an integrated glass cup, and the temperature of the lower plate was controlled by recirculating fluid through the base. Hydrogel samples at the desired equilibrated temperature were taken directly from the jars, blotted and placed at the center of the lower plate held at the same temperature. The hydrogels were compressed to their 90% of their equilibrium thicknesses to ensure good contact (no slip) between the hydrogel surface and parallel plates. Dynamic frequency sweeps (oscillatory shear) were performed for each sample using a 0.2-5.0 % shear strain (verified linear viscoelastic region) over a frequency range of 0.1 to 100 rad s<sup>-1</sup>.

## **3.4. Results and discussion**

### **3.4.1. Block copolymer synthesis**

The syntheses of all SO diblock and SOS triblock copolymers were carried out using basic anionic polymerization techniques according to a previously reported multi-step protocol.<sup>15,20</sup> The initial synthesis of a hydroxyl terminated polystyrene homopolymer was carried out in bulk quantities such that all subsequent diblock copolymers could be synthesized

from the same S-OH macroinitiating chain homopolymers. Coupling of SO diblock copolymer was used to generate SOS triblock copolymer, ensuring the symmetry of the block distribution with respect to the PS chain ends. The S-OH macroinitiator for all three SO-Y diblock copolymers was synthesized with a molecular weight of 8390 Da (SEC, PS standards) targeted to ensure a glass transition temperature above the PEO crystallization temperature ( $T_{m, PEO} \sim 65 \text{ }^\circ\text{C}$ ,  $T_{g, PS} \sim 80 \text{ }^\circ\text{C}$ , Appendix).<sup>21</sup>

This design criterion was enforced such that PS spherical domains assembled in the melt-state would have a chance to vitrify prior to the onset of PEO crystallization during sample cooling. Given the strong dependence of PS glass transition temperature on molecular weights below 10 kDa, the realistic lower limit for PS in these studies is in the 8 kDa range. This lower limit, in turn, dictates the formation of very large SO block copolymer molecules. That is, the consequence of utilizing the BCP spherical morphology is that very asymmetric molecules with low PS volume fractions ( $f_{PS} = 0.08 - 0.13$ ) are required.<sup>22,23</sup> To reach this level of asymmetry, the PEO block has to be very large (Table 3.1), even for 8 kDa PS blocks. Three SO diblock copolymers were synthesized: SO-1, SO-1.6, and SO-2.3. SO-1 was synthesized to be the majority component in all SO-1/SOS-Y blends used in this study (Figure 3.1), and as the coupling precursor to the SOS-1 triblock copolymer. SO-1.6 and SO-2.3 were synthesized simply as precursors to triblock copolymers SOS-1.6 and SOS-2.3. The molecular weights of the SO-Y diblock copolymers spanned the range of 76000 to 175000 g mol<sup>-1</sup> in this study. SEC of all SO-X diblock copolymers showed the absence of S-OH homopolymer, confirming quantitative initiation from the alkoxide of the S-OH homopolymer. The molecular weights and volume fractions were calculated from <sup>1</sup>H-NMR peak integrations in combination with the known S-OH molecular weight established using SEC. Molecular weight distributions for both

**Table 3.1. Block copolymer characterization data**

Sample Names	$M_n$ (g/mol) <sup>a</sup>	$M_{n,PS}$ (g/mol)	$M_{n,PEO}$ (g/mol) <sup>d</sup>	$f_{PS}$ <sup>e</sup>	PDI <sup>b</sup>
SO-1	84390	8390 <sup>b</sup>	76000	0.11	1.03
SO-1.6	129690	8390 <sup>b</sup>	121300	0.07	1.04
SO-2.3	183190	8390 <sup>b</sup>	174800	0.05	1.15
SOS-1	168780	16780 <sup>c</sup>	152000	0.11	1.10 <sup>f</sup>
SOS-1.6	259280	16780 <sup>c</sup>	242500	0.07	1.08 <sup>f</sup>
SOS-2.3	366380	16780 <sup>c</sup>	349600	0.05	1.08 <sup>f</sup>

<sup>a</sup> The sum of the calculated PS and PEO molecular weights. <sup>b</sup> Determined from GPC (THF, PS std.). <sup>c</sup> Accounts for both PS chain ends. <sup>d</sup> Calculated from <sup>1</sup>H-NMR in combination with  $M_n$  of PS. <sup>e</sup> Volume fraction of PS, based on <sup>1</sup>H-NMR and nominal densities at 140 °C ( $\rho_{PS}=0.969$ ,  $\rho_{PEO}=1.064$  g/cm<sup>3</sup>).<sup>24</sup> <sup>f</sup> PDI of the fractionated SOS triblock copolymers.

SO-1 and SO-1.6 diblock copolymers were very narrow as expected from the living chain kinetics of anionic polymerization. ( $PDI_{SO-1} = 1.03$  and  $PDI_{SO-1.6} = 1.04$  for SO-1.6). The polydispersity of SO-2.3 was slightly elevated, ( $PDI=1.15$ ), a result that is consistent with the anionic polymerization of higher molecular weight PEO in THF solvent. This observation has been correlated to the changing solubility and equilibrium dynamics involving propagating species of differing ion pair associations, as molecular weights increase.<sup>25</sup> We have found lowering the polymer concentration in the reaction solution can improve PDI values. SOS-Y triblock copolymers were synthesized from coupling the corresponding SO-Y diblock copolymers, first forming the potassium alkoxide of the SO diblock copolymer and then using dibromoxylene (DBX) as a coupling agent. Coupling efficiencies were variable in the range of 44 - 84 wt%, but generally consistent with those traditionally achievable in large molecular weight systems.<sup>26</sup> The crude coupling reaction product contained both SOS triblock copolymer

and partially reacted or unreacted SO diblock copolymer. Fractionation was used to isolate each of the triblock copolymers, SOS-1, SOS-1.6 and SOS-2.3 from their crude reaction mixtures. Fractionation was performed using chloroform/*n*-hexane as the solvent/non-solvent pair. Non-solvent addition was carried out holding the polymer solution at or above 40 °C to avoid (non)solvent-induced PEO crystallization. Previously reported to occur around 35 °C in chloroform/*n*-hexane solutions, such crystallization triggers generalized precipitation which is non-selective for SOS triblock copolymer.<sup>27</sup> The fractionation procedure was repeated multiple times to reduce SO-Y content to less than 2 wt%. Data from repeated fractionations of SOS-1 are shown in Figure 3.2. The original coupling reaction yielded approximately 84 wt% SOS-1, as shown in Figure 2a. Figure 3.2b, 3.2c and 3.2d represent the SEC traces of the fractionation product (bottom layer) collected after the first, second, and third fractionations. Fractionation of SO-1.6 and SO-2.3 produced similar results after a slightly larger number of fractionation cycles. Molecular weights and compositions of the isolated SOS-Y triblock copolymers remained consistent with the coupling of the SO-X diblock copolymers, as shown in Table 3.1. Interestingly, the fractionation decreased the PDI of triblock copolymer SOS-2.3 as compared with diblock copolymer SO-2.3, a likely result of both favorable coupling statistics and the subsequent fractionation processes.

### **3.4.2. Characterization of SO/SOS blends**

The series of SOS-Y<sub>x</sub> blends were prepared using simple solution blending in chloroform, with SOS-Y denoting the tether type and x representing the molar concentration (in mol%) of SOS-Y triblock copolymer in the sample. For each of the three SO-1/SOS-Y combinations outlined in Figure 3.1, blends were produced with 3.0, 5.0, 10.0, and 15.0 mol% SOS-Y. Importantly, in blends formed from the SO-1/SOS-1 pairing, the volume fraction of PS

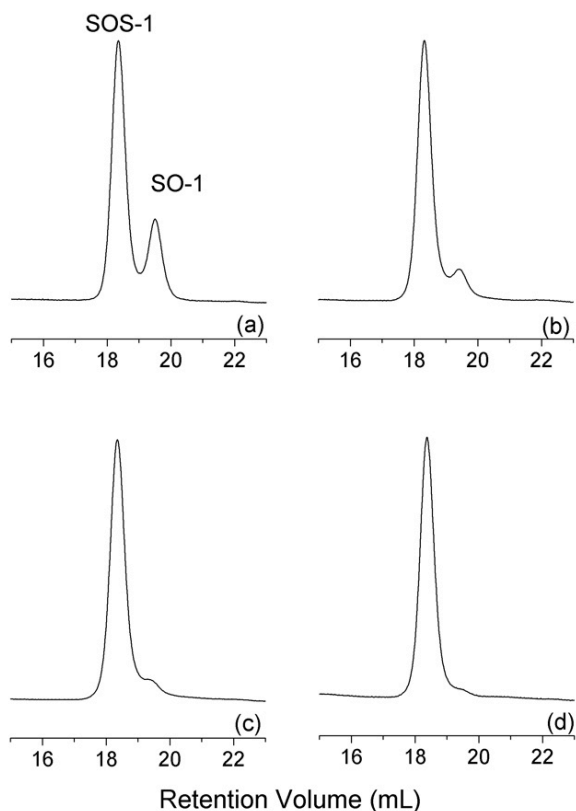


**Figure 3.2. SEC data (in THF) from fractionation of the SOS-1 coupling reaction product. (a) Crude reaction product showing initial coupling efficiency. (b) First fractionation product (bottom layer). (c) Second fractionation product (bottom layer). (d) Third fractionation product (bottom layer).**

$f_{PS}$ ) remains constant regardless of SOS-1 content, a consequence of the matched compositions of SO-1 and SOS-1. However, in blends formed from SO-1/SOS-1.6 or SO-1/SOS-2.3, the reduced PS content in the SOS component acts to lower the overall  $f_{PS}$ , relative to the matched SO-1/SOS-1 pair. This was of particular concern for the higher SOS-Y loadings, as a diminishing  $f_{PS}$  in the blends could begin to disfavor phase separation into the sphere-based morphology, a necessary constraint for tethered micelle network formation. Table 3.2 shows the  $f_{PS}$  values for each of the blends, which were ultimately maintained between 0.08 and 0.11.

**Table 3.2. Chemical and melt-state morphological characterization data of block copolymer blends**

Sample	Diblock	Tether type	Tether added (mol%)	$f_{PS}$	Percus-Yevick hard sphere model				
					$R_c^a$ /nm	$\phi_c^b$	$\theta_{PS}^c$	$R_{hs}^d$ /nm	$\phi_{hs}^e$
SOS-1_3	SO-1	SOS-1	3.0	0.11	9.2	0.097	227	16.6	0.57
SOS-1_5			5.0	0.11					
SOS-1_10			10.0	0.11					
SOS-1_15			15.0	0.11	9.4	0.099	242	16.7	0.56
SOS-1.6_3	SO-1	SOS-1.6	3.0	0.11	9.7	0.109	283	16.9	0.58
SOS-1.6_5			5.0	0.10					
SOS-1.6_10			10.0	0.10					
SOS-1.6_15			15.0	0.10	9.1	0.078	220	17.8	0.58
SOS-2.3_3	SO-1	SOS-2.3	3.0	0.10	9.7	0.104	283	16.8	0.54
SOS-2.3_5			5.0	0.10					
SOS-2.3_10			10.0	0.09					
SOS-2.3_15			15.0	0.08	9.5	0.082	250	17.4	0.50

<sup>a</sup> Micelle core radius, <sup>b</sup> Micelle core overall volume fraction,  $\phi_c = (R_c/R_{hs})^3 \phi_{hs}$ , based on the PY parameters, <sup>c</sup> Mean aggregation number (i.e., PS chains per sphere), based on the PY parameters, <sup>d</sup> apparent hard sphere radius, <sup>e</sup> hard sphere volume fraction.

While these values of  $f_{PS}$  were within the typical bounds for sphere formation in block copolymer melts,<sup>22,23</sup> we chose to verify phase separation and spherical domain formation for all samples using SAXS. A subset of the SAXS results are plotted in Figure 3.3a. Data for two blends, containing the lowest (3.0 mol%) and highest (15.0 mol%) SOS-Y amounts, are presented for each SO-1/SOS-Y combination. Notably, all blends share a common scattering profile which includes a prominent principal scattering peak at low values of the scattering wave

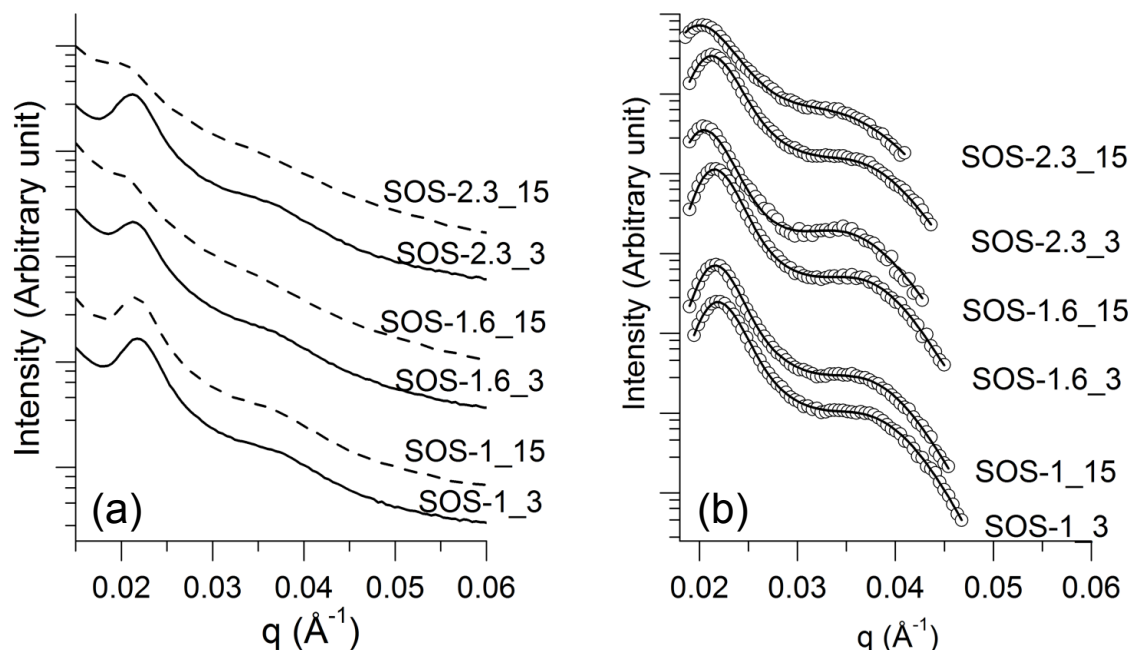


**Figure 3.3.** SAXS data for melts (100 °C) of SOS-1\_3, SOS-1\_15, SOS-1.6\_3, SOS-1.6\_15, SOS-2.3\_3 and SOS-2.3\_15 samples. **Figure 3b.** Background subtracted SAXS data (open circles) for SOS-1\_3, SOS-1\_15, SOS-1.6\_3, SOS-1.6\_15, SOS-2.3\_3 and SOS-2.3\_15 samples overlaid with nonlinear least square fits (solid line) to the Percus-Yevick hard sphere model for systems with liquid-like disorder.

vector  $q$ , followed by a less pronounced second hump at higher  $q$  values. This scattering signature is prototypical of sphere-forming block copolymer systems for which the packing structure of the micelle-like spherical domains can be described as "liquid-like". That is, due to the kinetic constraints associated with high molecular weight entanglements and limited macromolecular diffusion rates, these sphere-forming systems fail to develop a true bcc lattice that is typical in smaller molecular weight block copolymer systems.<sup>17</sup> Simple comparisons of the relative positions of the principal scattering peaks in each of these samples reveals the qualitative impact of adding unmatched SOS triblock copolymer to the SO-1/SOS-Y blends.

Inspection of the matched SO-1/SOS-1 SAXS data shows that blends containing 3 mol% and 15 mol% SOS-1 give very nearly identical scattering, suggesting small amounts of matched

triblock copolymer are largely inconsequential to the domain spacing produced during phase separation. This similarity is expected given the invariance of the blend composition to SOS-1 addition and the intrinsically matched lattice dimensions of the SO-1 and SOS-1 species in the self-assembled state. In contrast, increasing the amount of *unmatched* SOS-Y triblock copolymer in a blend with SO-1 does appear to have some influence on the characteristic dimensions of the system once the concentration is high enough. At only 3 mol% SOS-1.6 or SOS-2.3, the additional PEO contributed by the SOS-Y is small and the characteristic dimensions are still dominated by SO-1. These systems still appear to structurally mimic the SO-1/SOS-1 blends. However, when the amount of SOS-1.6 or SOS-2.3 was increased to 15 mol%, the principal scattering peaks of both melt blends shifted to smaller  $q$  values (from  $\sim 0.022 \text{ \AA}$  to  $\sim 0.021 \text{ \AA}$ ), indicating the increased PEO midblock molecular weights contributed by the SOS-Y triblock copolymer is pushing the average distance between PS cores to larger values. The exact source of this increase is impossible to characterize from the shift alone. That is, such a shift may be simply a result of the system expanding to accommodate the increase in PEO, but it may also be the result of a new thermodynamic preference to reorganize into PS cores of much higher aggregation number.

The scattering intensity for sphere forming systems can be expressed as a mathematical function which is proportional to the product of the form factor  $P(q)$ , which describes the intraparticle correlations, and the structure factor,  $S(q)$ , which describes the interparticle correlations. We were able to model the scattering data from these six data sets using  $P(q)$  for polydisperse solid spheres coupled with  $S(q)$  given by the Percus–Yevick (PY) model<sup>28</sup> for hard sphere liquids. Analysis of each of these data sets using fits to Percus-Yevick (PY) model adapted for polydisperse hard sphere liquids sheds a bit of light on the basic structural details of

the liquid-like packing (LLP) of micelles in the melt state, and perhaps the origin of the principal peak shift upon addition of unmatched SOS-Y triblock copolymer to SO-1 blends.

The details of the PY model used to fit the SAXS data have been described in detail in our previous publication,<sup>15</sup> and by others.<sup>29-32</sup> Figure 3.3b gives the background subtracted SAXS data for the six blend samples, overlaid with nonlinear least squares fits to the adapted PY model. The values of the key physical parameters producing these fits are given in Table 3.2.

At the heart of PY model is the hard sphere radius,  $R_{\text{hs}}$ , and the hard sphere volume fraction,  $\phi_{\text{hs}}$ .  $R_{\text{hs}}$  corresponds to the apparent radius over which the micelle acts as a hard sphere relative to other micelles, and therefore extends beyond the PS core to include a significant fraction of the dense PEO corona. The overall volume fraction of the sample occupied by these hard sphere constructs is then given by  $\phi_{\text{hs}}$ .  $R_{\text{hs}}$  is related to the average spacing between micelle domains, and  $\phi_{\text{hs}}$  provides information about how efficiently packed the micelles are. For example, hard spheres packed on a simple cubic lattice would produce a maximum packing fraction of  $\phi_{\text{hs}} = 0.52$ . A bcc lattice would produce  $\phi_{\text{hs}} = 0.68$ . Additionally, from the PY fit we are able to extract the radius of PS domains comprising the micelle core,  $R_{\text{c}}$ , and the volume fraction of PS in those micelle cores,  $\phi_{\text{c}}$ . Deviations between the true PS volume fraction,  $f_{\text{PS}}$ , and  $\phi_{\text{c}}$  are typically associated with the presence of free PS chain ends in the system.

Application of the PY model to the six blends shows the radii of the PS micelle cores,  $R_{\text{c}}$ , to vary over an particularly small range, bounded between 9.1 and 9.7 nm. These values lead to aggregation numbers in the mid 200's, as expected for spherical aggregates produced through melt-state self-assembly. Importantly, the model fit predicts micelle core volume fractions,  $\phi_{\text{c}}$ , that are very close to  $f_{\text{PS}}$  for each system, confirming the vast majority of the PS chain ends are

likely phase segregated into the micelle cores. In addition, the apparent hard sphere radii,  $R_{hs}$ , for matched blends SOS-1\_3 and SOS-1\_15, and the unmatched blends of lowest SOS-Y content, SOS-1.6\_3 and SOS-2.3\_3, are remarkably similar, falling in the 16.6-16.9 nm range. This is consistent with the coherence of the principal peak positions in the SAXS data for these four blends. Likewise, in the unmatched blends of highest SOS-Y content, SOS-1.6\_15 and SOS-2.3\_15, the hard sphere radii increase to 17.8 and 17.4 nm, respectively. This increase, which is consistent with the shift in the principal scattering peak to lower  $q$  values, suggests the impact of the additional PEO in the added tethers is to swell the size of the coronal layer, albeit by just a small fraction. Finally, it is noteworthy that the hard sphere volume fractions,  $\phi_{hs}$ , with the exception of the SOS-2.3\_15 sample (0.50), all fall above the packing efficiency of a simple cubic system (0.52). While these values (0.54 – 0.58) remain substantially below that of the bcc lattice (0.68) adopted by smaller molecular weight systems, their packing efficiency suggests these systems still act as relatively organized liquids.

### **3.4.3. Equilibrium swelling behavior**

Polymer disks formed from each blends were swollen in water over a 24 hour period to ensure equilibrium was reached. Each hydrogel (12 samples in total) was weighed gravimetrically over 10 °C increments from 10 °C to 50°C. The weights were measured four times for each hydrogel, to account for measuring errors associated with blotting to remove excess water. After each measurement, hydrogels were placed back in DI water and returned to a thermostatted water bath for at least one hour before the next measurement was performed. This was done to minimize error associated with losses due to evaporation or over-blotting during measurement. The equilibrium water content is defined by the swelling ratio,  $Q$ :

$$Q = \text{Equilibrium water content} = \frac{\text{Weight}_{\text{hydrogel at equilibrium}} - \text{Weight}_{\text{dry polymer disc}}}{\text{Weight}_{\text{dry polymer disc}}} \quad (2)$$

Figure 3.4a-c shows the equilibrium water content for each hydrogel at 10 °C, 30°C and 50°C, organized by the SOS-Y triblock copolymer used in the blend. The results of equilibrium water content for hydrogels at 20 and 40 °C have been excluded for clarity. Globally speaking, as the temperature increased from 10 °C to 50 °C, about a 30 -35% decrease in the water content was observed for all hydrogels. This is simply a result of the decreasing solubility of PEO in water with increasing temperature. Also, with increased concentration of SOS-Y from 3 to 15 mol%, about a 40 - 45 % decrease in the water content could be achieved. This is a direct result of the increased number of entanglements between the tethering midblocks of the bridging SOS triblock copolymer molecules, which scales with their concentration. Importantly, this behavior was across hydrogels from all SO-1/SOS-Y combinations investigated, and is consistent with the behavior observed in previous pre-structured hydrogels systems studied by our group.<sup>15, 17</sup>

However, the impact of lengthening the tethering PEO midblock on the quantity of water absorbed by the hydrogel under equilibrium swelling conditions was rather remarkable. When the PEO midblock molecular weight was increased to 1.6 times (SOS-1.6\_x hydrogels, Figure 3.4b) the molecular weight of the matched system (SOS-1\_x hydrogels, Figure 3.4a), swelling ratios of samples at identical SOS concentrations confirmed increases in water content from 65 to 80 wt%. Interestingly, if the swollen dimensions of the hydrogel were determined solely by the tether adopting its preferred coil size in the presence of a theta solvent, we would expect a molecular weight increase of 1.6 times to coincide with the approximate doubling of the swelling ratio (100% increase). That these systems are able to achieve a considerable fraction of that given the constrained environment (entanglements with other tethers, fixed ends) inherent to

these tethered micelle networks is quite impressive. Even at SOS loadings of 15 mol%, the additional swelling is consistently in this range. Rough estimates suggest the linear expansion of the hydrogel scales with the tether length to 0.35 – 0.42 power (cf. with 0.5 for a coil in a theta solvent), although the swelling results from the SOS-2.3 blends suggest the application of that power law may have limitations.

As shown in Figure 3.4c, an additional increase in the tether molecular weight to 2.3 times (SOS-2.3\_x hydrogels) that of the matched system has a substantially different impact on the swelling of the hydrogel. The large increase in tether length does not continue to increase the equilibrium swelling ratio, but instead produces swelling capabilities comparable to that exhibited by the original SO-1/SOS-1 hydrogel blends. In fact, the swelling behavior at each concentration of SOS-2.3 was almost identical to the matched system at each temperature tested.

We believe these curious results can be interpreted using the organizational concepts outlined in Figure 3.5. For tethers of matched, or 1.6 times matched, molecular weights, the preferred melt-state conformation of the midblocks restrict bridging to nearest neighbor micelles only. As a result, the longer tether length can act to expand the inter-sphere distance during swelling. However, the increase to 2.3 times is sufficient to enable some fraction of the SOS-2.3 triblock copolymers to bridge into micelles occupying the shell of second nearest neighbors. Those chains in particular then act to restrict swelling to a state that more closely resembles the original capabilities of the matched SO-1/SOS-1 system. It is not clear at this point what tether length is sufficient to permit bridging to the second shell of nearest neighbors, whether the fraction of chains bridging to second shell matters, whether the transition to matched system swelling behavior is sharp or gradual in nature. Polydispersity in the mid-block is likely critical in the determination any of these swelling characteristics.

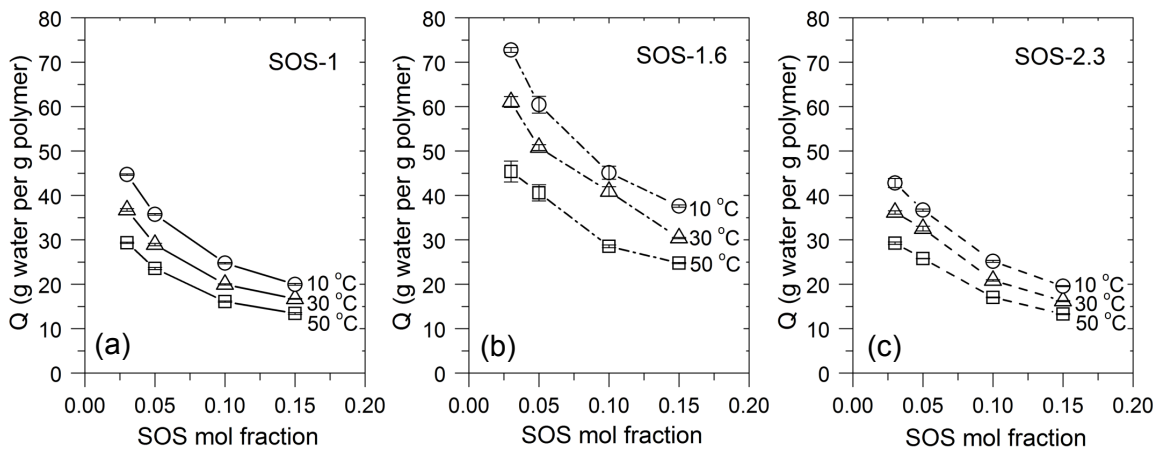


Figure 3.4. Equilibrium water content for combinations of SO-1 with (a) SOS-1, (b) SOS-1.6, and (c) SOS-2.3 at 10, 30 and 50 °C. All values determined gravimetrically. Error bars denote standard deviations from four measurements.

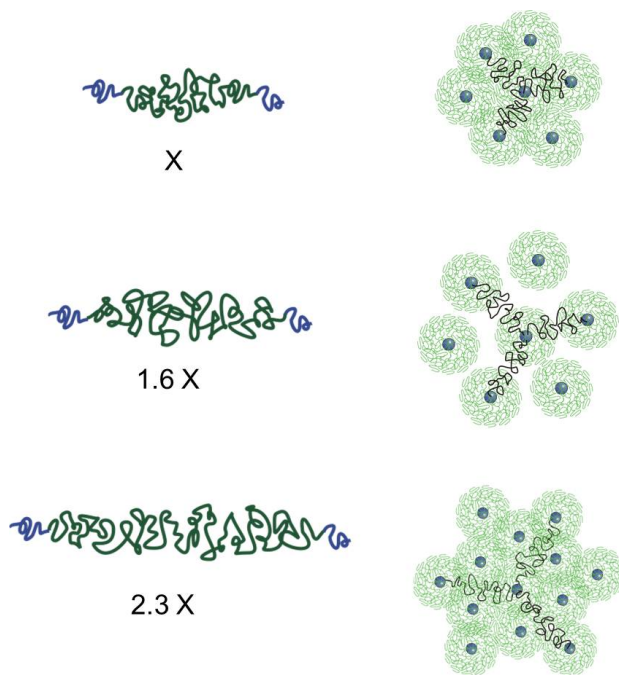
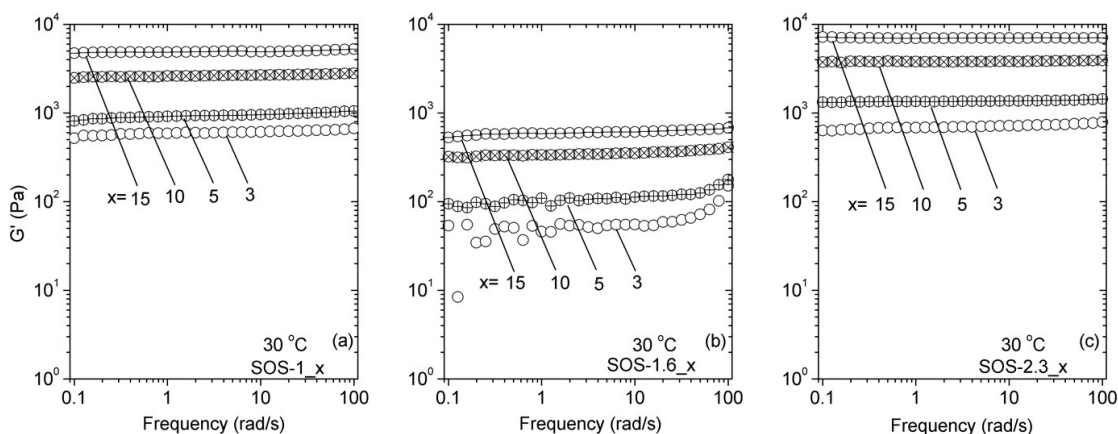


Figure 3.5. Proposed mechanism. When midblock size is 1X to 1.6X, the SOS triblock copolymers bridge only to the first shell of nearest neighbor micelles. Once the midblock molecular weight is increased to 2.3X, the SOS triblock copolymers are able to bridge into the second shell of nearest neighbor micelles.

#### 3.4.4. Impact on mechanical properties

The mechanical response of each hydrogel under dynamic oscillatory shear at 30 °C is presented in Figure 3.6a-c. Small strain values (0.2 - 5.0%) in the linear viscoelastic region were used to eliminate slip at the hydrogel-platen interface. Elastic moduli ( $G'$ ) for each hydrogel are plotted versus angular frequency in the range of 0.1 rad/s to 100 rad/s. As the plots show, the elastic moduli for all hydrogels at 30 °C were independent of frequency over the entire range tested. The impact of increasing the tether molecular weight from matched to 1.6 times matched is immediately evident, and quite dramatic. At equivalent concentrations of SOS triblock copolymer, increasing the tether length 1.6 times matched decreases the elastic modulus by almost a full order of magnitude. This substantial decrease has several implications concerning the origin of the elastic modulus in these tethered micelle networks. Clearly, the concentration of tethering molecules in and of itself is not the factor determining the magnitude of the  $G'$ , given the equivalence in concentrations between the two systems. However, coupling this precipitous drop in modulus with the swelling data suggests that the proximity of the micelles in the network is critical in the determination of mechanical response. That is, when the tether lengths are matched in the system, the degree of coronal layer overlap is high, and the chain interactions (dynamic entanglements, e.g.) between those coronal layers dictates a majority of the elastic response (under small strain oscillation, at least). A comparison of the elastic moduli between hydrogels containing 15 mol% SOS-1 (4.8 kPa) and SOS-1.6 (0.51 kPa) suggests that nearly 89% of the modulus (at least) originates from coronal layer interactions. This percentage assumes there is no residual coronal overlap still contributing to the elastic modulus in the SOS-1.6\_15 sample. If that is untrue, this percentage may be even higher. Interestingly, the majority of chains comprising the coronal brush layer of PEO surrounding the PS core would be



**Figure 3.6. Dynamic frequency sweeps for hydrogels based on combinations of SO-1 with (a) SOS-1, (b) SOS-1.6, and (c) SOS-2.3 at 30 °C. 'x' denotes the mol% SOS-Y triblock copolymer in the network.**

dangling ends in standard network nomenclature. Often, small concentrations of dangling ends are ignored because they have minimal influence on the mechanical properties of the network. However, in these tethered micelle systems, the concentration (and molecular weights) of these dangling ends is so high that their interactions actually dominate the mechanical behavior of the network.

Comparison with the SOS-2.3<sub>x</sub> hydrogels appears to be consistent with the hypothesis put forward in Figure 3.5. As with swelling ratio, the use of the SOS-2.3 tethers produces dynamic elastic properties more reminiscent of the original matched SO-1/SOS-1 system, but in this case displaying about a 50% increase in elastic modulus when compared with matched systems of equal SOS content. We suspect this modest yet significant increase in modulus is correlated to the increased number of neighboring micelles to which each individual PS domain is mechanically correlated (connected) within the network.

Finally, in Figure 3.7 we present the effect of temperature-induced swelling changes on the elastic moduli of the hydrogel systems. Noticeably, there is no particular correlation with temperature that can be decoupled from simple sample-to-sample variation. Importantly, changing temperature (see Figure 3.4) has a significant effect on the water content in the hydrogel, with swelling ratios decreasing by up to 50%. However, the elastic modulus data in Figure 3.7 show that such large changes in water content from *uniform* expansion or contraction of the system do not influence the mechanical response to shear strain. It seems clear that while water intake does, for example, dilute the overall polymer concentration in the system, the simultaneous expansion of both the tethers and PEO coronal layers leaves the number of chain interactions between overlapping micelles essentially constant. We believe the significance of this data is that it underscores the minimal effects of water content, in and of itself, as a major contributor to the mechanical response of tethered micelle networks, and supports the contention that coronal layer overlap, for which temperature changes have very little effect, is the dominant factor in determining the dynamic mechanical response of these systems.

These results further emphasize the versatility of using melt-state pre-structuring of tethered micelle networks as platforms for mechanically robust, tunable hydrogel systems. The data presented show that through a simple combination of tether concentration and tether length, the mechanical properties of the resultant tethered micelle network can be tuned across a very significant range. The key is that both serve as simple knobs through which the coronal layer overlap in the system can be tuned. Furthermore, the tethered micelle networks fabricated in this manner appear to have mechanical properties that are largely invariant over the temperature ranges examined here. Obviously, the reliance on PS vitrification specific to this system has temperature limitations, but such can be overcome through alternate block selection

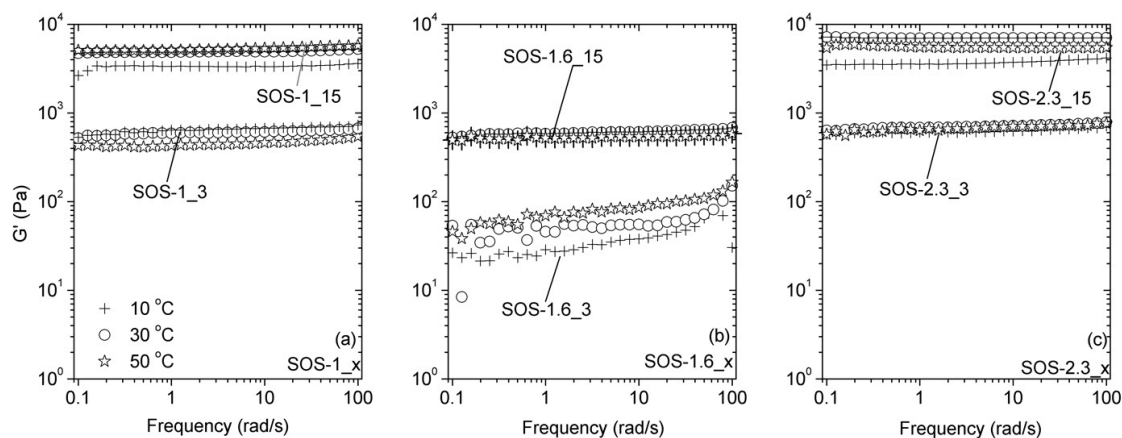


**Figure 3.7. Dynamic frequency sweeps for hydrogels based on combinations of SO-1 with (a) SOS-1, (b) SOS-1.6, and (c) SOS-2.3 at 10, 30, and 50 °C. Data only for hydrogels containing 3 mol% and 15 mol% SOS-Y triblock copolymer in the network are shown.**

and the use of chemical crosslinking.<sup>17</sup> Notably, such control over mechanical properties is simply not possible using traditional solution-based assembly of tethered micelle networks.

### 3.5. Conclusions

In this report we used tethering molecules of different lengths to extend our understanding of mechanical property control in tethered micelle networks. The work is based on the use of a previously published solvent-free fabrication methodology exploiting the melt-state self-assembly of (lattice matched) sphere-forming SO diblock and SOS triblock copolymer blends. Importantly, solvent-free pre-structuring of tethered micelle networks via this approach is capable of producing highly elastic and mechanically robust hydrogel systems not typically possible using solution assembly techniques. By introducing SOS triblock copolymer with PEO midblocks that were 1.6 times that of the lattice matched system, we were able to increase swelling ratios by 65 to 80% (up to 73 g H<sub>2</sub>O/g polymer), and effectively eliminate coronal layer overlap between adjacent micelles. In doing so, we were able to establish coronal layer overlap

as the primary contributing factor (at least 90%) in determining the dynamic elastic moduli exhibited by the matched systems. Extending the tether length to 2.3 times, in contrast, produced swelling and coronal layer overlap identical to the lattice matched system. We hypothesize that tethering molecules of that length are able to bridge into the second shell of nearest neighbor micelles, precluding any increased swelling capabilities and reproducing the overlap present in the matched system. Notably, we were able to show that either tether concentration or tether length can be used to provide control over coronal layer overlap, and provide avenues through which the system mechanical properties can be tuned. We contend such accurate control over mechanical properties is simply not possible using traditional solution-based assembly of tethered micelle networks.

### **3.6. Recognitions**

This work was supported by the National Science Foundation (DMR-0645781) and the Colorado State University.

### 3.7. References

- [1] B. Jeong, Y. H. Bae, D. S. Lee, and S. W. Kim, "Biodegradable block copolymers as injectable drug-delivery systems," *Nature*, vol. 388, pp. 860-862, 1997.
- [2] Y. T. Yinghua Ma, Norman C. Billingham, Steven P. Armes, Andrew L. Lewis, "Synthesis of Biocompatible, Stimuli-Responsive, Physical Gels Based on ABA triblock copolymers," *Biomacromolecules*, vol. 4, pp. 864-868, 2003.
- [3] Y. Qiu and K. Park, "Environment-sensitive hydrogels for drug delivery," *Advanced Drug Delivery Reviews*, vol. 53, pp. 321-339, 2001.
- [4] B. Jeong, Y. H. Bae, and S. W. Kim, "Drug release from biodegradable injectable thermosensitive hydrogel of PEG-PLGA-PEG triblock copolymers," *Journal of Controlled Release*, vol. 63, pp. 155-163, 2000.
- [5] C. He, S. W. Kim, and D. S. Lee, "In situ gelling stimuli-sensitive block copolymer hydrogels for drug delivery," *Journal of Controlled Release*, vol. 127, pp. 189-207, 2008.
- [6] S. E. Kirkland, R. M. Hensarling, S. D. McConaughy, Y. Guo, W. L. Jarrett, and C. L. McCormick, "Thermoreversible Hydrogels from RAFT-Synthesized BAB Triblock Copolymers: Steps toward Biomimetic Matrices for Tissue Regeneration†," *Biomacromolecules*, vol. 9, pp. 481-486, 2008.
- [7] K. T. Nguyen and J. L. West, "Photopolymerizable hydrogels for tissue engineering applications," *Biomaterials*, vol. 23, pp. 4307-4314, 2002.
- [8] J. L. Drury and D. J. Mooney, "Hydrogels for tissue engineering: scaffold design variables and applications," *Biomaterials*, vol. 24, pp. 4337-4351, 2003.
- [9] I. K. Kwon and T. Matsuda, "Photo-iniferter-based thermoresponsive block copolymers composed of poly(ethylene glycol) and poly(N-isopropylacrylamide) and chondrocyte immobilization," *Biomaterials*, vol. 27, pp. 986-995, 2006.
- [10] K. A. Aamer, H. Sardinha, S. R. Bhatia, and G. N. Tew, "Rheological studies of PLLA-PEO-PLLA triblock copolymer hydrogels," *Biomaterials*, vol. 25, pp. 1087-1093, 2004.
- [11] T. Fujiwara, T. Mukose, T. Yamaoka, H. Yamane, S. Sakurai, and Y. Kimura, "Novel Thermo-Responsive Formation of a Hydrogel by Stereo-Complexation between PLLA-PEG-PLLA and PDLA-PEG-PDLA Block Copolymers," *Macromolecular Bioscience*, vol. 1, pp. 204-208, 2001.
- [12] K. Park, K. Kim, I. C. Kwon, S. K. Kim, S. Lee, D. Y. Lee, and Y. Byun, "Preparation and Characterization of Self-Assembled Nanoparticles of Heparin-Deoxycholic Acid Conjugates," *Langmuir*, vol. 20, pp. 11726-11731, 2004.
- [13] L. Bromberg, "Scaling of Rheological Properties of Hydrogels from Associating Polymers," *Macromolecules*, vol. 31, pp. 6148-6156, 1998.
- [14] N. Sanabria-DeLong, A. J. Crosby, and G. N. Tew, "Photo-Cross-Linked PLA-PEO-PLA Hydrogels from Self-Assembled Physical Networks: Mechanical Properties and Influence of Assumed Constitutive Relationships," *Biomacromolecules*, vol. 9, pp. 2784-2791, 2008.
- [15] C. Guo and T. S. Bailey, "Highly distensible nanostructured elastic hydrogels from AB diblock and ABA triblock copolymer melt blends," *Soft Matter*, vol. 6, p. 4807, 2010.
- [16] T. Kissel, Y. Li, and F. Unger, "ABA-triblock copolymers from biodegradable polyester A-blocks and hydrophilic poly(ethylene oxide) B-blocks as a candidate for in situ forming hydrogel delivery systems for proteins," *Advanced Drug Delivery Reviews*, vol. 54, pp. 99-134, 2002.

- [17] V. F. Scalfani and T. S. Bailey, "Access to Nanostructured Hydrogel Networks through Photocured Body-Centered Cubic Block Copolymer Melts," *Macromolecules*, vol. 44, pp. 6557-6567, 2011/08/23 2011.
- [18] M. W. Matsen and R. B. Thompson, "Equilibrium behavior of symmetric ABA triblock copolymer melts," *The Journal of Chemical Physics*, vol. 111, pp. 7139-7146, 1999.
- [19] T. P. L. Paul C. Hiemenz, *Polymer Chemistry*, 2 ed.: CRC Press, 2007.
- [20] J. J. M. R. P. Quirk, "Characterization of the functionalization reaction product of poly(styryl)lithium with ethylene oxide," *Part A: Polym. Chem.*, vol. 26, pp. 2031-2037, 1988.
- [21] "Effect of Molecular Weight on Glass Transition by Differential Scanning Calorimetry," *Canadian Journal of Chemistry*, vol. 52, pp. 3170-3175, 1974/09/15 1974.
- [22] F. S. Bates, "Polymer-Polymer Phase Behavior " *Science*, vol. 251, pp. 898-905, 1991.
- [23] M. F. S. F. S. Bates, A. K. Khandpur, S. Foerster, J. H. Rosedale, "Fluctuations, conformational asymmetry and block copolymer phase behaviour," *Faraday Discuss*, vol. 98, pp. 7-18, 1994.
- [24] D. J. L. L. J. Fetters, D. Richter, T. A. Witten, A. Zirkel, *Macromolecules*, vol. 27, 1994.
- [25] D. Baskaran and A. Muller, "Anionic vinyl polymerization—50 years after Michael Szwarc," *Progress in Polymer Science*, vol. 32, pp. 173-219, 2007.
- [26] G. G. Nossarev and T. E. Hogen-Esch, "Living tert-butyllithium initiated anionic polymerization of 2-vinylnaphthalene in toluene-tetrahydrofuran mixtures," *Journal of Polymer Science Part A: Polymer Chemistry*, vol. 39, pp. 3034-3041, 2001.
- [27] H. I. Panagiota G. Fragouli, Nicko Hadjichristidis, "Synthesis and characterization of linear diblock and triblock copolymers of 2-vinyl pyridine and ethylene oxide," *Polymer*, pp. 7141-7144, 2002.

## CHAPTER 4

### IMPROVING TOUGHNESS IN HIGHLY SWOLLEN BLOCK COPOLYMER BASED HYDROGEL NETWORKS<sup>4</sup>

#### 4.1 Summary

This report introduces a unique method of improving hydrogel toughness in an entirely independent manner from equilibrium swelling state in block copolymer-based hydrogel networks. The approach is based on a step-wise installation of two networks, the first during *melt-state* self-assembly of the block copolymer blend, and a second following equilibrium swelling of the primary network. The first determines the equilibrium swelling ratio, while the second determines the ultimate tensile properties of the hydrogel. The hydrogel system described consists of sphere-forming polystyrene-poly(ethylene oxide) (PS-PEO) diblock copolymer which has been pre-blended with small concentrations of polystyrene-poly(ethylene-oxide)-polystyrene (PS-PEO-PS) triblock copolymer. During melt-state self-assembly, the PEO midblock in the PS-PEO-PS triblock copolymer serves to tether adjacent PS spherical aggregates and provides the primary mesh. In a previous report we demonstrated such hydrogels are incredibly elastic, mechanically robust, preserve their shape, and can produce swelling ratios ranging from 3 to 37 g water per g polymer depending on PS-PEO-PS content (3.3 - 72.0 mol%). In this report, we

---

<sup>4</sup> The content of this dissertation chapter have been adapted from a manuscript submitted to *Soft Matter*. Chen Guo and Travis S. Bailey developed and designed the experiments. Chen Guo performed the experiments with Jackson Lewis and Miriah Schwartz. The manuscript and dissertation chapter were written by Chen Guo with editing by Vincent Scalfani and Travis S. Bailey.

advance the utility of this framework by taking advantage of the hundreds of hydroxyl end-capped PS-PEO diblock copolymers per spherical aggregate, exploiting them as reactive handles easily substituted to other functional groups. Here, we use the facile transformation to azide and alkyne groups as a means to install additional tethering chains between the spherical aggregates subsequent to initial equilibrium swelling of the hydrogel. By coupling diblock copolymer chain ends post-swelling, a secondary mesh is formed free of the osmotic stress imposed on the primary network. This secondary mesh provides significant improvement to the hydrogel tensile properties without altering water content in the hydrogel. Notably, these improvements could be made while simultaneously maintaining the shape, dynamic shear moduli, and unconfined compressive properties of the original hydrogel.

#### **4.2. Introduction**

The investigation of polymeric based hydrogels has been an attractive research field due to their applicability in a wide range of biocompatible technologies including bioseparations<sup>1-3</sup>, encapsulation matrices, biomedical implants, tissue engineering<sup>4</sup> and drug delivery<sup>5-8</sup>. A range of hydrogel platforms have been previously developed for such applications which are most often based on the random physical or chemical cross-linking of hydrophilic polymers in solution.<sup>9-12</sup> Such systems allow for the high water content necessary for use in the aforementioned environments, however, most hydrogel systems with water content above 80% (g/g) inevitably suffer from substandard mechanical properties.

Our group has been actively developing strategies to improve mechanical performance capabilities of high water content hydrogels by effectively pre-structuring tethered micelle networks in the absence of solvent. Our hydrogels are fabricated by melt blending sphere-

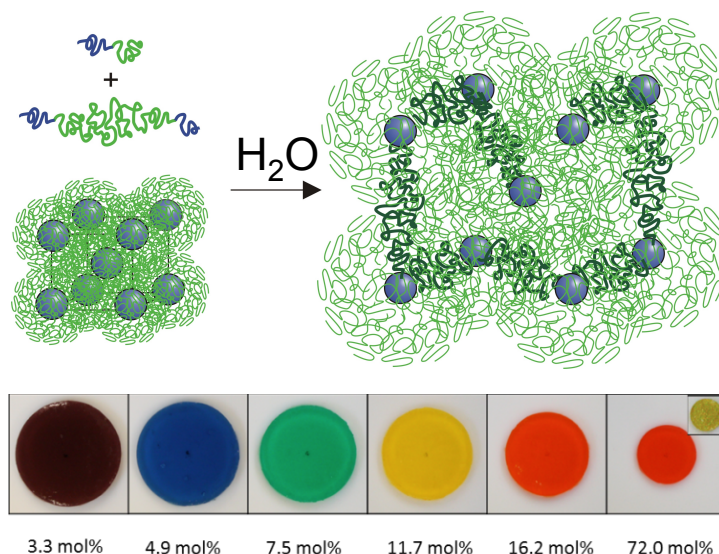


**Figure 4.1. Generalized fabrication strategy for block copolymer based hydrogels based on sphere-forming SO diblock and SOS triblock copolymer blends. Constituent block copolymers are pre-assembled in the melt and vitrified prior to swelling. SOS triblock copolymer (in bold) acts to tether adjacent spherical PS domains. Changing the amount of SOS triblock copolymer (labeled in mol%) influences the equilibrium swelling dimensions due to topological entanglements produced during self-assembly.**

forming<sup>13-15</sup> AB diblock and ABA triblock copolymers and subsequently vitrifying<sup>13, 14</sup> or chemically cross-linking<sup>15</sup> the isolated spherical domains of block A which form during the self-assembly process (Figure 4.1). Each sphere is comprised of several hundred minority component (A) blocks, which are necessarily (by block connectivity) enveloped by a dense corona brush of equal number majority component (B) blocks, giving rise to the micelle like appearance. Without solvent present, a highly regular and periodic lattice of densely packed micelles is produced. Vitrifying or cross-linking the interior spherical domain (A blocks) allows one to completely preserve the melt state self-assembled structure both on the micro and macroscale.

Upon selectively hydrating the majority component (B blocks), the lattice of micelles expands as water penetrates the dense coronal brush layer of each micelle. However, the added ABA triblock copolymer, even at small quantities, acts to tether the individual micelles together

into an infinite network; each sphere acting as a junction point in the hydrogel. Equilibrium swelling dimensions are determined by the balance of solvent-induced osmotic swelling, the entropic restoring force of the ABA tethering midblock, and the quantity of topological ABA entanglements present within the network (Figure 4.1).<sup>14</sup>

In our initial studies with hydrogels based on polystyrene-*b*-poly(ethylene oxide)/polystyrene-*b*-poly(ethylene oxide)-*b*-polystyrene (PS-PEO/PS-PEO-PS or SO/SOS) we found the melt-organized blends preserved their original shape, were highly elastic, and easily tunable; the mechanical properties (dynamic elastic moduli and compression-decompression were evaluated) of the model SO/SOS hydrogels were controllable through simple adjustment of triblock copolymer content, while the overall swelling was controllable with either triblock copolymer content or temperature. For example, by adjusting the amount of SOS content from 3 mol% to 72 mol% in the SO/SOS mixture, highly elastic hydrogels were produced having dynamic elastic moduli over a range of  $10^3$ – $2 \times 10^5$  Pa and swelling ratios from 3.8–36.9 g water per g polymer, respectively. Mechanical performance in unconfined compression was also highly tunable through adjustment of triblock copolymer content. At 40 % strain, samples with only 3 mol % SOS produced compressive moduli of 7.5 kPa, while samples with 72 mol % SOS produced compressive moduli of over 1000 kPa. Fine-tuning of the swelling could be achieved through adjustment of temperature (10°C to 50°C), without significantly influencing any mechanical properties examined.

In this first publication (Chapter 2),<sup>14</sup> we focused primarily on establishing the structure of the network in these model SO/SOS hydrogel systems, and their mechanical performance under dynamic shear and cyclic compression.<sup>13, 14</sup> In a subsequent report from our group, we were able to extend this melt-state prestructuring approach to systems based on polydiene-PEO

block copolymers in which the polydiene spherical aggregates could be chemically cross-linked (in contrast to vitrification of PS) following self-assembly.<sup>15</sup> In this report we return to the PS-PEO based systems and focus on the inherent toughness provided by this uniquely structured network, the ease through which latent functionality can be incorporated, and a method for exploiting such latent functionality to further enhance toughness while maintaining fixed swelling ratios.

One of the most common strategies for improving hydrogel tensile properties is to incorporate a second network to help absorb and distribute stress imposed on the system. Conventional double-network (DN) hydrogels, usually consist of networks comprised of two distinct hydrophilic polymers, one stiff and brittle and the other soft and ductile. These systems tend to exhibit high toughness in general and have proven quite effective, although the range of water contents in which enhanced toughness is achieved can be limited.<sup>16, 17</sup> The fabrication process typically consists of two steps. By adding small amount of cross-linker to a polymerization solution, the first network is made. Then the first network is immersed in the solution where the second network is polymerized and cross-linked. Even though DN hydrogels significantly improve hydrogel mechanical properties, the sol-gel fabrication process is susceptible to heterogeneity in local structure in both networks (due to differences in monomer, initiator and cross-linker diffusion rates), and can be challenging to adapt to shape specific hydrogel applications. In addition, unreacted monomer, crosslinker, and small oligomers or oligomeric networks can take weeks to be removed, particularly when leaching or cytotoxicity is of concern.

As we demonstrate in this report, the homogeneity in structure provided by melt-state self-assembly of macromolecular block copolymers produces a primary or first network that is

inherently quite tough when compared with most hydrogel systems. In fact, these networks are able to absorb strains elastically to a few hundred percent, with the exact modulus exhibited tunable through the triblock copolymer content used in the original melt-state blend. Given these advantages over many hydrogel systems, we decided to explore the installation of a second network that, instead of altering the mechanical performance directly, would remain largely passive under small strain conditions. That is, the secondary mesh would only become actively engaged when the primary network was approaching its own strain limitations. The goal was to be able to improve the high strain toughness of the hydrogel without impacting the smaller strain mechanical response of the primary network, previously tuned through triblock copolymer content in the melt blend.

Our approach is based on exploiting the large number (in excess of 200)<sup>14</sup> of hydroxyl terminated SO diblock copolymers comprising each micellar domain. By converting these hydroxyl groups to clickable alkyne and azide functionalities, we established a means of coupling excess diblock block copolymer to form additional SOS triblock copolymer, although *after* the hydrogel has already reached its equilibrium-swollen dimensions. Our hypothesis was that, while the SOS triblock copolymer added in the original melt blend is molecularly identical (ignoring the coupling fragment) to the SOS triblock copolymer formed via Cu(I)-catalyzed coupling in the hydrated state, the stress state of these two triblock copolymer populations would be significantly different. The SOS triblock copolymer present during melt-state self-assembly of the spherical morphology becomes trapped in its current conformation during sample vitrification. Upon exposure to aqueous media, infinite swelling and micelle dispersal is restricted by the entropic restoring force in the tethering midblocks of the triblock copolymer population, combined with topological entanglements present among nearby tethers. The

concentration of topological entanglements scales with triblock copolymer concentration, and has a dramatic influence on the equilibrium dimensions (Figure 4.1). Effectively, the osmotic driving force to swell is opposed by an equal and opposite force supplied by the entangled triblock copolymer adjoining the spherical PS domains. In contrast, triblock copolymer formed through diblock copolymer coupling at swelling equilibrium would incorporate a secondary mesh of tethers free of the osmotic stress imposed on the primary network. Importantly, with the exception of the Cu(I) catalyst specific to this particular choice of chemistry, formation of the secondary mesh by this route is absent of small molecule reagents or sol fractions associated with leaching concerns in traditional DN hydrogel systems.

Within, we 1) establish the baseline tensile toughness of the AB/ABA pre-structured hydrogel system, 2) demonstrate the successful incorporation of latent azide and alkyne functionality without network disruption, and 3) exploit that functionality to increase the tensile toughness of high water content (~ 95 mass%) forms of these hydrogels.

### **4.3. Experimental**

#### **4.3.1 Materials**

Styrene (99%, 4-tert-butylcatechol inhibitor, Aldrich) and ethylene oxide (99.5+%, compressed gas, Aldrich) monomer were each purified by successive vacuum distillations (10–20 mTorr) from dried di-n-butylmagnesium ( $0.1 \text{ mmol g}^{-1}$  monomer, 1.0 M solution in heptane, Aldrich) before use. Both purified styrene and ethylene oxide monomer were stored in glass burettes in the dark, at room temperature (styrene) and 3 °C (ethylene oxide), respectively, before use (typically less than 24 h). Argon degassed cyclohexane (CHX) was purified by passing the solvent over activated alumina followed by Q-5-like supported copper catalyst (Glass Contour,

proprietary). Argon degassed tetrahydrofuran (THF) was purified by passing the solvent over activated alumina. High-purity argon (99.998%, Airgas) was passed through additional oxygen and moisture traps prior to use. Glassware and polymerization reactors were flamed under vacuum and backfilled with argon (3x). Polymerizations and functionalization reactions were carried out using standard air-free techniques. All other materials were used as received.

#### 4.3.2 Synthesis of PS-PEO diblock copolymer (SO-H) and PS-PEO-PS (SOS) triblock copolymer

SO-H and SOS were prepared as reported previously using two-step anionic polymerization of styrene and ethylene oxide monomers.<sup>14, 18, 19</sup> The fractionation process used for triblock copolymer purification was previously discussed where chloroform and n-hexane were used as solvent/non-solvent system and the temperature was maintained higher than 40 °C to avoid PEO crystallization.<sup>13, 20</sup> SEC: (THF, PS std):  $M_w/M_n=1.04$ .  $M_{n,SO} = 70000 \text{ g mol}^{-1}$ .  $M_w/M_n=1.06$ .  $M_{n,SOS} = 140000 \text{ g mol}^{-1}$ , (calculated using SO  $M_n$ );  $\delta_H$  (300 MHz;  $\text{CDCl}_3$ ): 6.20-7.26 (b,  $-\text{C}_6\text{H}_5, -\text{OCH}_2(\text{C}_6\text{H}_4)\text{CH}_2\text{O}-$ ), 4.55 (s,  $-\text{OCH}_2(\text{C}_6\text{H}_4)\text{CH}_2\text{O}-$ ), 3.1–4.0 (b,  $-\text{CH}_2\text{CH}_2\text{O}-$ ,  $-\text{CH}(\text{C}_6\text{H}_5)\text{CH}_2\text{CH}_2\text{O}-$ ), 1.0-2.30 (b,  $-\text{CH}_2\text{CH}(\text{C}_6\text{H}_5)-$ ,  $\text{CH}_3\text{CH}(\text{CH}_2\text{CH}_3)-$ ,  $-\text{CH}(\text{C}_6\text{H}_5)\text{CH}_2\text{CH}_2\text{O}-$ ), 0.5-0.78 (m,  $\text{CH}_3\text{CH}(\text{CH}_2\text{CH}_3)-$ ).

#### 4.3.3 Synthesis of SO-azide<sup>21, 22</sup>

SO-H (5.42 g,  $7.8 \times 10^{-5}$  mol) was added to a 300 mL flask, which was then evacuated and backfilled with Ar (3x). 100 mL of distilled methylene chloride was then added to dissolve the polymer. The flask was placed to a pre-heated oil bath at 45 °C before adding methane sulfonylchloride (MsCl, 0.12 mL, 20 equiv.) and triethyl amine (0.2 mL, 20 equiv.). The reaction was allowed to stir overnight and the crude product was filtered before being

precipitated into pentane (1 L). The solid was collected via vacuum filtration and dried under vacuum overnight to produce a white solid. Yield 5.25 g, 95+%. SEC: (THF, PS std):  $M_w/M_n=1.05$ .  $M_{n,SO\text{-azide}} = 70000 \text{ g mol}^{-1}$ ;  $\delta_H$  (400 MHz;  $CDCl_3$ ): 6.20-7.26 (b,  $-C_6H_5$ ,  $-OCH_2(C_6H_4)CH_2O-$ ), 4.55 (s,  $-OCH_2(C_6H_4)CH_2O-$ ), 4.2-4.4 (t,  $-CH_2-SO_3-CH_3$ ), 3.1-4.0 (b,  $-CH_2CH_2O-$ ,  $-CH(C_6H_5)CH_2CH_2O-$ ), 2.7 (s,  $-CH_2-SO_3-CH_3$ ), 1.0-2.30 (b,  $-CH_2CH(C_6H_5)-$ ,  $CH_3CH(CH_2CH_3)-$ ,  $-CH(C_6H_5)CH_2CH_2O-$ ), 0.5-0.78 (m,  $CH_3CH(CH_2CH_3)-$ ).

SO-Ms (4.75 g,  $6.9 \times 10^{-5}$  mol) was placed in a 300 mL round bottom flask containing purified DMF under Ar in a pre-heated oil bath at 60 °C. After the polymer was completely dissolved, sodium azide ( $NaN_3$ , 0.089g, 20 equiv.) was added to the reaction with vigorous stirring. The crude reaction mixture was filtered after an overnight reaction and then precipitated into ethyl ether. The collected powder was then dissolved in chloroform to be washed with DI water. The polymer solution in chloroform was dried using magnesium sulfate and then filtered. White powder was collected through filtration under vacuum after the precipitation into pentane. The polymer was then dried under vacuum at room temperature overnight. Yield 4.2 g, 88%. SEC: (THF, PS std):  $M_w/M_n=1.05$ .  $M_{n,SO\text{-azide}} = 70000 \text{ g mol}^{-1}$  (difference between end-groups did not calculated);  $\delta_H$  (400 MHz;  $CDCl_3$ ): 6.20-7.26 (b,  $-C_6H_5$ ,  $-OCH_2(C_6H_4)CH_2O-$ ), 4.55 (s,  $-OCH_2(C_6H_4)CH_2O-$ ), 3.1-4.0 (b,  $-CH_2CH_2O-$ ,  $-CH(C_6H_5)CH_2CH_2O-$ ), 1.0-2.30 (b,  $-CH_2CH(C_6H_5)-$ ,  $CH_3CH(CH_2CH_3)-$ ,  $-CH(C_6H_5)CH_2CH_2O-$ ), 0.5-0.78 (m,  $CH_3CH(CH_2CH_3)-$ ).

#### 4.3.4 Synthesis of SO-alkyne<sup>23</sup>

SO-H (6.31 g,  $9.1 \times 10^{-5}$  mol) was placed into a 500 mL two-neck round bottom flask. Dry THF (250 mL) was added to the flask. The solution was heated in a pre-heated oil bath at 50 °C under Ar. Once SO-H was completely dissolved, NaH (0.23 g, 100 equiv.) was added to

the solution and stirred for 20 minutes. Propargyl bromide solution in toluene (80 wt%, 0.31 mL, 20 equiv.) was injected to the reaction via an air-free syringe. The reaction was increased to 65 °C to reflux overnight. The reaction mixture was filtered and precipitated three times into pentane (1 L). The suspension was filtered and dried under vacuum overnight to give pale yellow powder. Yield 5.65 g, 89%. SEC (THF, PS std):  $M_w/M_n=1.05$ .  $M_{n,SO-alkyne} = 70000$  g mol<sup>-1</sup> (difference between end-groups did not calculated);  $\delta_H$  (400 MHz; CDCl<sub>3</sub>): 6.20-7.26 (b, -C<sub>6</sub>H<sub>5</sub>, -OCH<sub>2</sub>(C<sub>6</sub>H<sub>4</sub>)CH<sub>2</sub>O-), 4.55 (s, -OCH<sub>2</sub>(C<sub>6</sub>H<sub>4</sub>)CH<sub>2</sub>O-), 4.2 (d, -OCH<sub>2</sub>C≡C), 3.1–4.0 (b, -CH<sub>2</sub>CH<sub>2</sub>O-, -CH(C<sub>6</sub>H<sub>5</sub>)CH<sub>2</sub>CH<sub>2</sub>O-), 2.46 (t, -C≡CH), 1.0-2.30 (b, -CH<sub>2</sub>CH(C<sub>6</sub>H<sub>5</sub>)-, CH<sub>3</sub>CH(CH<sub>2</sub>CH<sub>3</sub>)-, -CH(C<sub>6</sub>H<sub>5</sub>)CH<sub>2</sub>CH<sub>2</sub>O-), 0.5-0.78 (m, CH<sub>3</sub>CH(CH<sub>2</sub>CH<sub>3</sub>)-).

#### 4.3.5 SO/SO-alkyne/SO-azide/SOS blends

Each blend sample was prepared by solution blending (1 g total polymer in 20 mL benzene) the appropriate amounts of SO, SO-alkyne, SO-azide and SOS (10 mol% for all blends) to produce blends containing the specified amount of the “clickable” SO moieties. Solutions were frozen using an ethanol/liquid nitrogen slush bath and then dried under vacuum at room temperature overnight.

#### 4.3.6 Dry polymer disk formation

Dry polymer disks with 8 mm diameter and 0.25 mm thickness were melt-pressed using a washer between Teflon covered kapton sheets on a Carver press at 150°C.

#### 4.3.7 Hydrogel swelling and general protocol of click chemistry

Dry polymer disks were placed into a 300 mL round-bottom flasks containing degassed DI water (100 mL) until the equilibrium swelling conditions were reached (~1 hr) at room

temperature. Swollen hydrogels at equilibrium state were taken out from the degassed DI water and placed on a teflon surface. After excess water was blotted, the hydrogels were weighed. Then, the hydrogels were placed back into the flasks with freshly degassed water (100 mL) and degassed for another 10 minutes. Copper sulfate solution (0.25 mL, 0.007 M, in degassed DI water) and sodium ascorbate solution (1 mL, 0.009 M, in degassed DI water) were then injected into the flasks via air-free syringes. The reaction was kept at room temperature overnight. Finally, the hydrogels were left in degassed DI water for one hour to wash off the catalyst before any characterization was performed.

## **4.4 Characterization**

### **4.4.1 Molecular characterization**

<sup>1</sup>H NMR spectra were collected at room temperature in CDCl<sub>3</sub> on a Varian Inova 400 MHz Spectrometer (n = 32, delay = 30 s). Size exclusion chromatography (SEC) was performed on a Viscotek GPC-Max chromatography system fitted with three 7.5 × 340 mm Polypore<sup>TM</sup> (Polymer Laboratories) columns in series, an Alltech external column oven, and a Viscotek differential refractive index (RI) detector. S-OH molecular weight and polydispersity, and the polydispersity of the SO and SOS samples were determined using a THF (40 °C) mobile phase (1 mL/min) with PS standards (Polymer Laboratories).

### **4.4.2 Dynamic Shear and Unconfined Compression Testing**

The rheology and unconfined compression test results were collected on a TA Instruments ARES rheometer at room temperature using parallel plate geometry with an infinite lower plate and an 8 mm upper plate. The bottom plate was the bottom of an integrated glass

cup outfitted with a humidified cover. The swollen hydrogels were placed onto the bottom plate with excess water blotted away. The hydrogel thicknesses were measured on the rheometer and determined by the gap value between the parallel plates when the normal force on the upper plate reached 2 grams force. Since all unstrained hydrogels in this study exceeded 8 mm diameters, the stresses were calculated based on the fixed upper plate dimensions. To eliminate slip between the upper plate and the hydrogel samples during the rheological property measurements, 10% compressive strain was applied on each hydrogel sample. Dynamic frequency sweeps were performed on each sample using a shear strain in the range of 0.15-3% (linear viscoelastic region) over a frequency of 0.1 to 100 rad/s. For unconfined compression tests, the gels were compressed to 40% using a rate of 20%/min. Two compression-decompression cycles were performed to study the possible hysteresis also using the rate of 20%/min during decompression.

#### **4.4.3 Tensile Testing**

Tensile tests were carried out on rectangular pieces of hydrogel sample cut to approximately 14 mm width with thickness that varied from 0.424 to 0.758 mm. All tensile tests were run at room temperature using the normal force transducer of a TA ARES rheometer. TA rectangular torsion geometry test fixtures were used as tensile test grips, although the grip surfaces were modified with 600 grit sand paper to eliminate slip. The experimental setup and strain rate used were similar to that reported Schmidt et al.<sup>24</sup> with some minor adjustments. A strain rate of 5 mm/s was applied until complete hydrogel fracture. The strain rate was chosen to minimize slip while ensuring the maximum travel distance could be covered in less than 0.5 minutes, such that surface evaporation during testing could be minimized. Stress was calculated as the force normalized by the initial cross sectional area of each sample (engineering stress).

## 4.5 Results and discussion

### 4.5.1 Block Copolymer Synthesis, Physical Characterization and Blend Formation

The hydrogel systems used in this study originate from a set of just four distinct block copolymers. One of these four block copolymers, a hydroxyl-terminated PS-PEO diblock copolymer, serves as the parent molecule from which the remaining three block copolymers were derived.

The parent block copolymer, designated SO, was prepared via a two-step anionic polymerization of styrene and ethylene oxide as previously reported.<sup>14, 18, 19</sup> <sup>1</sup>H NMR was used to confirm the targeted volume fraction of polystyrene ( $f_s = 0.13$ ), and SEC confirmed the narrow polydispersity of 1.04. From this parent diblock copolymer the first of the three derivative molecules, a PS-PEO-PS (SOS) triblock copolymer was synthesized. This SOS triblock copolymer was prepared by re-activating the terminal alcohol on SO with potassium naphthalenide and then slowly (several hours) adding,  $\alpha,\alpha'$ -dibromo-*p*-xylene as a coupling agent. The coupled triblock copolymer product was found to be a 60:40 (mass%) mixture of SOS:SO via SEC peak integration, which is consistent with other reported coupling yields,<sup>20</sup> including our own prior work.<sup>13</sup> The SOS triblock copolymer was isolated from this mixture (98+%) using an iterative fractionation process in which chloroform and n-hexane were used as a solvent/non-solvent pair and the temperature was maintained higher than 40 °C to avoid PEO crystallization.<sup>13, 20</sup> Importantly, the SOS triblock copolymer formed in this manner has a molecular weight and contour length essentially double that of the SO diblock copolymers used in this study. This was done in order to ensure domain size compatibility between the SO and SOS block copolymers during self-assembly.

Blends formed from these two block copolymers (SO and SOS) comprise the first set of hydrogel materials considered. These hydrogels serve as baseline materials through which the intrinsic tensile properties of the model system, containing only a primary network, could be established. Six SO/SOS blends containing SOS contents ranging from 4.1 to 45.1 mol% were prepared via solution blending in benzene. Solid powder mixtures were recovered via freeze drying the blend solutions. Reported SOS triblock copolymer concentrations are based on integration of SEC traces following solution blending. Uniform discs (8 mm diameter, 0.24-0.28 mm thickness, 0.015-0.016g) at each SOS concentration were prepared via melt pressing at 150 °C for five minutes. Melt pressing serves both to mold the powders into a homogeneous solid and provide the chain mobility needed for self-assembly into the sphere-based morphology. A LLP of spheres was verified by SAXS for all samples. Detailed analysis of the morphological structure of these materials by SAXS can be found in a previous publication.<sup>14</sup> SEC analysis of samples before and after melt pressing showed no observable sample degradation or change in SOS content.

The second set of materials considered were based on substituting various fractions of the parent (hydroxyl functional) SO diblock copolymer with SO diblock copolymer that had been modified with click functionality (SO-azide; SO-alkyne). In these four component blends, the SOS triblock copolymer continues to serve as the component forming the primary network in the hydrogel. The azide and alkyne functional SO diblock copolymers provide a latent ability to generate more triblock copolymer at a future time, that is, once the vitrified blend has been hydrated and the primary network of triblock copolymer tethers has been established and osmotically engaged.

SO-alkyne and SO-azide were both prepared via straightforward substitution reactions after conversion of the terminal alcohol groups on the parent SO diblock copolymer to their corresponding sodium or potassium alkoxides. To generate SO-azide, the terminal alkoxide was first converted to a mesyl leaving group before displacement in the presence of sodium azide.<sup>21-23</sup> Generation of SO-alkyne was achieved by treatment of the SO alkoxide with propargyl bromide. <sup>1</sup>H-NMR was able to confirm transformation of the hydroxyl groups to -alkyne and -mesyl groups to be essentially quantitative given the uncertainty associated with end-group analysis by <sup>1</sup>H NMR of large polymer molecules. Quantification of the azide functionalization efficiency was more difficult to ascertain. The methylene protons adjacent to the azide group overlap with the ethylene oxide backbone and could not be resolved. However, the complete disappearance of the methyl protons of the mesyl group was indicative of a successful substitution reaction with complete mesyl group displacement. In addition, FTIR confirmed the presence of an azide vibration (2110 cm<sup>-1</sup>) (See appendix for the NMR spectra of SO-Ms and SO-azide). While

**Table 4.1. Hydrogel composition and post-swelling click chemistry reaction conversion**

Sample	SOS <sub>pre</sub>	SO-X <sub>pre</sub>	SO-azide:SO-alkyne:SO-H	SOS <sub>max</sub>	SOS <sub>post</sub>	Coupling conversion
A1					20.2	60.0
A2	9.3	90.7	1:1:4	28.8	18.4	50.8
A3					21.2	65.0
A4					20.3	60.0
B1					29.0	59.4
B2	9.8	90.2	1:1:8/5	46.5	30.7	63.8
B3					29.8	61.4
B4					22.7	41.9
C1					39.7	60.2
C2	10.4	89.6	1:1:4/7	69.4	42.9	65.3
C3					37.5	56.6
C4					32.4	47.7
D1					48.0	58.0
D2					48.4	58.4
D3	8.9	91.1	1:1:0	100	52.0	62.3
D4					52.1	62.3
D5					45.1	54.8

complete functionalization of the SO-azide could not be confirmed, blends involving SO-azide and SO-alkyne were assembled assuming functionalization of both block copolymers was quantitative. The possibility of non-quantitative functionalization and its impact on coupling efficiency is considered in subsequent sections.

Polymer blends containing approximately 8.5 - 10 mol% SOS and varying, equimolar amounts of SO-azide and SO-alkyne were prepared via solution blending (with freeze-drying) from benzene. The SO-azide: SO-alkyne ratio was held constant at 1:1 and the blend was diluted with reactively inert SO, producing four distinct blends ( $A_{pre}$  -  $D_{pre}$ ) with varying SO-azide/SO-alkyne content as shown in Table 3.1. Reported SOS triblock copolymer concentrations are based on integration of SEC traces following solution blending (Figure 4.4, left). Notably, there is some unintended variation in the amount of pre-blended SOS triblock (8.9 - 10.4 mol %) across the four blends, which is attributable to a combination of error associated with massing, SEC peak integration, and local fluctuations blend composition. Uniform discs (8 mm diameter, 0.24-0.28 mm thickness, 0.015-0.016g) of samples A through D were prepared via melt pressing at 150 °C for five minutes. It is well established that azide-alkyne Huisgen cycloadditions can occur at high temperatures with the absence of a metal catalyst.<sup>25</sup> We ran several control experiments before and after melt pressing azide-alkyne functional SO and found no indication of additional triblock copolymer formation in the SEC traces. Molecular weight degradation was also not observed. Functional group integrity during melt pressing proved difficult to accurately assess (via <sup>1</sup>H NMR, e.g.) given the reduced concentration of end groups in the blends. However, independent melt processing of neat SO-alkyne showed no apparent change in chain end functionality occurred during heating for such short times.

## 4.5.2 Baseline Performance of SO/SOS Hydrogels

Dry polymer discs of SO/SOS blends were swollen in DI water until reaching the equilibrium swollen state (approximately one hour, evident by constant mass and size). The equilibrium swelling ratios ( $Q$ 's) were calculated based on gravimetric analysis of the discs before and after swelling. As found in previous studies,  $Q$  could be altered through environmental temperature in addition to tether (SOS) concentration.<sup>14</sup> To eliminate temperature effects, all hydrogels were swollen at room temperature (thermostated 25 °C). Figure 4.2a shows

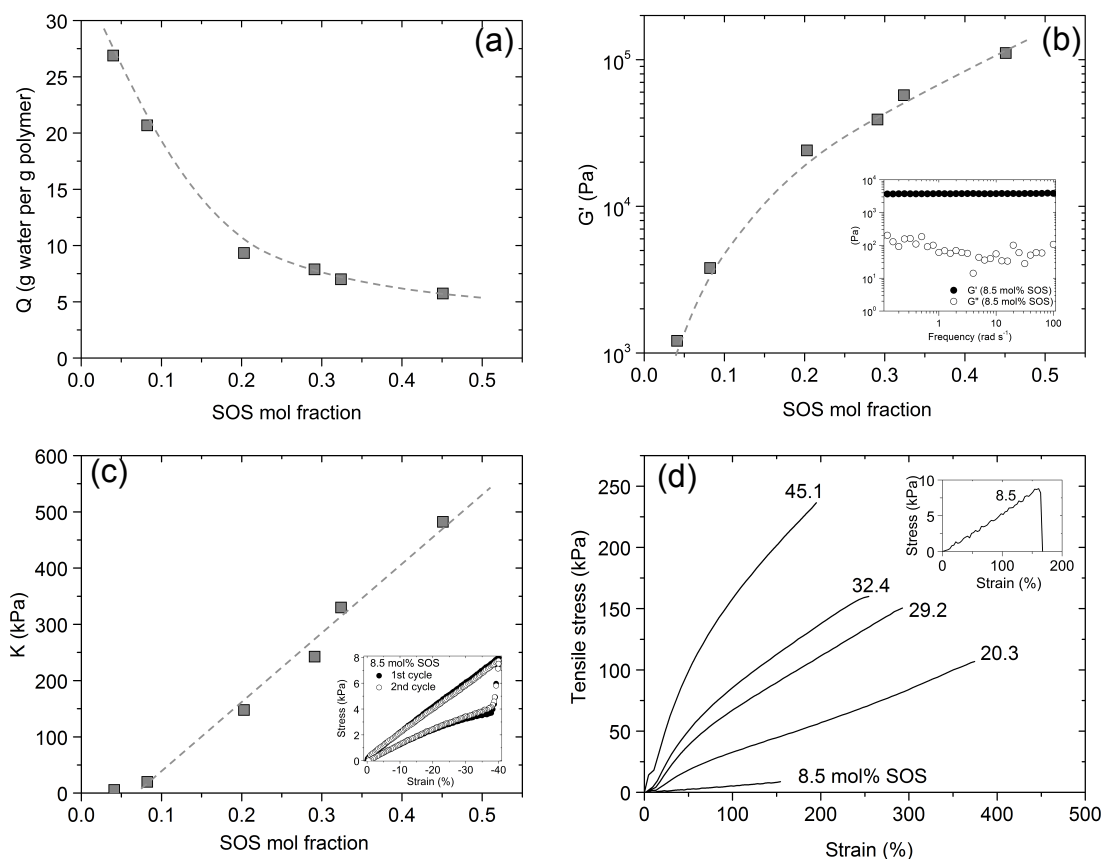


**Figure 4.2. Behavior of baseline SO/SOS hydrogels as a function of SOS triblock copolymer concentration. (a) Swelling ratio ( $Q$ ). (b) Elastic modulus ( $G'$ ) under dynamic shear ( $\omega = 1$  Hz); (c) Compressive modulus ( $K$ ) in unconfined compression (strain rate = 20% min<sup>-1</sup>). (d) Tensile tests, (strain rate = 5 mm s<sup>-1</sup>). Insets in (b) and (c) describe the dynamic frequency sweep and unconfined compression data for the baseline SO/SOS hydrogel containing 8.5 mol% SOS triblock copolymer. The inset in (d) provides a zoomed representation of the 8.5 mol% SOS hydrogel.**

the variation in  $Q$  with SOS concentration for the six SO/SOS blends. The values of  $Q$  varied from 5.5 g H<sub>2</sub>O/g polymer (45.1 mol% SOS) to 27 g H<sub>2</sub>O/g polymer (4.1 mol% SOS). Importantly, the change in equilibrium  $Q$  with decreasing SOS concentration was entirely consistent with that observed in our prior studies employing this sphere based network,<sup>14, 15</sup> once the differences in overall molecular weight used in those studies are accounted for. A detailed discussion of the influence of SOS concentration on hydrogel swelling behavior can be found in a previous publication.<sup>14</sup> Of notable importance is the role that SOS concentration and the associated concentration of topologically fixed entanglements play in determining  $Q$ . As alluded to in the introduction, polystyrene end blocks of the SOS triblock copolymer become fixed within the spherical domains during sample vitrification, producing topologically constrained entanglements among nearby tethers. These entanglements act to restrict expansion of the hydrogel. The concentration of topological entanglements scales with triblock copolymer concentration, and therefore has a dramatic influence on the equilibrium dimensions and swelling ratio obtainable by the hydrogel (Figure 4.1).

The mechanical properties evaluated in this study include dynamic shear modulus, compressive modulus, tensile strain at break, tensile stress at break, Young's modulus and toughness. All quantities were taken at first indication of fracture. Of this set, the dynamic shear modulus and compressive modulus have been investigated previously for similar SO/SOS based hydrogel systems.<sup>14</sup> Given the SO and SOS molecules used in this study are of slightly smaller molecular weights, measurements of both moduli are included here in order to establish the baseline performance of these particular SO/SOS blends, and provide a means of assessing the impact of installing a secondary network of tethers.

Figure 4.2b shows the elastic moduli of all six SO/SOS hydrogels as a function of their SOS triblock copolymer concentration. The elastic moduli for hydrogels based on all six blends were found to be independent of frequency over the range of 0.1-100 Hz. Importantly these are small strain (< 3%) experiments maintained in the linear viscoelastic region for each sample. The frequency sweep data for the blend containing 8.5 mol% SOS triblock copolymer is highlighted in the inset of Figure 4.2b. The plateau behavior in modulus is typical of elastic solids, and our hydrogel systems in particular. The major axes of Figure 4.2b plot the elastic modulus ( $G'$ ) (at a shear frequency of 1 Hz) for each of the hydrogels as a function of the SOS triblock copolymer concentration. The elastic moduli span a significant range ( $10^3$  to  $10^5$  Pa), increasing with increasing SOS triblock copolymer concentration. This ability to tune the modulus over such a dramatic range using SOS concentration is consistent with our previous studies and is a consequence not only of adding additional strands (tethers) between junction points (spheres and topological entanglements), but of increased coronal layer overlap (among PEO chains) imposed by the entanglement restricted swelling.<sup>13, 14</sup>

Figure 4.2c shows the compressive moduli of the six hydrogel samples as a function of SOS triblock copolymer concentration. Unconfined compression/decompression was carried out to 40% strain for each sample at a strain rate of  $20\% \text{ min}^{-1}$ . Each sample was subjected to two continuous compression/decompression cycles, with no delay between cycles. Example stress-strain data for the sample containing 8.5 mol% SOS triblock copolymer is shown in the Figure 4.2c inset. The basic cycle shape exhibited by the 8.5 mol% SOS sample was consistent across all hydrogels regardless of SOS triblock copolymer concentration, and indicates several shared characteristics of hydrogels constructed using this pre-structured network of tethered spheres. For example, the modulus under compression remains constant (stress linear in strain) up to 40%

**Table 4.2. Hydrogel Q and tensile properties**

Sample	SOS <sub>post</sub> (mol%)	Q (g water/g polymer)	Strain to break (%)	Stress to break (kPa)	Young's modulus (kPa)	Toughness (kJ/m <sup>3</sup> )
Baseline Hydrogels	4.1	26.9	-	-	-	-
	8.5	20.7	154	8.7	5.3	6.2
	20.3	9.3	375	107	38	203
	29.2	7.9	293	150	82	246
	32.4	7.0	254	160	110	240
	45.1	5.7	195	237	209	280
A	20.0 ± 1.2	18.5 ± 1.0	287 ± 58	68 ± 21	12.0 ± 1.5	74 ± 33
B	28.1 ± 3.6	18.3 ± 0.7	458 ± 85	163 ± 53	12.5 ± 1.2	269 ± 116
C	38.1 ± 4.4	18.8 ± 0.4	567 ± 56	169 ± 34	11.2 ± 1.5	361 ± 93
D	49.1 ± 3.0	19.2 ± 0.7	479 ± 103	135 ± 30	13.1 ± 1.2	276 ± 127

strain for all samples. The compressive modulus, indicated by the slope of the compression leg of the cycle is plotted on the major axes of Figure 4.2c for each hydrogel as a function of its SOS triblock copolymer concentration. Like the dynamic shear modulus, the compressive modulus increases with increasing SOS concentration, covering an impressive range of nearly two orders of magnitude, from approximately 5.3 kPa (4.1 mol% SOS) to 480 kPa (45.1 mol% SOS). Each hydrogel also exhibits complete elastic recovery (with reproducible hysteresis) such that the first and second compression/decompression cycles are experimentally equivalent.

Figure 4.2d shows the stress-strain behavior for five of the six SO/SOS baseline hydrogels under tensile strain. The resolution of the normal force transducer used was insufficient to accurately examine the tensile properties of smallest SOS content (4.1 mol%) and therefore weakest hydrogel. As with the dynamic shear modulus and compressive modulus, increasing the SOS triblock copolymer content had a significant influence on the tensile properties exhibited by the hydrogel. Table 4.2 shows the values for the Young's modulus (initial slope), strain at break, stress at break and toughness for the baseline hydrogels as a function of their SOS triblock copolymer content. The Young's modulus increases quite dramatically with increasing SOS triblock copolymer content, improving from 5.3 to 209 kPa between 8.5 mol%

and 45.1 mol% SOS triblock copolymer. The hydrogel toughness seems to also improve with the SOS concentration, although the most significant jump takes place between 8.5 mol% and 20.3 mol% SOS triblock copolymer (from 6.2 to 203 kJ m<sup>-3</sup>). After that, the improvement is far less dramatic, with the toughness of the 45.1 mol% SOS sample topping out at 280 kJ m<sup>-3</sup>.

This non-linear dependence on SOS concentration suggests a transition in the failure mechanism from one that is quite dependent on the concentration of tethering molecules at low concentrations to one that is much less dependent at higher concentrations. At low concentrations, the tethering molecules are responsible for absorbing most of the load, and their number appears to be the primary factor limiting the total energy absorbable by the hydrogel. We believe once the concentration of tethering molecules reaches a critical value, the entanglement density produced among them more effectively distributes the load across the entire network and provides a higher overall modulus. However, those entanglements, just as they limit strain under osmotic swelling forces (as their number increases), also limit the strain available to the hydrogel under a tensile loading event. As a result, the strain at break decreases as the tether concentration increases above that 20 mol% threshold. We suspect that once the hydrated matrix reaches its strain limit, failure is likely a consequence of bond rupture in the hydrated PEO matrix, rather than chain pull out from, or brittle fracture within, the vitrified PS spheres. This hypothesis has yet to be examined.

Clearly, additional SOS triblock copolymer added during the melt-state self-assembly process has considerable influence on hydrogel mechanical properties. The next section of this article is focused on how the installation of additional SOS tethering molecules after equilibrium swelling has taken place can enhance the toughness exhibited by these systems. We chose to focus our efforts on hydrogels with original SOS triblock copolymer concentrations in the 9 to

10 mol% range. These hydrogels exhibited significantly high Q values in the range of 18 to 20 g H<sub>2</sub>O/g polymer and could be handled easily due to reasonable shear, compressive and tensile moduli, but lacked the toughness of the higher SOS content hydrogels by a significant margin. The goal was to use latent azide and alkyne chain end functionality as a means of performing diblock copolymer coupling in situ, once self-assembly, vitrification, and swelling were already complete. The diblock copolymer coupling effectively creates additional SOS triblock copolymer in the system, but absent of the osmotic stress imposed on the original SOS triblock copolymer present during the swelling event. This strategy is shown pictorially in Figure 4.3. It was our hypothesis that this second population of SOS triblock copolymer tethers, given their initial, unstrained state would serve to improve toughness by extending the strain limitations of the first tether population.

#### **4.5.3 Chemical Characterization and Swelling in “Click” Enhanced Hydrogels**

Four blends (A through D), each containing approximately (1) 8.9 to 10.4 mol% SOS triblock copolymer, (2) varying, equimolar amounts of SO-azide and SO alkyne diblock copolymer, and (3) a balance of reactively inert SO diblock copolymer, were prepared. The composition of SO-azide and SO-alkyne were chosen such that the baseline values of 8.9 – 10.4 mol% SOS present in each at swelling could be theoretically increased to values ranging from 28.8 mol% (blend A) to 100 mol% (blend D) total SOS triblock copolymer post swelling (Table 4.1).

Multiple polymer discs were melt-pressed from each of the block copolymer blends A through D (Table 4.1). The discs were individually swollen in excess DI water until reaching equilibrium dimensions (about one hour evident by constant mass and size). The Q values for the

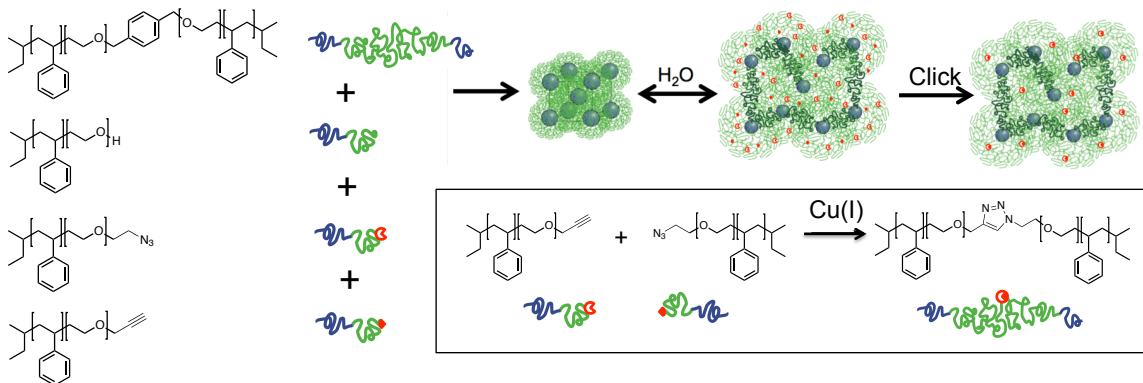


**Figure 4.3. Pictorial schematic showing the strategy for introducing a secondary network of SOS triblock copolymer tethers using aqueous phase click chemistry at swelling equilibrium.**

hydrogel discs formed from each of the blends A through D prior to exposure to Cu(I) catalyst are shown in Figure 4.5. The inclusion of SO diblock copolymer that contains terminal azide or alkyne functionality appeared to have no particular influence on the equilibrium swelling dimensions when compared to that expected from baseline SO/SOS type hydrogels with similar SOS triblock copolymer concentrations. That is, all hydrogels from the blends exhibited pre-click Q values in the 18 – 20 g H<sub>2</sub>O/g polymer range, consistent with an SOS tether content in the 8.9 – 10.4 mol% range. This behavior confirmed the hypothesis that the integration of chain end functionality other than the native hydroxyl at the PEO chain end could be done without disruption of the basic network swelling behavior.

Each hydrogel solution (hydrogel in excess DI water) was degassed with argon prior to the addition of sodium ascorbate and copper (II) sulphate. The combination of copper sulfate and sodium ascorbate produces the Cu(I) catalyst in-situ to facilitate the Huisgen cycloaddition reaction between terminal azide and alkyne functional groups of the hydrated PEO blocks.<sup>26</sup> In the absence of oxygen removal from the hydrogel solutions prior to catalyst addition, we

observed significant PEO degradation (verified with SEC, data not shown). This is in accordance with reports by the Madras<sup>27</sup> and Crowley groups<sup>28</sup> who observed similar degradation phenomena. Hydrogel samples were left in the catalyst solution for 24 hours prior to removal, followed by sequential dialysis against fresh DI solutions to remove residual catalyst. Preliminary kinetic experiments were used to confirm the 24-hour reaction time was sufficient to reach maximum conversion. Coupling efficiencies were calculated based on the percent of azide (or alkyne) functional groups reacted, as quantified through the observed SOS triblock copolymer added to the system following exposure to the Cu(I) catalyst. Representative SEC data is shown in Figure 4.4 for each of the blends with the results of all coupling reactions summarized in Table 4.1.

Importantly, a control sample composed of only SO diblock and SOS triblock copolymer, absent of any azide/alkyne functionality was also run in parallel to determine the effect of sodium ascorbate and copper (II) sulfate solution on the constituent polymer species. The SEC traces of the control sample before and after exposure to the catalyst system for 24 hours showed no significant change, suggesting neither degradation nor significant side-reactions occurred (Figure 4.4). To ensure that coupling in the sample was homogeneous and not influenced by diffusion limitations in either copper sulfate or sodium ascorbate, SEC was performed on sections taken from both inner and outer regions of a disc. No significant differences in regional coupling were detected in any samples tested.

SEC analysis of the total SOS triblock copolymer after the post-swelling click chemistry varied from 18.4 - 52.0 mol%, depending on blend composition. Importantly, these values were reflective of a coupling efficiency that remained almost constant ( $58.1\% \pm 6.3\%$ ) across all

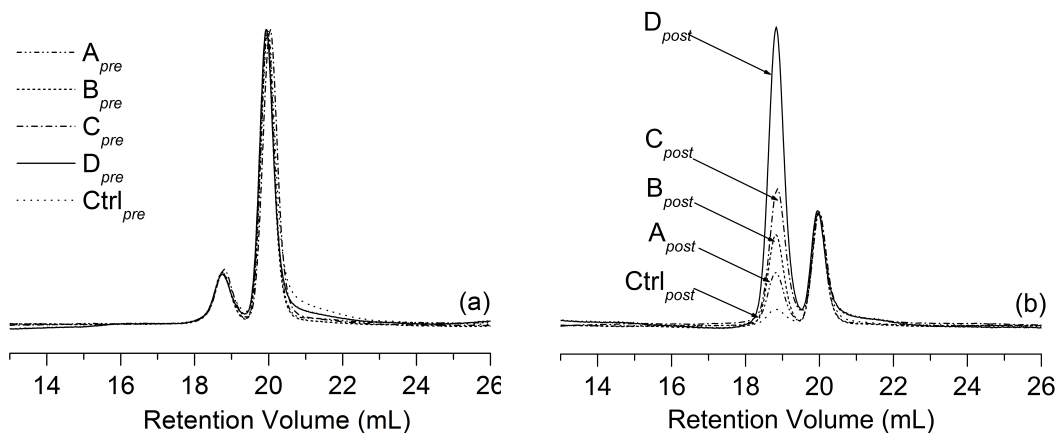


**Figure 4.4. Representative SEC data for hydrogels formed from blends A through D (a) before (pre) and (b) after (post) exposure to the Cu(I) catalyst. All SEC traces are normalized to a constant area under the SO-X diblock copolymer peak (right) in order to show the relative amounts of SOS triblock copolymer (left peak) more clearly. Control samples contain only SO and SOS and verify that exposure to the catalyst solution has no degradative effects on the constituent block copolymers.**

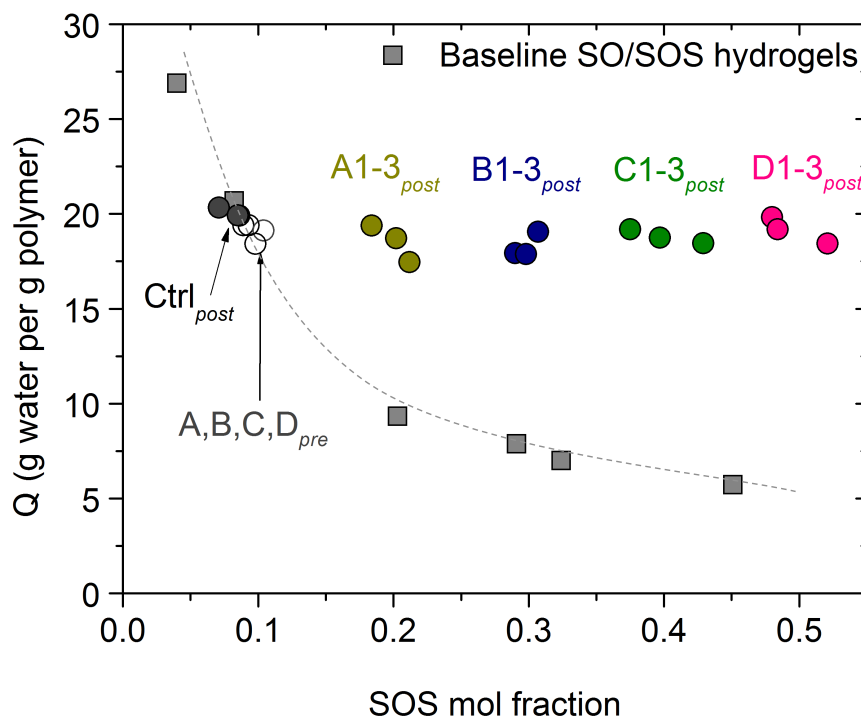


**Figure 4.5. Hydrogel swelling ratio ( $Q$ ) as a function of SOS triblock copolymer concentration. Data show the installation of a secondary network of SOS tethers has no impact on the swelling ratio determined by the primary SOS network.**

samples despite variation in the amount of azide/alkyne functional polymer present. This is likely indicative that some degree of non-quantitative functionality is present in the initial materials (e.g. PS-PEO-azide at < 100% functionality). However, post-reaction  $^1\text{H}$  NMR and FTIR seem to indicate both azide and alkyne groups are still present in small amounts, although the size of the block copolymers have made quantification unreliable. We suspect that in addition to non-quantitative functionality in SO-azide (or SO-alkyne), performing the reaction within the context of a fixed morphology is also playing an active role in determining coupling efficiency. On the positive side, the self-assembled sphere morphology uniquely places PEO chains of the corona in close proximity with those belonging to adjacent spherical domains. This structure spatially directs or concentrates terminal azide and alkyne groups into defined regions, which should enhance coupling efficiencies when the number of functional chain ends in the region is high (e.g. at low conversions). On the negative side, the reaction volume available to each functional group is constrained by the limited travel available to each PEO chain end, given the opposite end is anchored to a fixed junction point (spherical domain) in the network. As the conversion proceeds to higher values, and residual functional group concentrations diminish, the occurrence of orphaned chain ends is likely. Finally, the preferred location of azide and alkyne functional chain ends during self-assembly process is unknown. It is also possible the sphere morphology produces a consistent ratio of functional chain ends that are sequestered deep in the coronal PEO layer, in proximity with the PS domains. Such buried chain ends would have severely hindered mobility therefore would not be able contribute to the in-situ generation of triblock copolymer. We also note that our polymers are of much greater molecular weight than what is commonly employed in azide/alkyne click reactions ( $M_n < 30,000 \text{ g/mol}$ )<sup>26</sup> and that coupling efficiency between high molecular weight species is commonly much lower than that found in small

molecular weight systems. It is unclear at present if the moderate conversion yield is a result of limitations associated with phase separation, morphology, non-quantitative functionality in one or both species, or a combination of these factors.

The post-click Q values for three hydrogels from each blend type are given in Figure 4.5 as a function of their new total SOS triblock copolymer concentrations. Clearly, the installation of additional SOS triblock copolymer through click coupling under equilibrium swelling conditions has no significant influence on the water content of the hydrogel. That is, the Q values still reflect the SOS triblock copolymer concentration present prior to swelling. Q values for the baseline SO/SOS hydrogels are included in Figure 4.5 and provide a direct comparison between hydrogels of similar *total* SOS triblock copolymer concentrations, differing only in the manner in which the triblock copolymer was introduced into the system. To summarize, one can predetermine water content by selecting the percentage of SOS triblock copolymer used during melt-state self-assembly. The post-swelling click chemistry then provides a means of adding an additional, secondary network of SOS tethers while preserving the original Q values. The impact of this secondary network on the mechanical properties of the hydrogel is the subject of the next section.

#### **4.5.4 Mechanical Performance of “Click” Enhanced Hydrogels**

Figure 4.6 shows the pre-click and post-click elastic moduli of hydrogels formed from the four blends A through D. In addition, the elastic moduli of the six baseline SO/SOS hydrogels are also included for direct comparison of the post-click hydrogels with baseline hydrogels of similar SOS content. As a control experiment, baseline SO/SOS hydrogels with approximately



the four blends prior to the addition of the catalyst solution all appear to fall along the trajectory expected for the baseline SO/SOS hydrogel systems. That is, the chain end functionality in its uncoupled state has a negligible effect on the elastic properties of the hydrogels under dynamic shear, as expected. A comparison of the elastic moduli of hydrogels containing azide/alkyne functional groups both pre- and post-click reveals an apparent increase in elastic modulus (20 to 40%) upon installation of additional SOS triblock copolymer. However, when compared with baseline hydrogels of similar *total* SOS triblock copolymer concentrations, these increases in modulus (as a result of introducing the second network of tethers) are actually quite modest. For example, adding tethers post-swelling to get from 8.9 mol% SOS to 48 mol% SOS triblock copolymer (sample D1) produces an increase in elastic modulus from 4.7 to 6.3 kPa (appendix). By comparison, baseline SO/SOS hydrogels with 45.1 mol% SOS triblock copolymer in which the entire population of tethers was introduced during melt-state self-assembly exhibits an elastic modulus just over 100 kPa. This type of comparison underscores the very limited impact the secondary network, installed post-swelling, has on the small strain shear response of these hydrogels. At small oscillatory strains ( $< 3\%$ ), the secondary network, containing almost four times the number of tethers as the primary network, remains largely passive. This is a direct reflection of the stress free environment under which these tethers are installed. Notably, in a parallel study we have shown the elasticity of these hydrogel networks is governed predominately by the degree of PEO coronal overlap with adjacent spherical domains.<sup>13</sup> The small improvement in elastic modulus is likely product of the changes in the way in which adjacent coronal layers are connected, however, without a pronounced difference in coronal layer overlap, the changes detected remain quite modest.

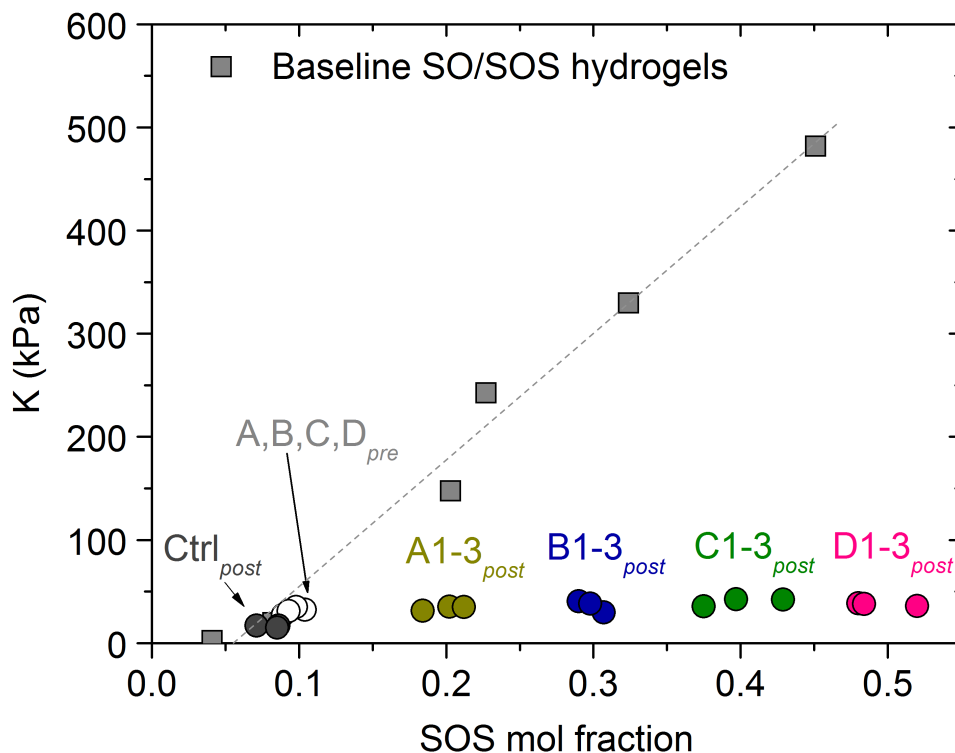


**Figure 4.7. Compressive moduli in unconfined compression (strain rate = 20% min<sup>-1</sup>) as a function of total SOS triblock copolymer concentration.**

The behavior of the post-click hydrogels in unconfined compression (to 40% strain) produced similar conclusions (Figure 4.7). As with the baseline SO/SOS hydrogels, all samples, regardless of treatment, produced linear stress-strain relationships to 40% strain (strain rates at 20% min<sup>-1</sup>) and exhibited some hysteresis during decompression, but ultimately showed complete elastic recovery with second compression/decompression cycles coinciding the first cycle. Baseline SO/SOS control samples exposed to catalyst solutions for the required 24 hour reaction time performed similarly to unexposed baseline hydrogels in agreement with the previous experiments involving elastic modulus. Pre-click samples gave compressive moduli consistent with those produced by baseline SO/SOS hydrogels of similar SOS triblock

copolymer concentrations, also in agreement with the previous experiments involving elastic modulus. The effects of installing the additional SOS triblock copolymer post-click resulted in small increases in compressive modulus across all samples when compared with their pre-click counterparts, but as with elastic modulus, the increase was very modest when compared with baseline SO/SOS hydrogels of similar *total* SOS content. Using sample D1 as an example once again, the pre-click (8.9 mol% SOS) and post-click (48.0 mol% SOS) compressive moduli were 27 and 38 kPa respectively, demonstrating the marginal effect of the secondary SOS network on compression response of the hydrogel. By comparison, the baseline SO/SOS hydrogel of 45.1 mol% SOS exhibited a compressive modulus of 482 kPa. Perhaps unexpectedly, the post-click data suggest that even at 40% compression, the secondary network of SOS tethers still does not engage to the extent that it contributes significantly to the mechanical response of the hydrogel, even contributes four times as many tethers as the primary network. The SOS triblock copolymer of the primary network introduced during melt-state self-assembly is still the dominant contributor. Original compression data for the baseline SO/SOS control samples, as well as the pre- and post-click samples A1 – D1 are included in the appendix.

The true impact of installing the secondary network of SOS tethers is the stunning enhancement in hydrogel toughness possible while maintaining very high Q values. Figure 4.8 shows the tensile tests from a series of post-click samples A through D. Similar control experiments on baseline SO/SOS hydrogels exposed to the catalyst solution for 24 hours, as well as pre-click blends A through D showed tensile behavior similar to that expected for baseline SO/SOS hydrogels of similar SOS content, in agreement with the previous hydrogel performance results under dynamic shear and unconfined compression. However, the post-click blends A

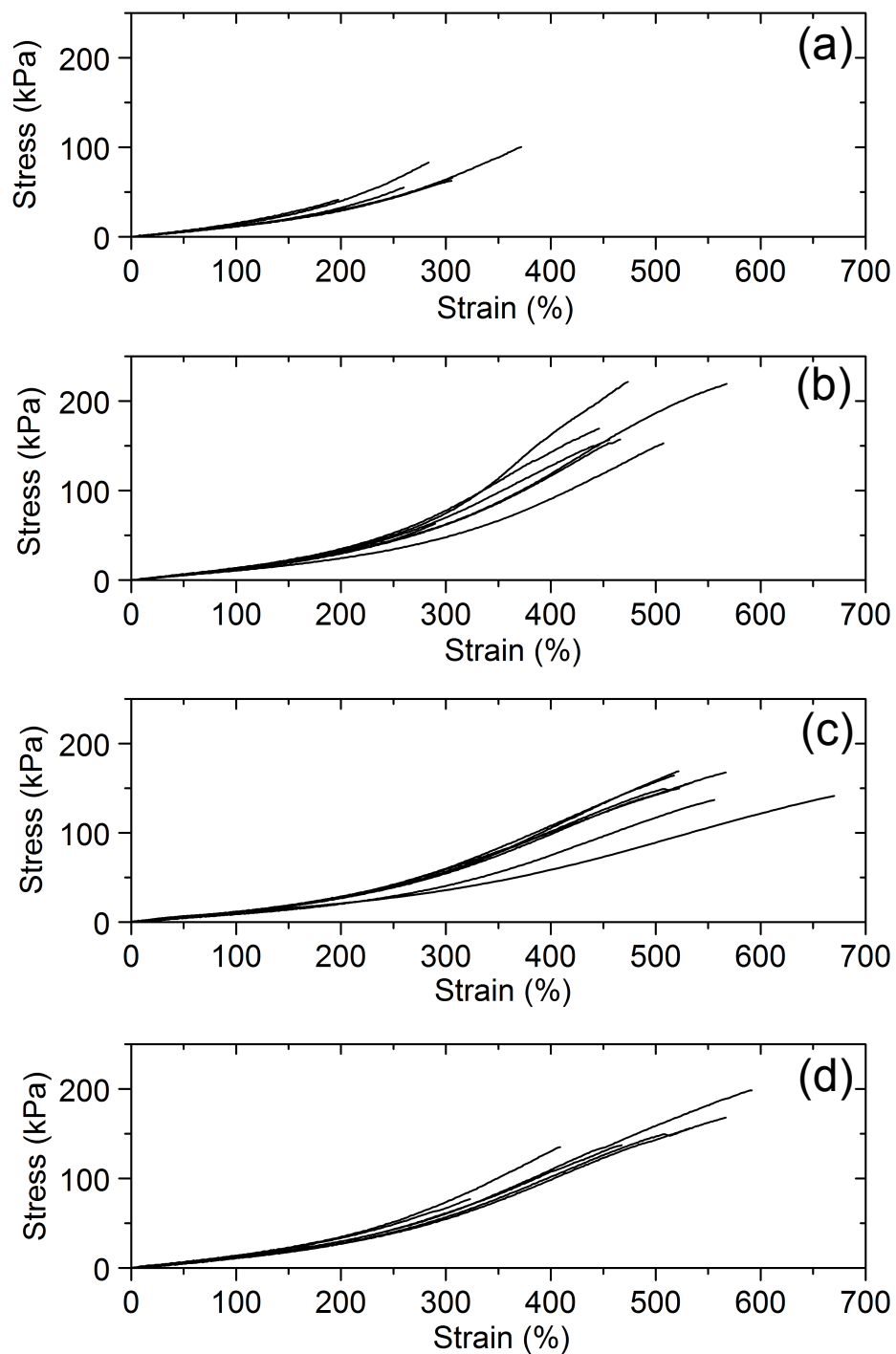


**Figure 4.8. Tensile test results for hydrogels formed from blends A through D, evaluated after installation of the secondary network of SOS triblock copolymer. Total SOS triblock copolymer concentrations can be found in Table 4.2.**

through D showed dramatic improvements in virtually all tensile property categories. Table 4.2 summarizes the basic tensile properties for each of the hydrogel blends A through D, along with analogous data for the performance of the baseline SO/SOS hydrogels. Importantly, each of the hydrogels formed from blends A through D has a swelling ratio in the range of 18 – 20 g H<sub>2</sub>O/g polymer, and is therefore comparable with the 8.5 mol% SOS baseline hydrogel.

One can see immediately from the entries in Table 4.2 as well as Figure 4.9 that the addition of the secondary network provides vast improvements in toughness. With only a single, primary network of SOS tethers, the 8.5 mol% SOS hydrogel (~ 95% H<sub>2</sub>O by mass) was able to absorb 6.2 kJ m<sup>-3</sup>. With the addition of the secondary network of tethers, the toughness could be improved dramatically, with samples from blend C reaching mean values of 361 kJ m<sup>-3</sup> (a 58-fold increase). Similarly, the secondary network of SOS tethers provides significant improvements in strain to break, stress to break, and Young's modulus when compared with the 8.5 mol% SOS baseline hydrogel of equivalent Q value. Incredibly, the installation of the secondary network, even at the moderate levels produced in the B blends, endows the hydrogels with Q values of 18 - 20 g H<sub>2</sub>O/g polymer with the tensile properties typically available only to hydrogels of much lower water content.

We believe the dramatic impact of the secondary SOS network under tension (in comparison to small strain shear or unconfined compression) is a product of its ability to reinforce the primary network at higher strains. Because it is largely formed in an unperturbed state, the topological entanglements of the secondary network require much higher strains to become mechanically engaged. As such, they provide the hydrogel network an improved range over which strain energy can be absorbed by the hydrogel. That is, as the primary network approaches its mechanical limit, it gradually begins to transfer load to the secondary network,

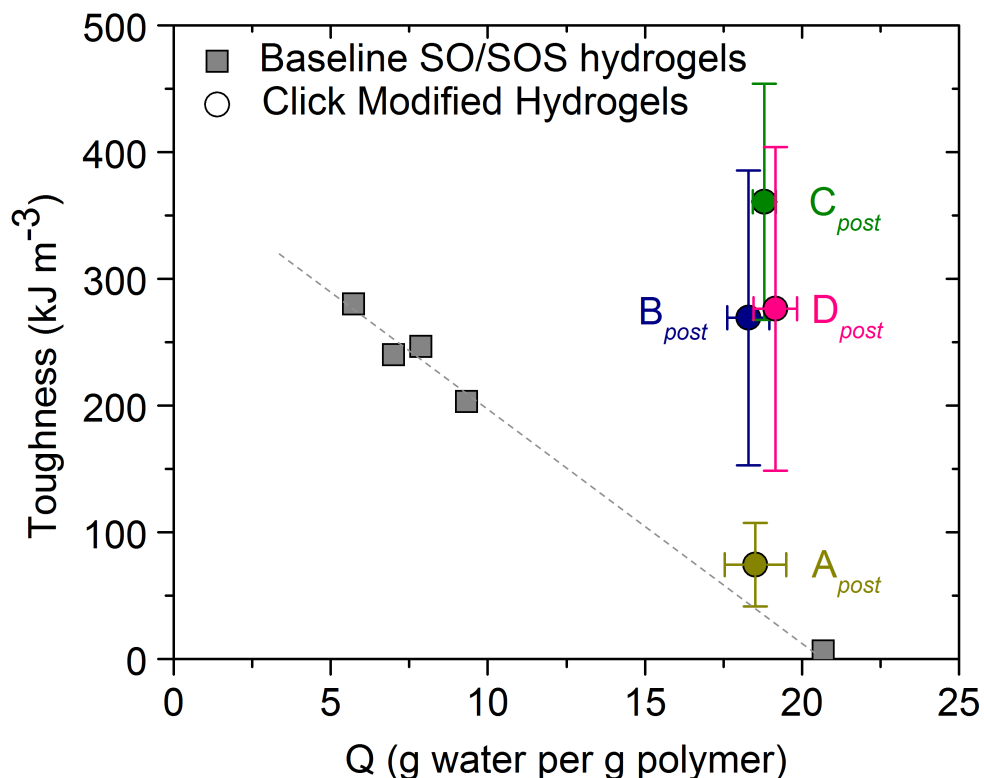


**Figure 4.9. Hydrogel toughness as a function of Q. Data show the installation of a secondary network of SOS tethers improves hydrogel toughness while remaining approximately the same Q. The toughness and Q data can be found in Table 4.2.**

extending the strain and stress to break. Consequently, these additional tethers improve the elongation capacity of the hydrogels, quite remarkably. Overall, the post swelling click chemistry provides a means of adjusting the tensile properties of these tethered micelle based hydrogels, in a manner that is largely independent of other mechanical properties of the system.

It should be noted that no particular processing strategies were developed to optimize the tensile performance of these samples. The stress-strain plots in Figure 8 give a sense of the scatter in the tensile response that was typical given simple melt-pressing under atmospheric

conditions. Thus the measured tensile properties are almost assuredly influenced by the presence of bubble, grain boundary and edge defects present before and after swelling. As a consequence, the vast improvements in tensile properties reported are likely understated. That is, the potential of the secondary network to enhance the tensile properties of these hydrogel systems may not be fully accessible until processing strategies are optimized to limit focal defects.

Finally, we reiterate the inherent simplicity of this hydrogel network, which is based effectively on a single parent PS-PEO block copolymer. Unlike traditional DN hydrogels, the first and second networks in this system derive from the same molecular constructs, with the precursors to the second network intrinsically present through selective chain end functionalization with orthogonally reactive coupling agents. The strategy preserves the chemical composition of the hydrogel while simply exploiting the stepwise installation process as a means to form two chemically identical tethering populations, each under a different degree of mechanical (osmotic) stress. Importantly, with the exception of the Cu(I) catalyst specific to this particular choice of chemistry, formation of the secondary network by this route could potentially eliminate concerns associated with leaching in traditional DN hydrogels. Systems based on alternate coupling chemistries are currently under development.

#### **4.6 Conclusions**

The homogeneity in structure provided by melt-state self-assembly of sphere-forming blends of PS-PEO diblock and PS-PEO-PS triblock copolymers produces a primary network of spherical domains that remains incredibly elastic when swollen in water. Such hydrogel networks were able to absorb tensile strains to a few hundred percent, with the exact modulus exhibited tunable through the triblock copolymer concentration of the original melt-state blend.

By incorporating azide and alkyne functional PS-PEO diblock copolymer into the hydrogel framework, a secondary network of tethers could be reactively installed subsequent to reaching swelling equilibrium. Importantly, the installation of the second network did not influence the equilibrium water content of the hydrogel system. Through mechanical testing of the new system containing both primary and secondary networks, we were able to establish the passive nature of the secondary network under small strain dynamic shear and larger strain unconfined compression experiments. However, the presence of the secondary network was able to dramatically improve the high strain tensile properties (strain to break, stress to break, Young's modulus and toughness) of high water content hydrogels. For example, the toughness of hydrogels containing 95% water by mass was increased nearly 58-fold through secondary network installation. The impressive increase is believed to drive from the system's ability to gradually transfer load to the secondary network, which becomes increasingly engaged as the strain on the system grows. Thus, the secondary network provides an improved range over which strain energy can be absorbed by the hydrogel, particularly at very high swelling ratios.

#### **4.7 Recognitions**

This work was supported by the National Science Foundation (DMR-0645781) and Colorado State University.

#### **4.8 Supporting information found in the appendix**

<sup>1</sup>H-NMR spectrum of PS-PEO-H (Figure 4S.1); <sup>1</sup>H-NMR spectrum of PS-PEO-Ms (Figure 4S.2); <sup>1</sup>H-NMR spectrum of PS-PEO-azide (Figure 4S.3); <sup>1</sup>H-NMR spectrum of PS-PEO-alkyne (Figure 4S.4); FTIR result for PS-PEO-azide (Figure 4S.5); Frequency sweep results (elastic shear moduli) for samples A1 - D1, baseline SO/SOS hydrogels of 4.1 and 20.3

mol% SOS (Figure 4S.6), and a catalyst control sample; Unconfined compression for samples A1 - D1, and a catalyst control sample (Figure 4S.7) in Appendix.

## 4.9 References

- [1] G. W. M. V. Annette Rösler, Harm-Anton Klok, "Advanced drug delivery devices via self-assembly of amphiphilic block copolymers," *Advanced Drug Delivery Reviews*, vol. 53, pp. 95-108, 2001.
- [2] R. Huang, L. K. Kostanski, C. D. M. Filipe, and R. Ghosh, "Environment-responsive hydrogel-based ultrafiltration membranes for protein bioseparation," *Journal of Membrane Science*, vol. 336, pp. 42-49, 2009.
- [3] K. P. Jung Ju Kim, "Smart hydrogels for bioseparation," *Bioseparation*, vol. 7, pp. 177-184, 1998.
- [4] A. Khademhosseini and R. Langer, "Microengineered hydrogels for tissue engineering," *Biomaterials*, vol. 28, pp. 5087-92, Dec 2007.
- [5] T. K. B. Serguei V. Vinogradov, Alexander V. Kabanov, "Nanosized cationic hydrogels for drug delivery preparation, properties and interactions with cells," *Advanced Drug Delivery Reviews*, vol. 54, pp. 135-147, 2002.
- [6] K. B. K. Nikolaos A Peppas, Madeline Torres-Lugo, Anthony M Lowman, "Poly(ethylene glycol)-containing hydrogels in drug delivery," *Journal of Controlled Release*, vol. 62, pp. 81-87, 1999.
- [7] K. P. Yong Qiu, "Environment-sensitive hydrogels for drug delivery," *Advanced Drug Delivery Reviews*, vol. 53, pp. 321-339, 2001.
- [8] A. K. Bajpai, S. K. Shukla, S. Bhanu, and S. Kankane, "Responsive polymers in controlled drug delivery," *Progress in Polymer Science*, vol. 33, pp. 1088-1118, 2008.
- [9] A. S. Hoffman, "Hydrogels for biomedical applications," *Advanced Drug Delivery Reviews*, vol. 54, pp. 3-12, 2002.
- [10] S. W. K. Byeongmoon Jeong, You Han Bae, "Thermosensitive sol-gel reversible hydrogels," *Advanced Drug Delivery Reviews*, vol. 54, pp. 37-51, 2002.
- [11] K. T. Nguyen and J. L. West, "Photopolymerizable hydrogels for tissue engineering applications," *Biomaterials*, vol. 23, pp. 4307-4314, 2002.
- [12] W. E. Hennink and C. F. van Nostrum, "Novel crosslinking methods to design hydrogels," *Advanced Drug Delivery Reviews*, vol. 54, pp. 13-36, 2002.
- [13] T. S. B. Chen Guo, "Tailoring the Nanostructures of Tethered-sphere Hydrogel Networks," *In preparation*, 2011.
- [14] C. Guo and T. S. Bailey, "Highly distensible nanostructured elastic hydrogels from AB diblock and ABA triblock copolymer melt blends," *Soft Matter*, vol. 6, p. 4807, 2010.
- [15] V. F. Scalfani and T. S. Bailey, "Access to Nanostructured Hydrogel Networks through Photocured Body-Centered Cubic Block Copolymer Melts," *Macromolecules*, vol. 44, pp. 6557-6567, 2011/08/23 2011.
- [16] K. Yasuda, J. Ping Gong, Y. Katsuyama, A. Nakayama, Y. Tanabe, E. Kondo, M. Ueno, and Y. Osada, "Biomechanical properties of high-toughness double network hydrogels," *Biomaterials*, vol. 26, pp. 4468-75, Jul 2005.
- [17] J. P. Gong, Y. Katsuyama, T. Kurokawa, and Y. Osada, "Double-Network Hydrogels with Extremely High Mechanical Strength," *Advanced Materials*, vol. 15, pp. 1155-1158, 2003.
- [18] R. P. Quirk and J. J. Ma, "Characterization of the functionalization reaction product of poly(styryl)lithium with ethylene oxide," *J. Polym. Sci., Part A: Polym. Chem.*, vol. 26, pp. 2031-7, 1988.

- [19] M. A. Hillmyer and F. S. Bates, "Synthesis and Characterization of Model Polyalkane-Poly(ethylene oxide) Block Copolymers," *Macromolecules*, vol. 29, pp. 6994-7002, 1996.
- [20] P. G. Fragouli, H. Iatrou, and N. Hadjichristidis, "Synthesis and characterization of linear diblock and triblock copolymers of 2-vinyl pyridine and ethylene oxide," *Polymer*, vol. 43, pp. 7141-7144, 2002.
- [21] J. H. Dmitri A. Ossipov, "poly(vinyl alcohol) based hydrogels formed by click chemistry," *Macromolecules*, vol. 5, pp. 1709-1718, 2006.
- [22] S. S. Iyer, A. S. Anderson, S. Reed, B. Swanson, and J. G. Schmidt, "Synthesis of orthogonal end functionalized oligoethylene glycols of defined lengths," *Tetrahedron Letters*, vol. 45, pp. 4285-4288, 2004.
- [23] I. T. Yassin A. Aggour, Takeshi Endo, "Synthesis and radical polymerization of end-allenoxy polyoxyethylene macromonomer," *Reactive and Functional Polymers* vol. 28, pp. 81-87, 1995.
- [24] A. K. Gaharwar, S. A. Dammu, J. M. Canter, C. J. Wu, and G. Schmidt, "Highly extensible, tough, and elastomeric nanocomposite hydrogels from poly(ethylene glycol) and hydroxyapatite nanoparticles," *Biomacromolecules*, vol. 12, pp. 1641-50, May 9 2011.
- [25] L. G. G. Vsevolod V. Rostovtsev, Valery V. Fokin, Barry Sharpless, "A Stepwise Huisgen Cycloaddition Process Copper(I)-Catalyzed Regioselective "Ligation" of Azides and Terminal Alkynes," *Angewandte Chemie International Edition*, vol. 41, pp. 2596-2599, 2002.
- [26] W. H. Binder and R. Sachsenhofer, "'Click' Chemistry in Polymer and Materials Science," *Macromolecular Rapid Communications*, vol. 28, pp. 15-54, 2007.
- [27] S. P. Vijayalakshmi, A. Raichur, and G. Madras, "Thermal degradation of poly(ethylene oxide) and polyacrylamide with ascorbic acid," *Journal of Applied Polymer Science*, vol. 101, pp. 3067-3072, 2006.
- [28] F. Z. Michael M Crowley, John J Koleng, James W McGinity, "Stability of polyethylene oxide in matrix tablets prepared by hot-melt extrusion," *Biomaterials*, vol. 23, pp. 4241-4248, 2002.

## CHAPTER 5

### CONCLUSIONS AND FUTURE WORK<sup>5</sup>

#### 5.1 Conclusion

The major achievements described in this dissertation include: 1) the development of a novel tethered micelle hydrogel system utilizing melt self-assembly of sphere forming SO and SOS blends (Chapter 2), 2) an improved understanding of the role of coronal layer overlap on the mechanical properties of these hydrogels and the synthetic parameters available to control that overlap, (Chapter 3), and 3) a demonstration of the functionalization potential intrinsic to these networks, by using chain end functionalization as a route to greatly improved hydrogel toughness.

Through the combination of environmental temperature (10 – 50 °C), SOS concentration (3 -72 mol%) and PEO mid-block molecular weight in the SOS tether (1, 1.6 and 2.3 times of the lattice matched length), we were able to successfully tune the equilibrium swelling ratios from 3 to 73 g H<sub>2</sub>O/g polymer, elastic modulus from 10<sup>2</sup> to 10<sup>5</sup> Pa, and compressive modulus from 10<sup>3</sup> to 10<sup>6</sup> Pa. We found the nanostructure formed using melt state self-assembly produced an intrinsic toughness in the range of 200 – 300 kJ m<sup>-3</sup> when the SOS concentration exceeded 20 mol%. However, toughness dramatically decreased to a few kJ m<sup>3</sup> as SOS mol fraction approached 10 mol%. Using post swelling click chemistry to install a secondary network of

---

<sup>5</sup> The contents of this dissertation chapter were written by Chen Guo.

tethers, we could produce a 58-fold increase in toughness without influence to hydrogel shape, swelling ratio, dynamic shear modulus or unconfined compressive performance.

## **5.2 Future work**

### **5.2.1 Sample preparation for tensile tests**

Measurements of hydrogel tensile properties are inherently plagued by defects produced during sample processing. Extraction of accurate toughness, strain at break, stress at break, and tensile modulus proved extremely difficult, especially on hydrogel systems exhibiting higher water contents. We found that defects caused by incomplete fusion of polymer particles and/or formation of air bubbles produced the weakest locations that could be easily fractured even under small strains. The problem was partially solved in Chapter 4 by carefully melt-pressing a single piece of polymer which was solution blended and then freeze-dried. Such simple processing changes provided significant improvement in the tensile strain to break values that could be measured. Optimum polymer processing and hydrogel sample preparation conditions need to be investigated in order to measure the tensile properties more accurately. Development of improved processing strategies is a critical topic for future work.

### **5.2.2 Mass transfer properties and pore structures in the hydrogels**

The potential application of these hydrogels as membranes was also preliminarily tested during the course of this thesis work using hydrogels formed from SO/SOS blends containing 7.5 mol% PS-PEO-PS triblock copolymer ( $f_{PS}=0.10$ ). A polymer thin film was prepared by hot-pressing the polymer sample between two Teflon sheets at 150 °C at 500 psi. The film (~10 μm) was removed from the Teflon sheets after cooling to room temperature and subsequently swollen in DI water. The hydrogel film swelled to equilibrium in less than 10 minutes and was then

carefully supported between sheets of filter paper (0.45  $\mu\text{m}$  pore size, Millipore). The membrane stack was placed in a membrane holder and connected to a FPLC. The flow rate was adjusted on the FPLC and the pressure values were measured under various flow rates. Water flux was calculated using the flow rate and the exposed membrane area (diameter = 1.4 cm). In this preliminary study, the flow rate was increased from 0.05 to 0.35 ml/min by 0.02 increments. As the pressure increased, the value of the water flux increased in an approximately linear fashion. The membrane stack could withstand pressures up to approximately 0.6 MPa, while the corresponding water flux reached close to 140 L/h  $\text{m}^2$ .

To better study the mass transfer properties of these hydrogels, a thin membrane preparation method which produces membranes with controllable, uniform thicknesses needs to be developed. More detailed membrane characterization methods also need to be employed. The fact that the film was extremely thin and delicate made handling difficult, and efficient methods for transfer to membrane supports are also needed to properly advance the potential of these hydrogels as viable membrane constructs.

### **5.2.3 Alternate Methods Towards Porosity Control**

Interestingly, one of our earlier attempts to control the porosity in our hydrogel network was to explore methods of shortening the coronal layer surrounding the PS micellar core. At that point we had not yet experimented with increasing the tether lengths, and did not yet fully understand the role of the coronal layer overlap in determining the mechanical properties of the tethered micelle network. Our approach was based on taking advantage of the miscibility of PEO and polylactide (PLA)<sup>1</sup> as a means of introducing a selectively etchable block (PLA) into the coronal layer previously occupied by only PEO. The key to being able to maintain the spherical

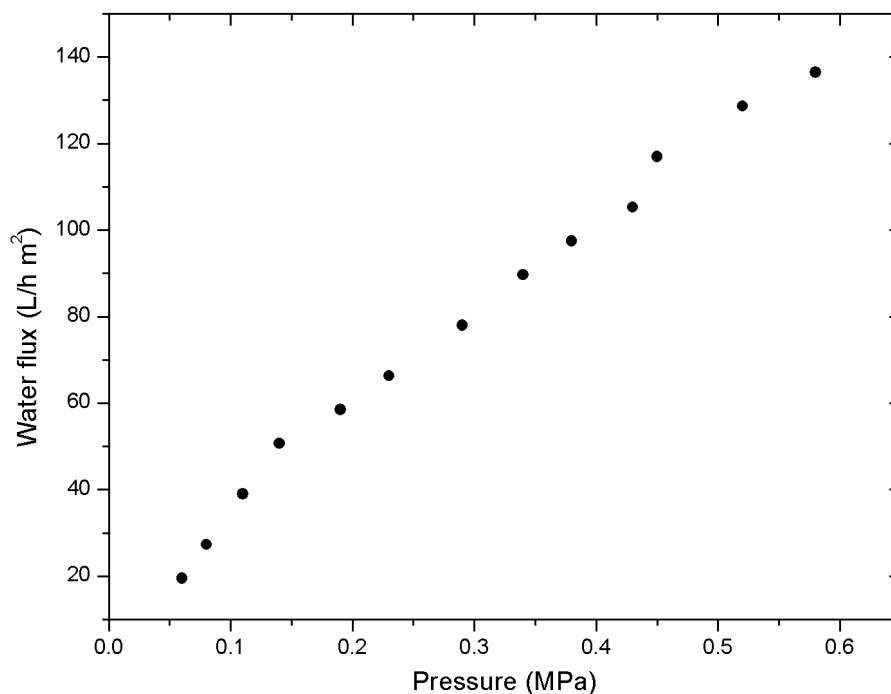


**Figure 5.1. Water flux of a tethered micelle hydrogel membrane (7.5 mol% SOS) sandwiched between two filter paper support layers.**

morphology in the melt was for the system to continue to phase separate as a diblock copolymer would, despite the introduction of a third PLA block. This constraint required the PEO and PLA be miscible, and phase separate from the PS as a single domain. Our hypothesis was that sphere-forming PS-PEO-PLA triblock copolymers with various PEO/PLA compositions could be synthesized and blended with tethering PS-PEO-PS triblock copolymers. The blends could then melt-pressed into polymer disks which could be placed in basic solutions, etching away the PLA block. Depending on the ratio of PEO and PLA, hydrogels with various coronal thicknesses could be produced. At that point, we were more focused on the open space created from material removal, and most often used the term increased porosity to describe our overriding goal.

As a preliminary study, a symmetric PS-PEO diblock copolymer ( $f_{PS} = 0.5$ ) was synthesized and used as a macroinitiator for the subsequent growth of a third PLA block. To demonstrate the etchability of the PLA block without destroying PS-PEO diblock copolymers, a PS-PEO-PLA triblock copolymer dry disk containing small amount of PS-PEO-PS triblock copolymer as tethers was hot pressed, cooled to room temperature, and immersed into an aqueous solution of NaOH (1.0M) for 24 hours. SEC traces of the original PS-PEO, PS-PEO-PLA and the polymer residue comprising the hydrogel after PLA degradation are shown in Figure 5.2. As shown in the figure, significant molecular weight increase is seen when the PLA block was grown onto the PS-PEO. Also, once the PLA block was removed, the remaining PS-PEO diblock copolymer shows no significant difference from the original PS-PEO, suggesting the etching process can be successfully performed on the material without degradation of the remaining PS-PEO diblock copolymer.

In the preliminary study, the PS-PEO-H had a PS volume fraction of 50% prior to PLA addition. Following PLA addition the PS volume fraction was reduced to around 13%. Since PLA is not water soluble, significant degradation of the hydrogel had to occur before the hydrogel disk could become noticeably swollen. To our dismay (at that time), the etched hydrogels were often too weak to handle. In retrospect, the long tether study discussed in Chapter 3 explains the fragile nature of these hydrogels. The weakness is caused by the dramatic reduction in (elimination of?) coronal layer overlap. Another significant difference in behavior observed in these systems from the standard SO/SOS block copolymer systems was that the etched hydrogels seemed to peel once placed in water, along what we suspected were Flory-Huggins parameter between PS and PLA that is much higher than the value between PS and PEO. Given our greater understanding of the importance of coronal layer overlap, it would

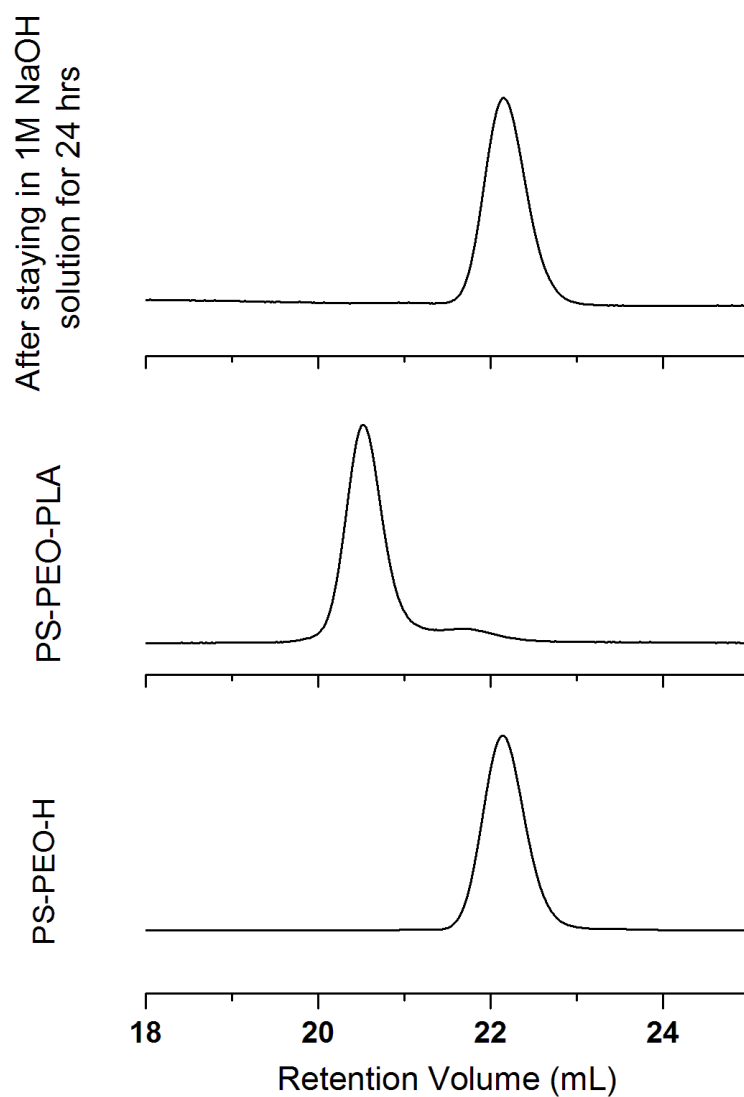


**Figure 5.2. SEC traces of PS-PEO-H, PS-PEO-PLA and the remaining polymer in the hydrogel following PLA degradation.**

inefficiently fused particle interfaces during melt-processing. This may be a consequence of a be interesting to revisit this approach with PS-PEO-PLA systems in which the etchable PLA block is significantly smaller.

#### **5.2.4 Ionic liquid gels and gels swollen in biological buffer solutions**

In addition to swelling in DI water, we recently started to exploit the possibility of preparing tethered micelle networks using other swelling media, including biologically relevant buffer solutions and room-temperature ionic liquids (RTILs). The buffer swollen gels were prepared as part of a preliminary protein immobilization study, which is now being continued by master's student Jackson Lewis. Early investigations of these hydrogels showed complete stability of the hydrogel in buffer environment. The RTIL project was started as a collaboration with the Douglas L. Gin group at University of Colorado at Boulder.<sup>2</sup> The Gin group had previously demonstrated the promising potential of imidazolium based RTILs as active media in light gas (CO<sub>2</sub>/N<sub>2</sub>, e.g.) separations. As a collaborative effort, our group proposed using the tethered micelle network as a supporting material for RTILs separations. In the initial work, polymer disks prepared from SO/SOS blends were placed into various RTILs to check their swelling behavior and mechanical properties. Preliminary studies showed that only water soluble RTILs would penetrate into the polymer disks to form swollen gels. These RTIL gels showed a significant difference in both the swelling and the mechanical properties when compared with water swollen gels. One of the challenges in this project was the limited RTIL available due to the difficulty of their synthesis and purification. However, the initial data suggests this area remains a good opportunity for future studies.

#### **5.2.5 Small molecule immobilization**

In chapter 4, the hydroxyl groups on the dangling PS-PEO chains were proven to be easily modified to alkyne and azide functional groups, and in that case used to achieve simple diblock copolymer coupling in situ. The results of this chapter imply that such functionalization

might be used in the future as a means of immobilizing other important ligands, including peptide sequences, enzymes, small molecule catalysts, or other biologically relevant molecules. Thus there is great potential for this hydrogel networks to be adapted to biological applications involving drug delivery, cell culture, wound healing, and tissue engineering.

### 5.3 References

- [1] A. J. Nijenhuis, E. Colstee, D. W. Grijpma, and A. J. Pennings, "High molecular weight poly(l-lactide) and poly(ethylene oxide) blends: thermal characterization and physical properties," *Polymer*, vol. 37, pp. 5849-5857, 1996.
- [2] A. L. LaFrate, J. E. Bara, D. L. Gin, and R. D. Noble, "Diol-Functionalized Imidazolium-Based Room-Temperature Ionic Liquids with Bis(trifluoromethanesulfonimide) Anions that Exhibit Variable Water Miscibility," *Industrial & Engineering Chemistry Research*, vol. 48, pp. 8757-8759, 2009/09/16 2009.

## APPENDIX

### SUPPLEMENTARY INFORMATION<sup>6</sup>

#### Supplementary Information for Chapter 2:

Highly Distensible Nanostructured Elastic Hydrogels from AB Diblock and ABA Triblock Copolymer Melt Blends

#### S 2.1 Determination of SOS triblock copolymer concentration in SOS-72.0 by regression analysis

The coupling efficiency of the **SOS-72.0** sample (referred to as SOS- $X_0$  below) was determined using linear least squares regression of the following equation, as described in the primary manuscript:

$$w_{i,SEC} = w_0 \cdot \left( \frac{m_{SOS-X_0}}{m_{SOS-X_0} + m_{SO}} \right) \quad (1)$$

---

<sup>6</sup> The contents of this dissertation Appendix consist of supporting information contained in the following publications and an example matlab calculation of the P-Y fitting:

Chapter 2 - Chen Guo and Travis S. Bailey. Highly Distensible Nanostructured Elastic Hydrogels from AB Diblock and ABA Triblock Copolymer Melt Blends. *Soft Matter*, 2010, **6**, 4807-4818.

Chapter 3 - Chen Guo and Travis S. Bailey. Effects of Tailored Coronal Layer Overlap in Tethered Micelle Hydrogel Networks, In preparation.

Chapter 4 - Chen Guo, Jackson T. Lewis, Vincent F. Scalfani, Miriah M. Schwartz and Travis S. Bailey. Improving Toughness in Highly Swollen Block Copolymer Based Hydrogel Networks. In preparation.

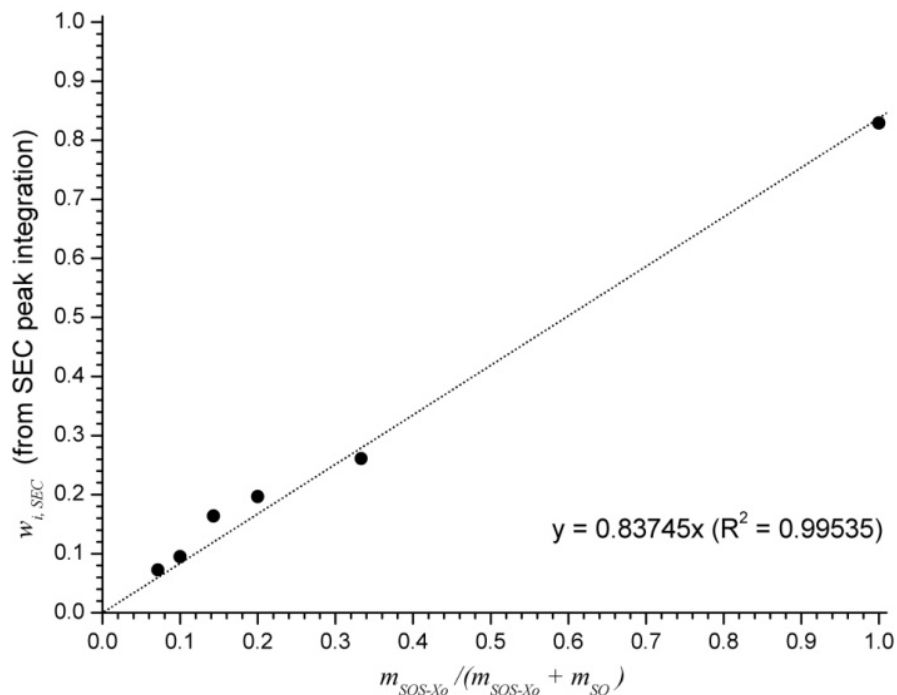


**Figure 2S. 1** The determination of  $w_0$  by linear regression helps minimize error associated with integrating relative chromatogram peak intensities in cases (such those found here) where peaks are both partially overlapping and of significantly different intensities. Compare with Fig. 4 in the primary manuscript.

Here,  $w_{i,SEC}$  represents the weight fraction of triblock copolymer in blend sample  $i$ ,  $i$  determined by integrating the relative areas under the SEC chromatogram, and the term in parentheses represents the weight fraction of the **SOS- $X_0$**  sample added to the blend. By plotting the pairs of these values for each blend in Table 2.2, the mass fraction of triblock copolymer in **SOS- $X_0$** ,  $w_0$ , could be obtained from the slope of the regressed line (Figure 2S.1). This analysis gave  $w_0 = 0.837$ , which equates to a molar concentration of triblock copolymer,  $X_0 = 72.0$  mol.

## S 2.2 Differential scanning calorimetry (DSC) data for the S-OH and SO samples

As discussed in the primary manuscript, DSC data was collected for the **S-OH** and **SO** samples using a heating rate of  $10 \text{ }^\circ\text{C min}^{-1}$ . The **S-OH** bulk PS sample (7.0 mg) exhibited a glass transition at  $80.16 \text{ }^\circ\text{C}$ , however no such transition was detected in the **SO** (6.2 mg) sample

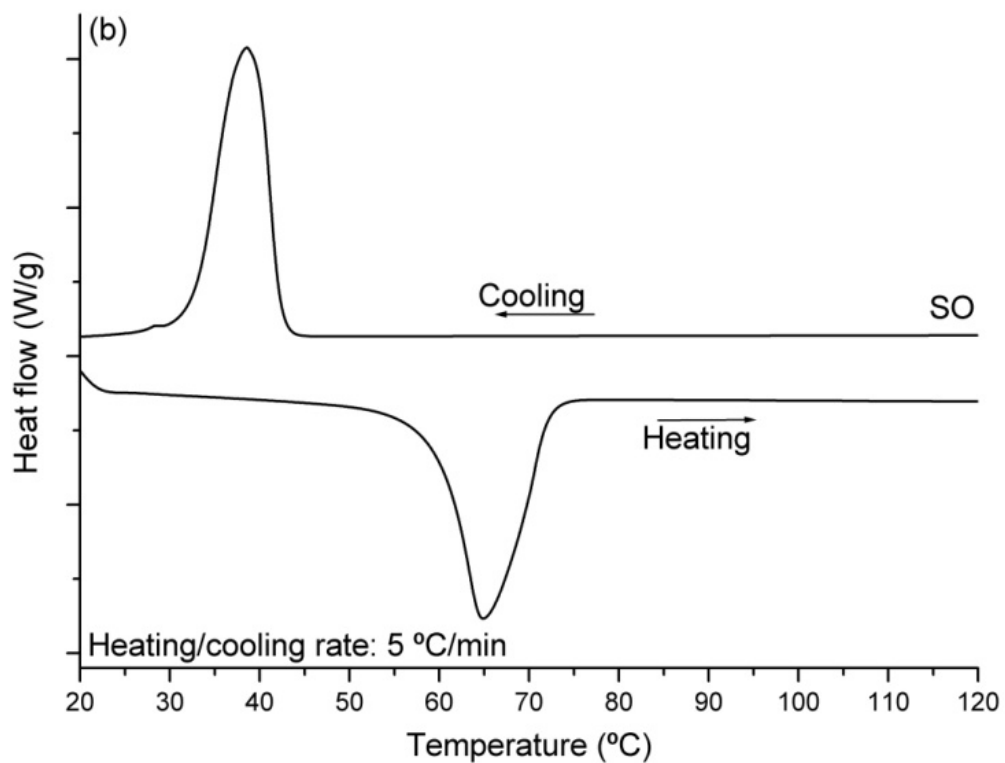
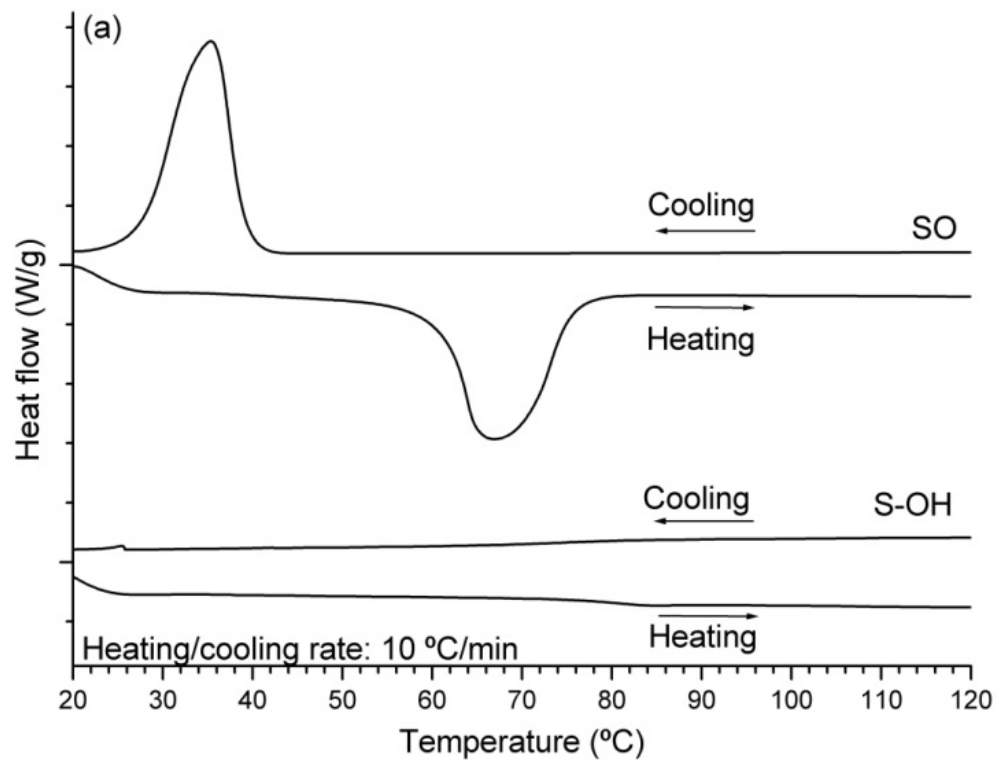


Figure 2S. 2 (a) DSC data for S-OH and SO samples ( $10\text{ }^{\circ}\text{C min}^{-1}$ ). (b) DSC data for SO ( $5\text{ }^{\circ}\text{C min}^{-1}$ ).

(Figure 2S.2a). Subsequent data collected on double the amount (12.7 mg) at  $5\text{ }^{\circ}\text{C min}^{-1}$  showed no detectable differences (Figure 2S.2b).

### S 2.3 Melt-state rheological analysis of the SO and SOS-72.0 samples

Melts of both **SO** and **SOS-72.0** samples exhibited elastic moduli in the  $10^3 - 10^5$  Pa range (typical of ordered block copolymer melts) up to  $150\text{ }^{\circ}\text{C}$  (Figure 2S.3). The transitions detected at around  $65\text{ }^{\circ}\text{C}$  correspond to the melting transition of PEO. The lack of a plateau region is typical of spherical morphologies with more liquid-like order.

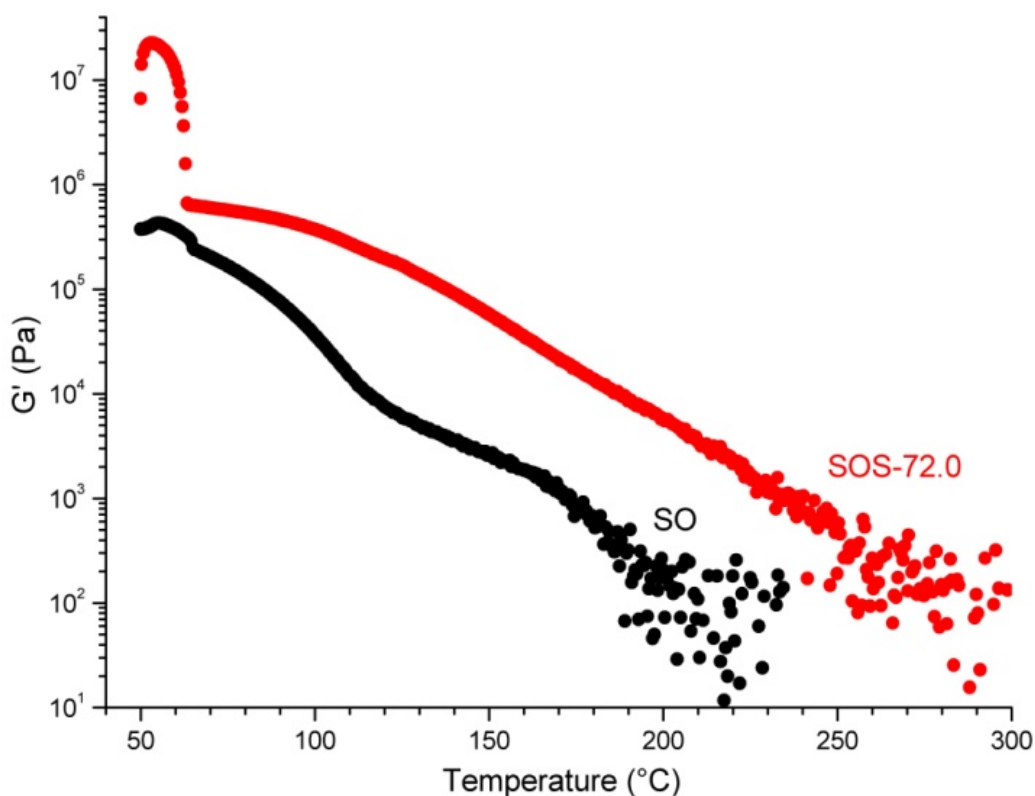


Figure 2S. 3 Dynamic temperature ramp data (oscillatory shear) for the SO and SOS-72.0 samples. Data were collected at  $1\text{ }^{\circ}\text{C min}^{-1}$  at a frequency of  $1\text{ rad s}^{-1}$  and a strain of 2%.

## S 2.4 Additional notes on the analysis of morphology from SAXS

The determination of the bcc unit cell lattice constant and the PS spherical domain radii from the SAXS data for the **SO** and **SOS-72.0** melts was based on the assumption that the principal scattering wave vector corresponded to the first allowed reflection for the Im3m (bcc) space group. The first allowed reflection corresponds to the 110 family of crystal planes, for which the d-spacing is given by:

$$d_{110} = \frac{2\pi}{q_{110}} \quad (2)$$

This distance corresponds one half of the face diagonal, such that the unit cell lattice constant is given by:

$$a_{bcc} = \sqrt{2}d_{110} \quad (3)$$

If one assumes that all of the PS is located within the spherical domains, then the radii of the PS domains can be estimated since the volume fraction of PS is known. Recalling the bcc lattice contains 2 complete spheres, the volume occupied by a sphere is:

$$V_{PS} = \frac{f_{PS} \cdot (\sqrt{2}d_{110})^3}{2} \quad (4)$$

And its radius is:

$$R_{PS} = \left( \frac{3}{4\pi} \cdot \frac{f_{PS} \cdot (\sqrt{2}d_{110})^3}{2} \right)^{1/3} \quad (5)$$

Finally, once the radius of the sphere is known, the aggregation number can be estimated using the density and molecular weight of the PS block:

$$\theta_{PS} = \left( \frac{4}{3} \pi R_{PS}^3 \right) \left( \frac{\rho_{PS}}{M_{n,PS}} \right) N_A \quad (6)$$

Note that this expression was used to calculate the aggregation numbers of the PS domains for both cases, that is when the radius was estimated using the bcc lattice as an approximation, and when the radius was determined using the more rigorous PY model to fit the SAXS data.

Finally, the nonlinear algebraic function  $G(q, R_{hs}, \phi_{hs})$  used in

$S(q, R_{hs}, \phi_{hs})$  is:

$$\begin{aligned}
G(q, R_{hs}, \phi_{hs}) &= \frac{\alpha}{(2qR_{hs})^2} (\sin(2qR_{hs}) - 2qR_{hs} \cos(2qR_{hs})) \\
&+ \frac{\beta}{(2qR_{hs})^3} (4qR_{hs} \sin(2qR_{hs})) \\
&+ \frac{\beta}{(2qR_{hs})^3} \left( (2 - (2qR_{hs})^2) \cos(2qR_{hs}) - 2 \right) \\
&+ \frac{\gamma}{(2qR_{hs})^5} \left( -(2qR_{hs})^4 \cos(2qR_{hs}) \right) \\
&+ \frac{\gamma}{(2qR_{hs})^5} \left( 4(3(2qR_{hs})^2 - 6) \cos(2qR_{hs}) \right) \\
&+ \frac{\gamma}{(2qR_{hs})^5} \left( 4((2qR_{hs})^3 - 6(2qR_{hs})) \sin(2qR_{hs}) + 24 \right) \\
\alpha &= \frac{(1 + 2\phi_{hs})^2}{(1 - \phi_{hs})^4} \\
\beta &= \frac{-6\phi_{hs} (1 + \phi_{hs}/2)^2}{(1 - \phi_{hs})^4} \\
\gamma &= \frac{\phi_{hs} (1 + 2\phi_{hs})^2}{2(1 - \phi_{hs})^4}
\end{aligned}$$

## Supplementary Information for Chapter 3:

### Effects of Tailored Coronal Layer Overlap in Tethered Micelle Hydrogel Networks

#### S 3.1 DSC of S-OH

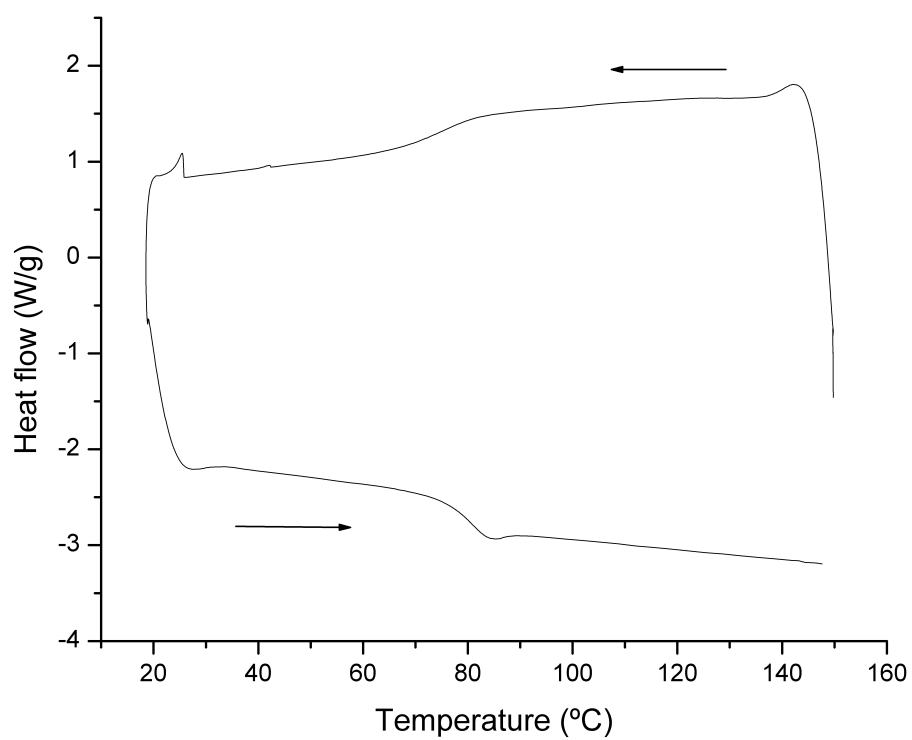
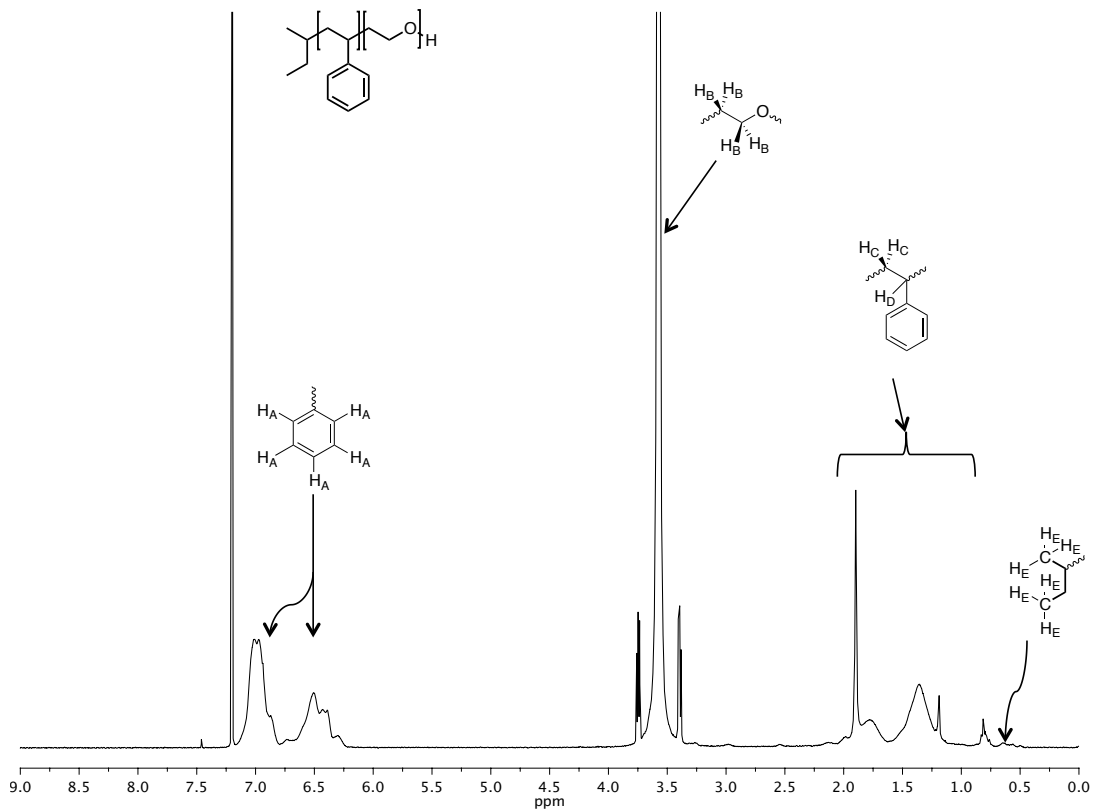


Figure S3.1. DSC of polystyrene homopolymer (S-OH) with molecular weight of 8390 g mol<sup>-1</sup>.

## Supplementary Information for Chapter 4:

### Improving Toughness in Highly Swollen Block Copolymer Based Hydrogel Networks

#### S4.1 $^1\text{H-NMR}$ spectrum of PS-PEO-H



**Figure 4S. 1.**  $^1\text{H-NMR}$  spectrum of PS-PEO-H diblock copolymer. The PS-PEO-PS triblock copolymer, PS-PEO-azide diblock copolymer, and PS-PEO-alkyne diblock copolymer were all generated from the above parent diblock copolymer molecule.

## S4.2 $^1\text{H-NMR}$ spectrum of PS-PEO-Ms

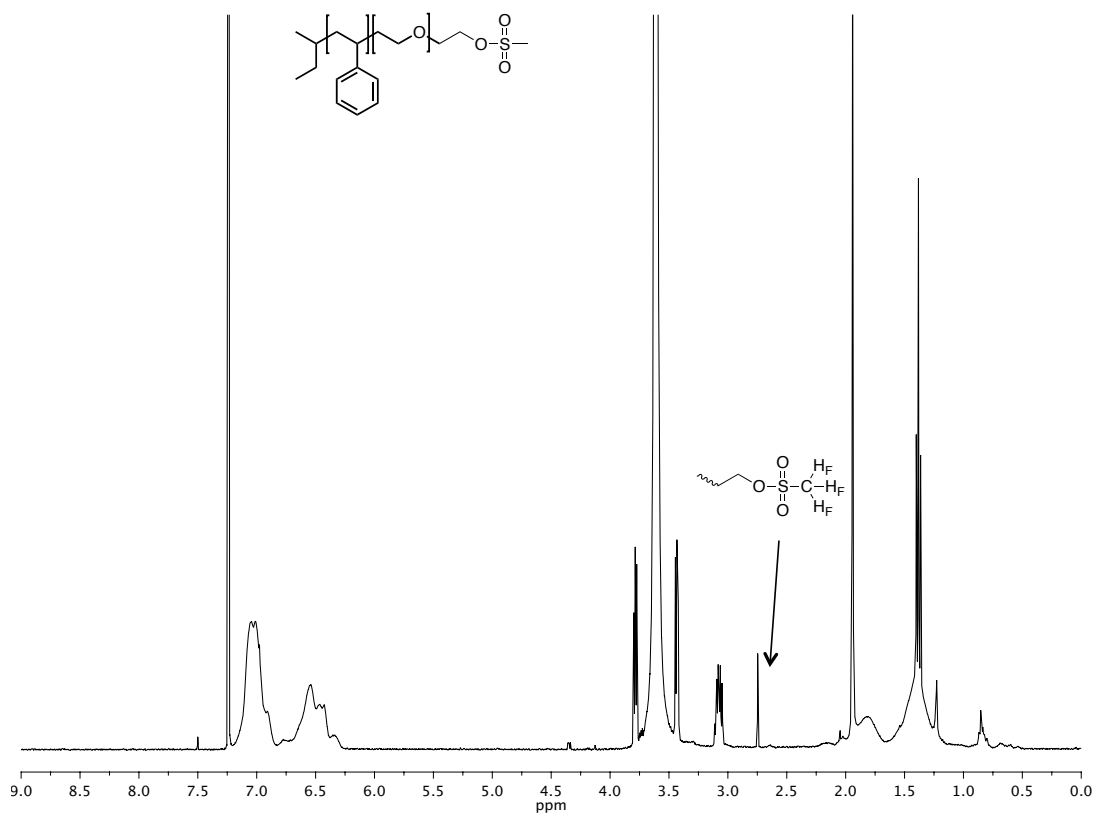
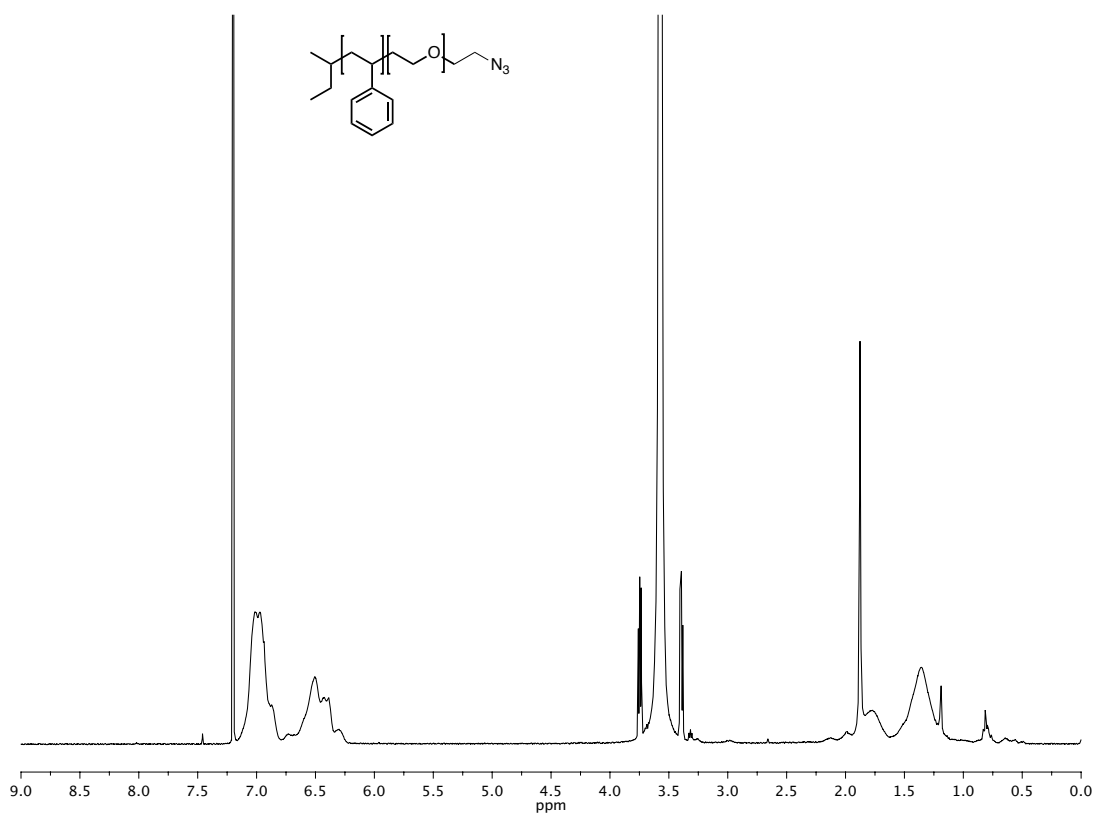


Figure 4S.2.  $^1\text{H-NMR}$  spectrum of PS-PEO-Ms (methanesulfonyl (mesyl)). This compound is the precursor of PS-PEO-azide.

### S4.3 $^1\text{H-NMR}$ spectrum of PS-PEO-azide



**Figure 4S.3.**  $^1\text{H-NMR}$  spectrum of PS-PEO-azide. The terminal methylene protons adjacent to the azide end group overlap with the methylene protons of the PEO backbone (4.0-3.2 ppm). Confirmation of azide group functionality is shown in the FTIR spectrum in Figure 4S.5.

#### S4.4 $^1\text{H-NMR}$ spectrum of PS-PEO-alkyne

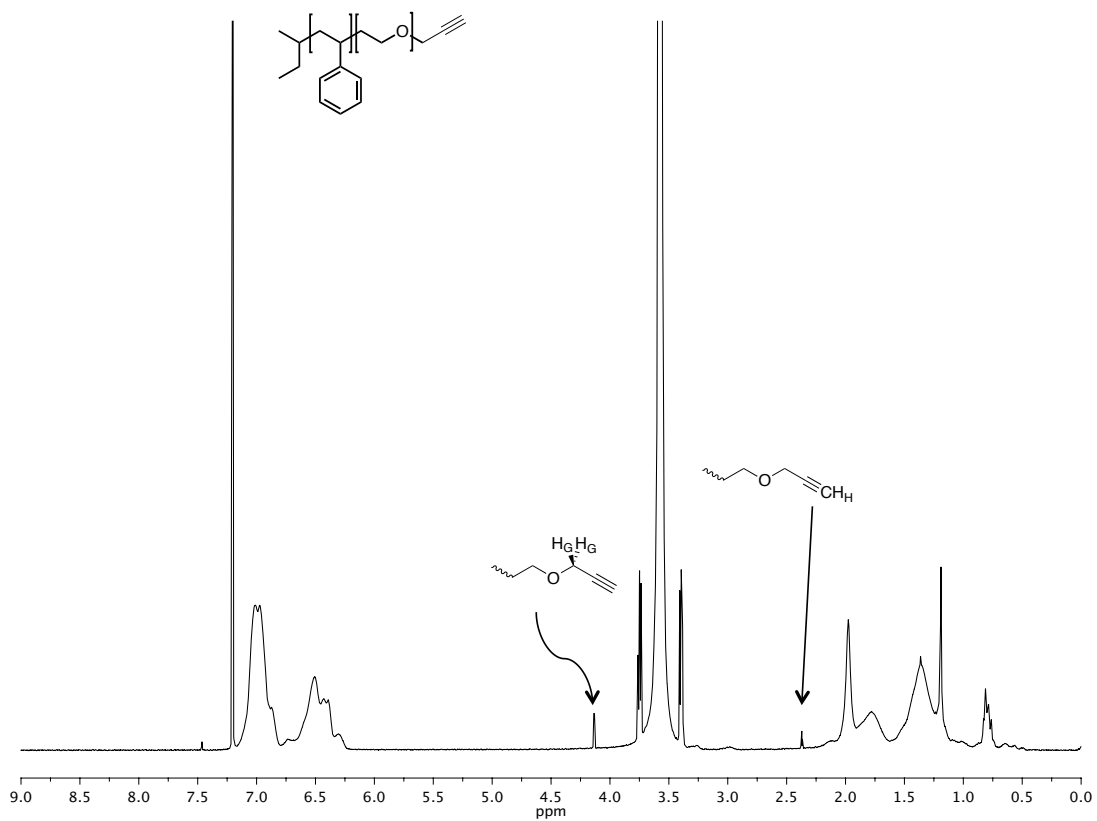


Figure 4S.4.  $^1\text{H-NMR}$  spectrum of PS-PEO-alkyne.

#### S4.5 FTIR spectrum of PS-PEO-azide

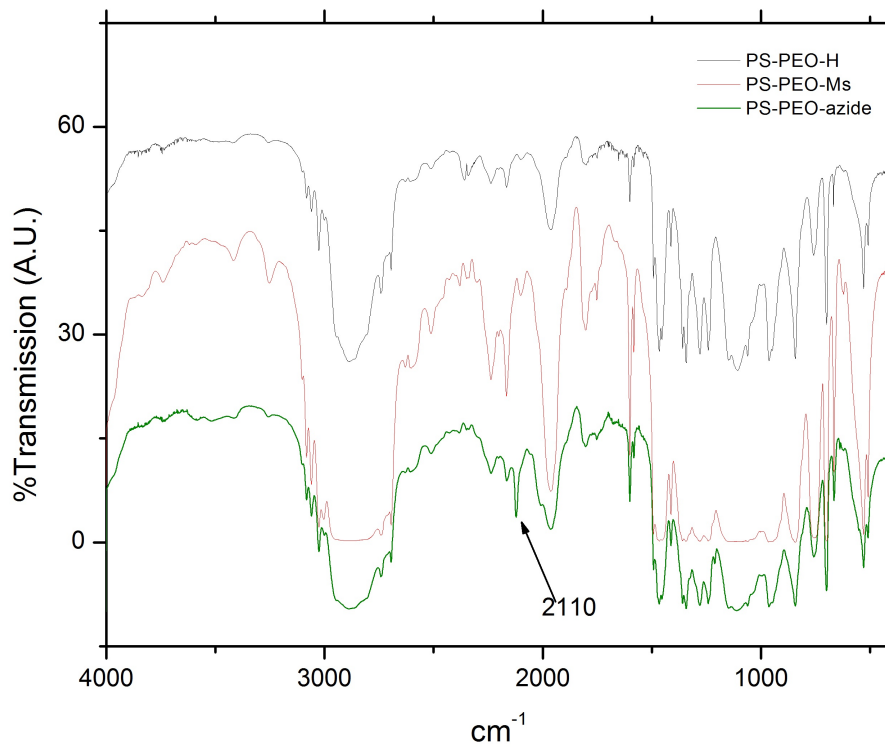
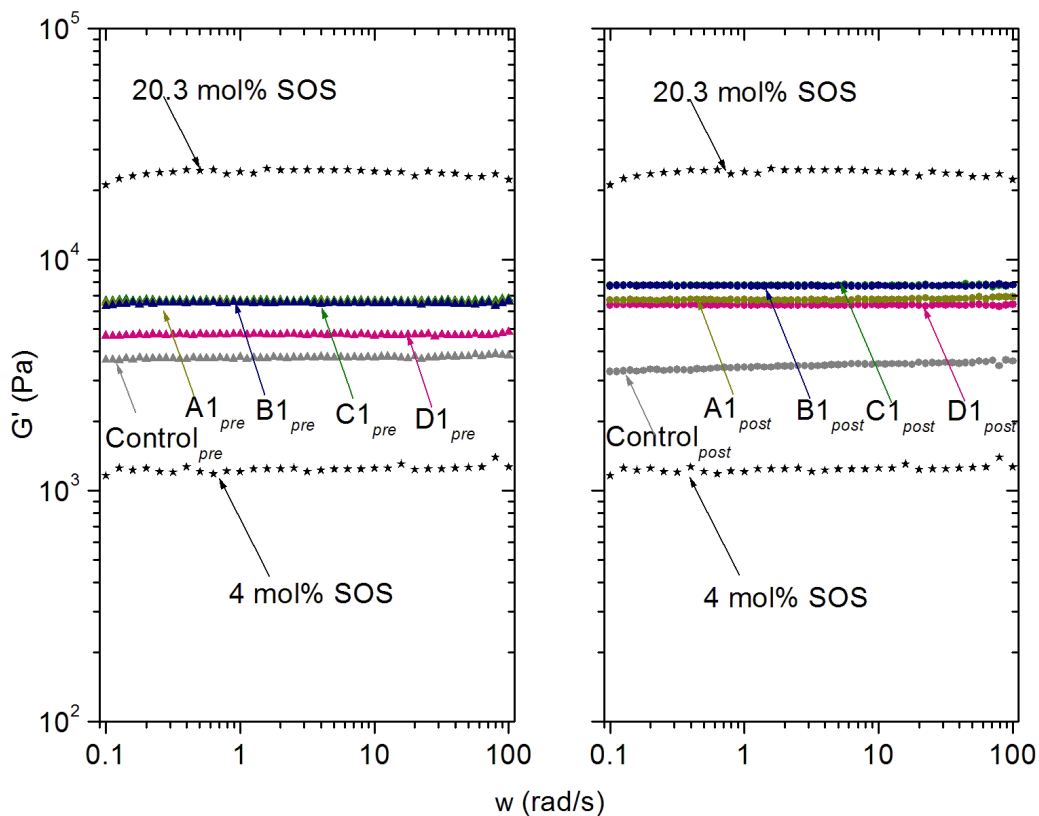


Figure 4S.5. FTIR spectra of PS-PEO-H, PS-PEO-Ms and PS-PEO-azide. The characteristic vibration for the azide group is shown at  $2110 \text{ cm}^{-1}$ .

**S4.6 Dynamic frequency sweep results (elastic shear moduli) for samples A1 - D1, baseline SO/SOS hydrogels of 4.1 and 20.3 mol% SOS, and a catalyst control sample**



**Figure 4S.6. Representative dynamic frequency sweep results showing the elastic moduli for samples A1 - D1, two baseline SO/SOS hydrogels of 4.1 and 20.3 mol% SOS, and a baseline SO/SOS hydrogel soaked in catalyst solution for 24 hours (control).**

### S4.7 Unconfined compression for samples A1 - D1, and a catalyst control sample

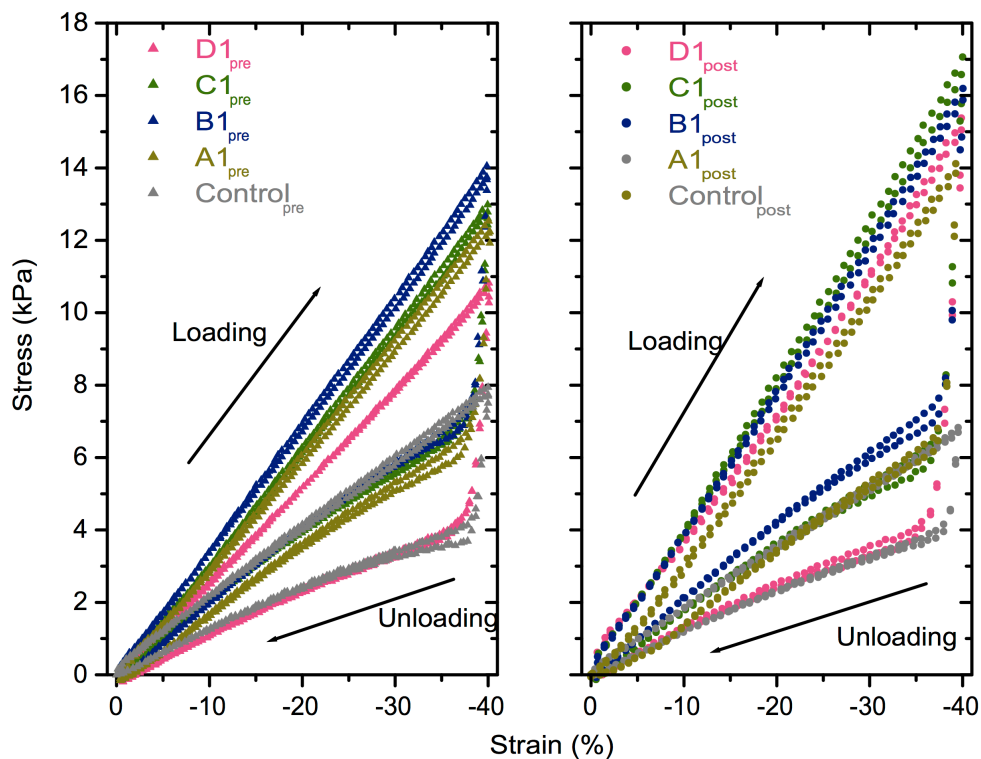


Figure 4S.7. Representative unconfined compression results showing the stress-strain relationships for samples A1 - D1, and a baseline SO/SOS control hydrogel soaked in catalyst solution for 24 hours (control).

## Example PY fitting using MATLAB

```
clc
clear

% Import raw data - full csv data file

file = 'SO_7200s_100C_raw_2.csv';
qvsI = importdata(file);
qrawfull = qvsI(:,1);
Irawfull = qvsI(:,2);

% Select subset of data set for background fit. Note this involves a little
% manual work to decide the regions to fit.

% low q region

lowrangemin = 20;
lowrangemax = 28;

% high q region

hirangemin = 105;
hirangemax = 130;

% Create single vector with all q and I data used to fit background

qbgfit = cat(1,qrawfull(lowrangemin:lowrangemax), qrawfull(hirangemin:hirangemax));
Ibgfit = cat(1,Irawfull(lowrangemin:lowrangemax), Irawfull(hirangemin:hirangemax));

figure(100)
plot(qrawfull, log10(Irawfull), qbgfit,log10(Ibgfit), '*');

% Creates functional form of background function

% a = [K tau beta]
a0 = [0.023 9 0.00625 0.5]; % guess
bgfit = @(a,qbgfit) log10(a(1)*10.^(a(2)*exp(-((qbgfit/a(3)).^a(4))));

bgguess = bgfit(a0,qbgfit);
figure(101)
plot(qrawfull, log10(Irawfull), qbgfit, bgguess, '*');

% Fit background

options = optimset('MaxFunEvals', 10000, 'MaxIter', 10000);
[afit, resnorm, residual, exitflag, output, lambda, jacobian] = ...
    lsqcurvefit(bgfit,a0,qbgfit,log10(Ibgfit),[],[],options);

% report fit parameters and plot fit with original data for comparison

afit
resnorm
Ibgfit = bgfit(afit, qrawfull);
figure (1)
plot(qrawfull,log10(Irawfull),qrawfull,Ibgfit, '*');

% Subtract Background

Isubfull = Irawfull - 10.^(Ibgfit);
```

```

% Save background corrected data

A = cat(2,qrawfull,Isubfull);
save SO_7200s_100C_raw_2_bgcor_full.txt A -ASCII
save SO_7200s_100C_raw_2_bgfitparam.txt afit -ASCII

% Select q (and corresponding I) region to PY fit

PYmin = 31;
PYmax = 97;

q = qrawfull(PYmin:PYmax);
I = Isubfull(PYmin:PYmax);

% Plot region prepared for PY fit

figure (2)
plot(q,log10(I), '*');

% determine the max in I and and its position in the vector. This is used
% in the next step to help create a good guess without worrying about the
% overall magnitude , i.e., K below.

[max, maxpos] = max(I);

% a = [K Rc sigmac xsi Rhs phihs sigmaq2]
b0 = [2.5 92 9.4 1.5 164 0.51 0.0002]; % guess

% define PY fitting function

PYfit = @(b,q) log10(b(1)*smear(q,b(2),b(3),b(4),b(5),b(6), b(7)*q.^2));

% Plot the PYfit with the guess against the background corrected data for
% comparison before running actual PYfit

PYguess = PYfit(b0,q);
normPYguess = (log10(I(maxpos))-PYguess(maxpos))+PYguess;
figure (3)
plot(q,log10(I),q,normPYguess, '*')

% Report calculated sphere core volume fraction produced from guess

fspguess = b0(6)*(b0(2)/b0(5))^3

% Perform Nonlinear PY fit

options = optimset('MaxFunEvals', 10000, 'Maxiter', 10000, 'TolFun', 1e-14);
[bfit,resnorm,residual,exitflag,output,lambda,jacobian] =...
    lsqcurvefit(PYfit,b0,q,log10(I),[],[],options);

bfit
resnorm
IPYfit = PYfit(bfit,q);

% Plot results with original data

figure (4)
plot(q,log10(I),'*',q,IPYfit)

```

```

% Calculate core volume fraction of fit

fsp = bfit(6)*(bfit(2)/bfit(5))^3

% write fit parameters and fit data to ascii files

B = cat(2,q,10.^(IPYfit));
save SO_7200s_100C_raw_2_fit.txt B -ASCII
save SO_7200s_100C_raw_2_fitparam.txt bfit -ASCII

```

Local minimum found.

Optimization completed because the size of the gradient is less than the default value of the function tolerance.

afit =

```

    0.0299    5.8111    0.0121    0.6738

```

resnorm =

```

    0.0014

```

fspguess =

```

    0.0900

```

Local minimum possible.

lsqcurvefit stopped because the final change in the sum of squares relative to its initial value is less than the selected value of the function tolerance.

bfit =

```

    2.5177   91.5060    7.0204    1.2593  166.2367    0.5331    0.0036

```

resnorm =

```

    0.0795

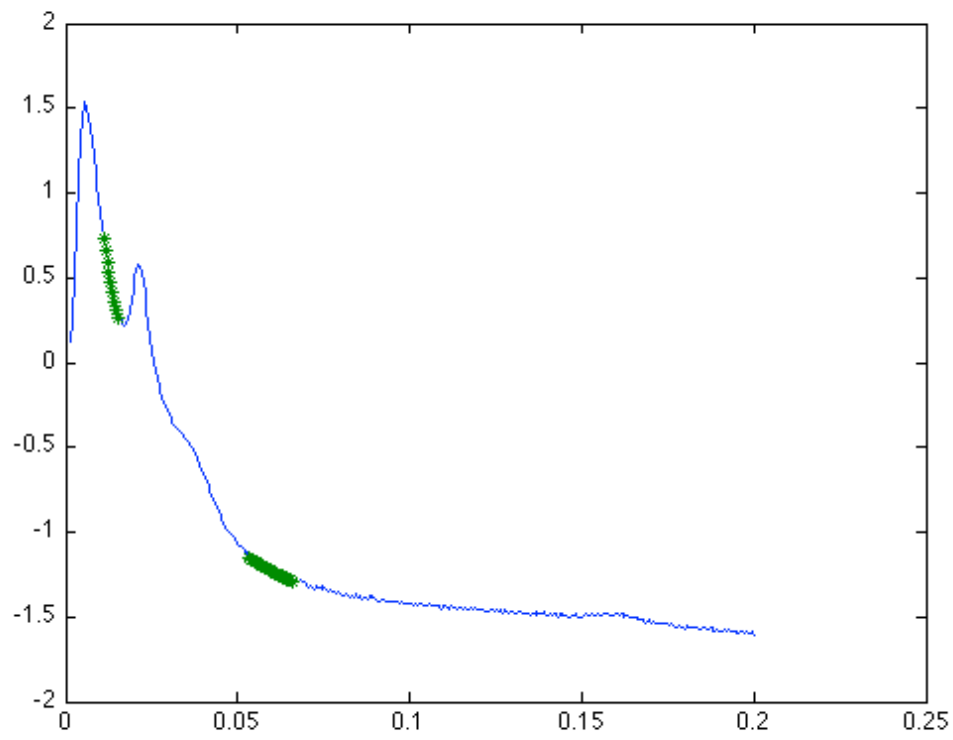
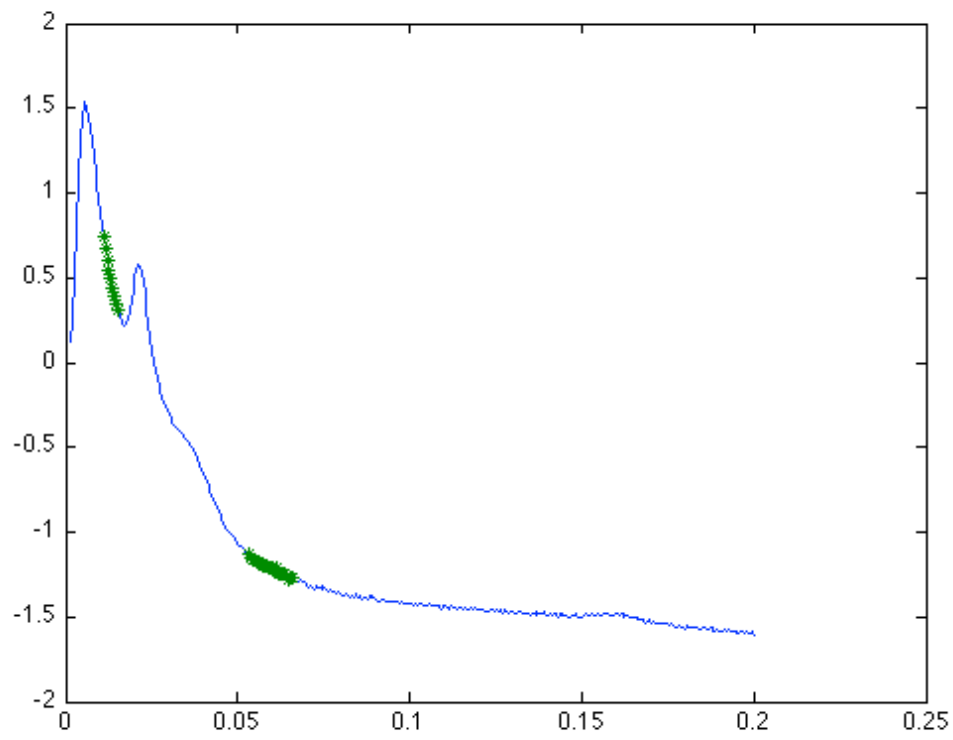
```

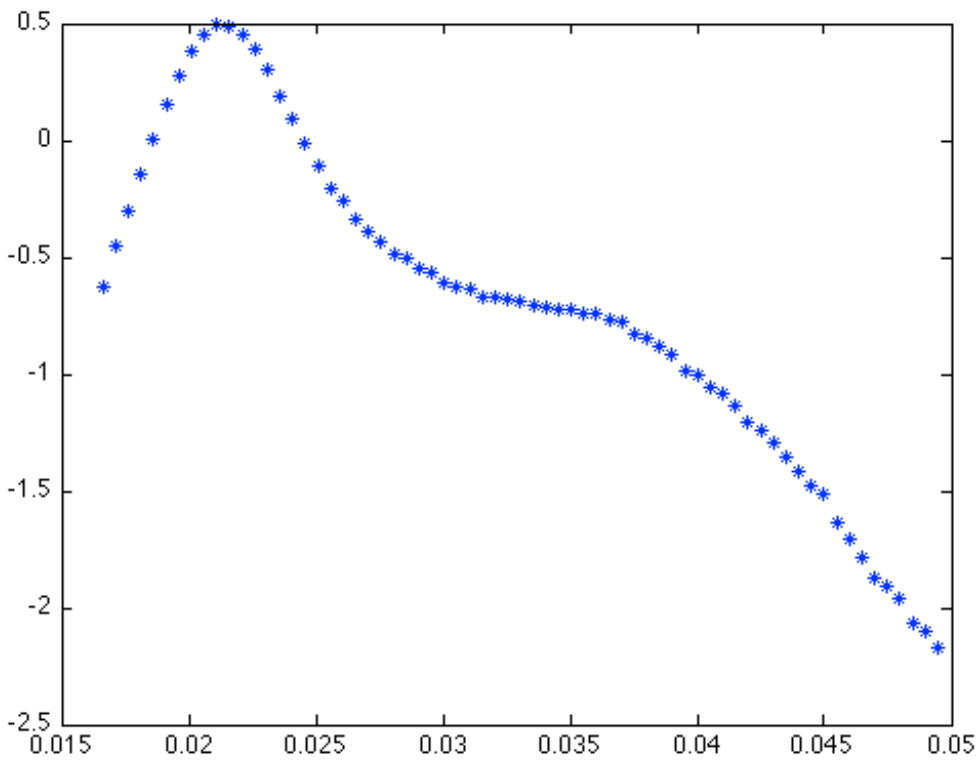
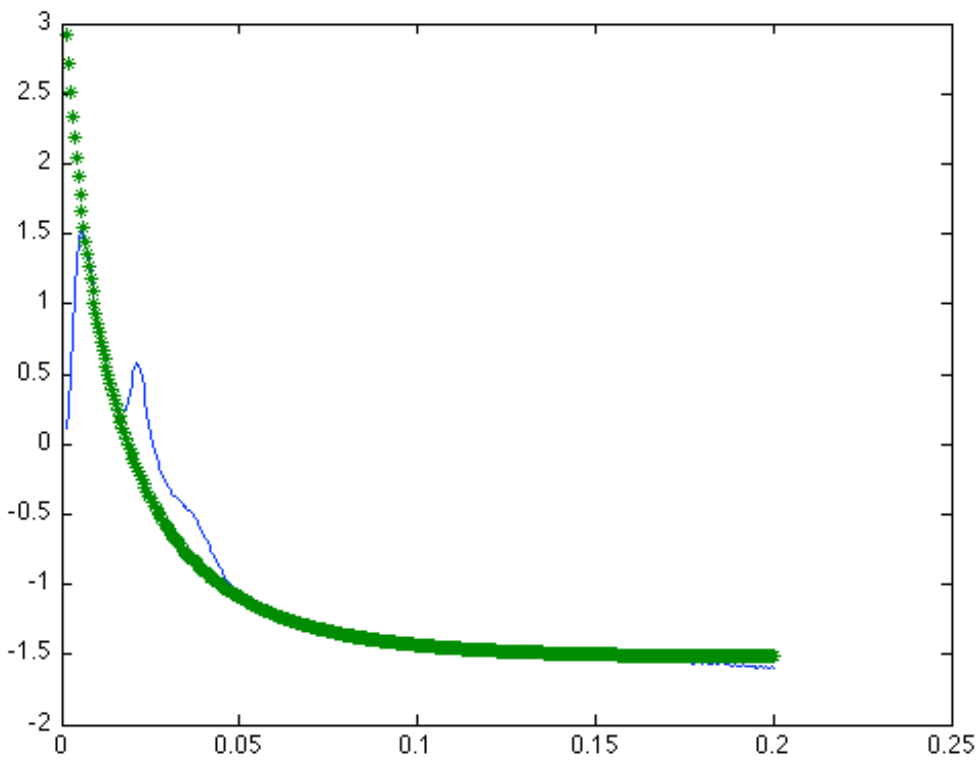
fsp =

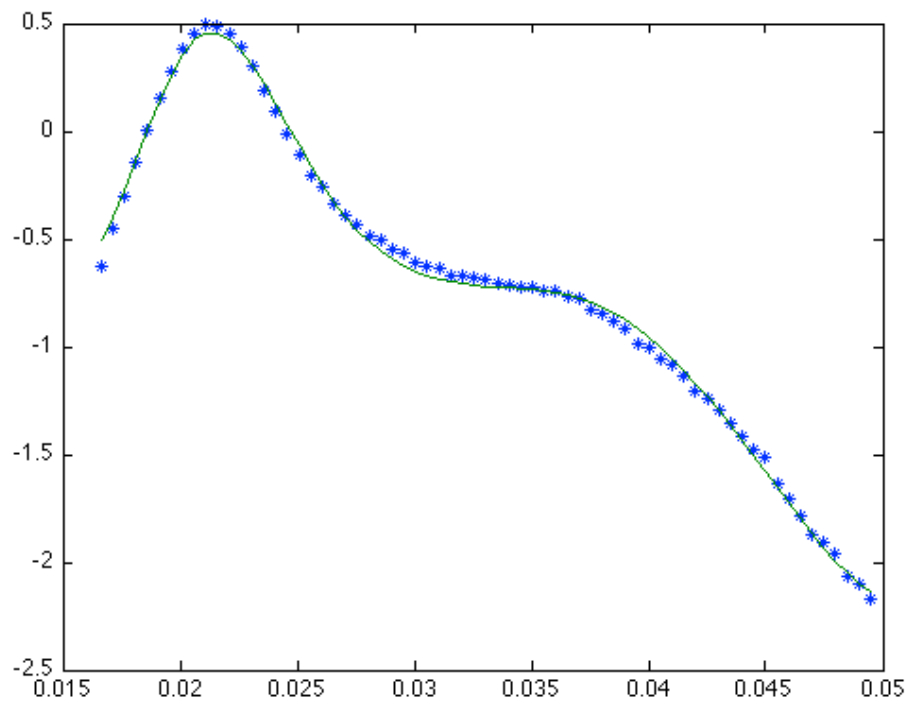
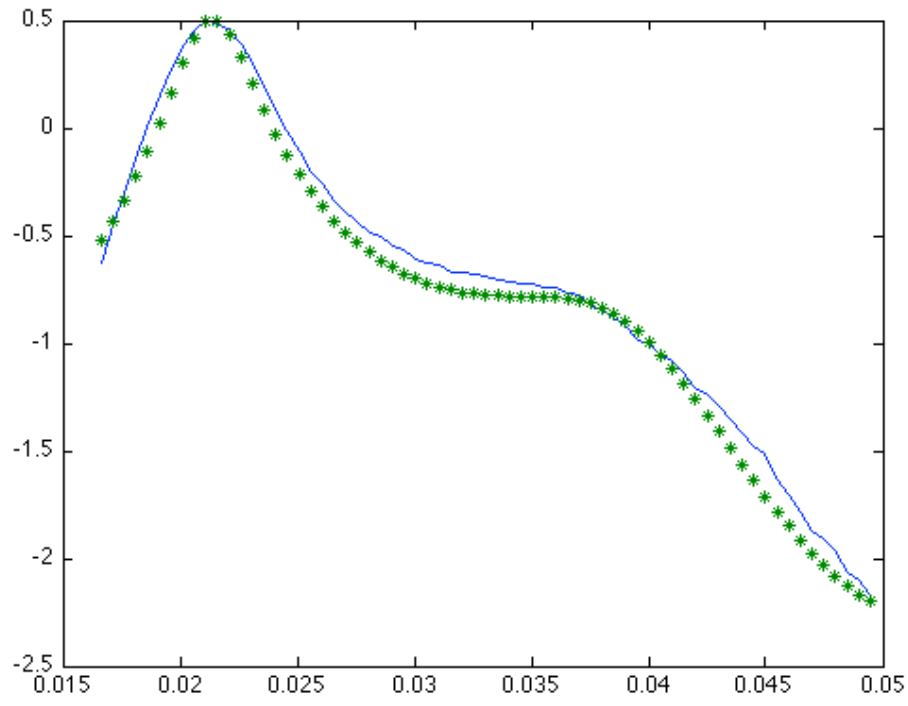
```

    0.0889

```







Published with MATLAB® 7.11

```

function Y=smear(q,Rc,sigmac,xsi,Rhs,phihs,sigmaq2)

Pgauss =@ (q,Rc,sigmac,xsi) (exp(-4*(pi*xsi*q).^2)/(sigmac*(2*pi)^0.5)).*gauss(q,Rc,sigmac);
alpha =@ (phihs) (1+2*phihs)^2/(1-phihs)^4;
beta =@ (phihs) -6*phihs*(1+phihs/2)^2/(1-phihs)^4;
gamma =@ (phihs) phihs*(1+2*phihs)^2/(2*(1-phihs)^4);
G =@ (q,Rhs,phihs) alpha(phihs)*(sin(2*q*Rhs)-2*q*Rhs.*cos(2*q*Rhs))./(2*q*Rhs).^2+...
    beta(phihs)*(2*2*q*Rhs.*sin(2*q*Rhs)+(2-(2*q*Rhs).^2).*cos(2*q*Rhs)-2)./(2*c...
    gamma(phihs)*(-(2*q*Rhs).^4.*cos(2*q*Rhs)+4*(3*(2*q*Rhs).^2-6).*...
    cos(2*q*Rhs)+(2*q*Rhs).^3-6*2*q*Rhs.*sin(2*q*Rhs)+6))./(2*q*Rhs).^5;
S =@ (q,Rhs,phihs) 1./(1+24*phihs*G(q,Rhs,phihs)./(2*q*Rhs));

% Y = Pgauss(q,Rc,sigmac,xsi).*S(q,Rhs,phihs);

Y = ones(numel(q),1);
for i = 1:numel(q)
Ismear =@ (qq) Pgauss(qq,Rc,sigmac,xsi).*S(qq,Rhs,phihs).*(1./(2*pi*sigmaq2(i)).^0.5).*exp(-0.5*
Y(i,1) = quadv(Ismear, q(i)-3*(sigmaq2(i))^0.5, q(i)+3*(sigmaq2(i))^0.5);
end
i;
end

```

Input argument "q" is undefined.

Error in ==> smear at 15  
Y = ones(numel(q),1);